

**POLITECNICO DI TORINO**

DEPARTMENT OF MECHANICAL AND AEROSPACE ENGINEERING

**Master of science level – Automotive Engineering**

Master's Degree Thesis

**A METHOD TO ENHANCE THE SPATIAL  
LAYOUT OF LATTICE INFILL IN  
ADDITIVE MANUFACTURING**



**Supervisor**

**Professor Giovanni Belingardi**

**Candidate**

**Gian Marco Tassi**

**March 2018**



# Contents

Abstract.....	4
Acknowledgment.....	6
1 Introduction to Additive Manufacturing.....	9
1.1 Additive Manufacturing Technologies .....	12
1.1.1 Vat Photopolymerization.....	14
1.1.2 Powder Bed Fusion (PBF).....	15
1.1.3 Material Extrusion.....	16
1.1.4 Material Jetting.....	18
1.1.5 Binder Jetting.....	19
1.1.6 Direct Energy Deposition (DED) .....	21
1.1.7 Sheet Lamination.....	22
2 Topology Optimization in Additive Manufacturing.....	24
2.1 2D Optimization Examples.....	28
2.2 3D Optimization Examples.....	31
3 Design Process.....	33
3.1 Starting Point and Objective .....	33
3.2 Choice of Additive Manufacturing Technology .....	34
3.3 FDM Manufacturing constraints.....	38
3.3.1 Bridging.....	38
3.3.2 Overhang Angle.....	40
3.3.3 Wall Thickness .....	41
3.3.4 Minimum Cylinder Diameter .....	42
3.3.5 Estimate of actual manufacturing constraints.....	43
3.4 Outline of the methodology proposed to enhance lattice infill distribution ....	48

4	Lattice Effective Properties .....	55
4.1	Effective properties from literature.....	55
4.1.1	Choice of BCC cell for the methodology .....	61
4.2	Effective properties of BCC cells through homogenization .....	62
4.3	Limits given by FDM manufacturing constraints.....	65
5	Partition into Subdomains of Constant Lattice Cell Size .....	67
5.1	Geometry Partition.....	68
5.2	Optional subdivision from feedback of Optimization problem 1 .....	70
6	Optimization Problems .....	72
6.1	Optimization Problem 1 .....	73
6.2	Optimization Problem 2.....	75
6.2.1	Cell Trimming Techniques.....	77
7	Practical Applications.....	80
7.1	Bottle Test Piece .....	81
7.1.1	Optimization Problem 1 on Bottle test piece.....	82
7.1.2	Subdivision Refinement .....	83
7.1.3	Optimization Problem 2 on Bottle test piece.....	85
7.1.4	Results .....	86
7.2	Upright.....	88
7.2.1	Definition of the Design Domain and Subdomains.....	90
7.2.2	Optimization Problem 1 – Upright.....	92
7.2.3	Optimization Problem 2 - Upright.....	93
7.2.4	Results .....	95
8	Conclusions .....	96
8.1	Future Work.....	97

Symbols List.....	99
Figure Index.....	101
Table Index.....	106
Bibliography.....	107

# Abstract

In this thesis, carried out at Michigan State University (Michigan, USA) with the supervision of Professor Alejandro R Diaz, a procedure to optimize the infill material distribution in the core of a three-dimensional object manufactured through additive manufacturing is presented. It was conceived to fit all requirements of Fused Deposition Modeling (FDM) printing technology but it is applicable to other technologies.

In this methodology, the infill geometry is characterized by the spatial repetition of a lattice cell printable without support material. The goal of the optimization is to maximize stiffness. In order to fit real 3D shape, that are possibly characterized by narrow and hefty regions, the design domain is divided in non-overlapping subdomain separated by solid walls. Each subdomain is characterized by a lattice infill which share the same cell size and topology, but the thicknesses of every bar is independent. The target of the subdivision is to use large cells in hefty regions which allows for a wider range of densities.

The placement of internal walls to separate adjacent subdomains is determined by an iterative procedure started with geometry considerations of the object and refined by the feedback coming from FEM simulations.

The spatial distribution of lattice material within each subdomain is determined through two optimization problems. The first problem makes use of effective properties of the cell to map the optimum relative density distribution and to assess the initial domain partition. It also provides a valuable feedback for the refinement of the subdivision of the design domain. The second problem optimizes the section properties of the lattice and it gives the actual material spatial distribution.

The methodology is illustrated using two examples: a test “bottle” shape to illustrate clearly all passages of the procedure, and a FSAE double wishbone upright which represent a possible automotive application of the methodology.

The results of the application of methodology are encouraging. This might be the first methodology that gives a printable, real 3D, optimized model that take in consideration

manufacturing constraints related to printability issues (in this case referred to FDM technology).

Main current problematics of this methodology are related to the choice of the internal walls, the absence of an efficient trimming algorithm and the anisotropy of additively manufactured objects not taken in consideration during optimization.

The parts optimized have been printed and shown during the presentation of this thesis.

The thesis is opened by an introduction on additive manufacturing technique and technologies. Then the application of topology optimization for additive manufacturing is explained through example of already existing methodologies (for 2D and 3D objects). Afterwards, the methodology proposed by this work is outlined, highlighting the starting point and the target. The following chapters explain in detail every step, supported by theory and examples. Once the methodology is fully outlined, two practical examples of pieces optimized through this methodology are shown to summarize the procedure and present the results and the improvements given by the optimization. The two examples have been printed with FDM technology without support material and presented at the final discussion. The thesis is closed by final remarks and discussion on future work.

# Acknowledgment

This final thesis is the result of six months of research in USA as part of the Fiat-Chrysler Project. An amazing experience made possible by Professor Giovanni Belingardi, FCA Group, Silvia Cigni and Raffaella Fiora, who believed in me, selected me, and supported me for all this period.

I would also like to thank Michigan State University which hosted me during this period and its kind staff that helped me whenever I needed. A special thanks to Professor Alejandro R. Diaz, who supervised my work there and look after me during all this period. He gave me knowledge, method, and steered me in the right the direction whenever he thought I needed it. The quality results of this thesis could not be reached without him. I would also like to thank my colleague at MSU Gao Qiren, who helped me during the progress of this thesis.

I would like to thank again my thesis advisor Prof. Giovanni Belingardi, who not only selected me, but was also present and willing to give me advices even when I was abroad.

And finally, a huge thank you to my family and my friends, the protagonists of my life.

Thanks to my mother Lucia and my father Marcello who supported me both economically and emotionally, who made possible for me to follow this path, and reach my goals. They allowed me and pushed me to discover the world, to make experiences abroad and taught me to not be afraid of the new, to keep chasing my dreams and my ambitions.

Thanks to my sister Barbara, who has always been my reference point, my guidance, ready to help me and support me. Also, a big thanks to Maurizio who became my brother in crime. And thanks to both of them, to give birth to Lorenzo and to have made me uncle of the most joyful and beautiful child.

Thanks to my uncle Maria Luisa who always cry when I come back and make me feel loved. Thanks to my aunt, uncle, cousins, Luca, Nicoletta, Sarah and Celine always present during the important step of my life.

A special thanks to my grandparents Agostino, Anna e Maria for the affection they have always given me. Thanks to my grandfather Igino, even if he cannot be here, I am sure he is looking down on me.

I would also like to thank Roberto and Cristiana who became both part of the family and took care of me since the first time we met.

Another big thank you to my godfather Gianluigi who since that day in the church became a guidance to me.

Thanks to my lifelong friends who know me better than myself and guided me through all my life. Thanks to all the colleagues I met during this fantastic academic journey who became great friends to me and always supported me



# 1 Introduction to Additive Manufacturing

Additive manufacturing (AM, or 3D printing) is a technology which allows the manufacture of intricate shapes that cannot be manufactured any other way, by printing them layer by layer. The process of adding material, as opposed to subtracting material, gives engineers an unprecedented opportunity to design lighter, more organic looking products.

This new manufacturing technology has started a real design and industrial revolution in many sectors such as automotive, aerospace and medical.<sup>1</sup> With the development of more accurate, faster and cheaper machine, additive manufacturing is not only used for prototyping, but it is becoming a suitable technology to efficiently produce small series of complex shapes, difficult (or impossible) to produce any other way.

For example, on January 6, 2014, SpaceX<sup>2</sup> launched its Falcon 9 rocket with a 3D-printed Main Oxidizer Valve (MOV) body in one of the nine Merlin 1D engines. This was the first time SpaceX launched a 3D printed part over a rocket successfully. SpaceX is investigating in this new manufacturing technology and today it is testing the “*SuperDraco*” engine which make use of a 3D-printed engine chamber developed entirely in-house. This engine will be part of the crewed spaceflight program (the ambitious program of make possible travel over space) and the Dragon Version 2 vehicle.

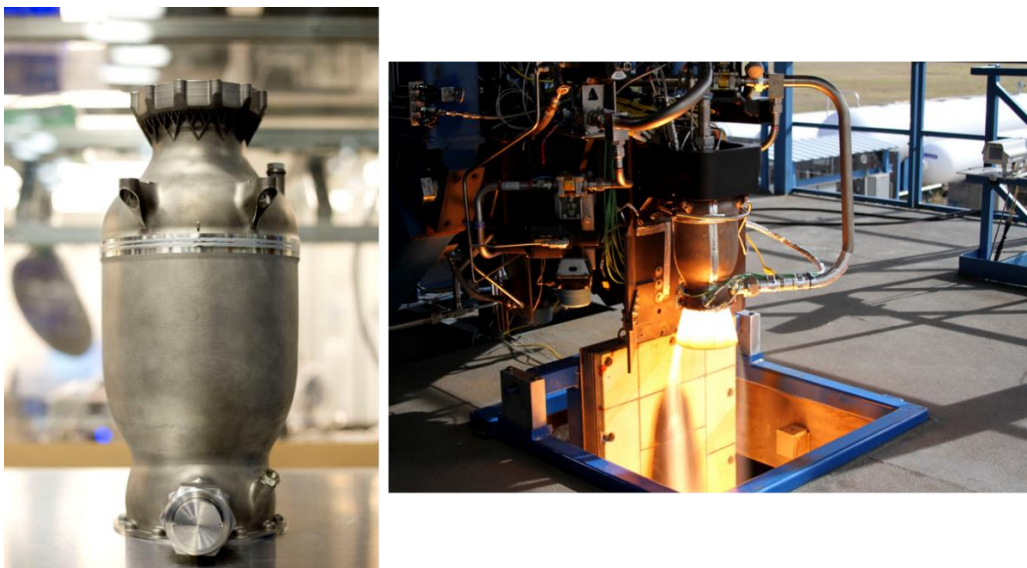


Figure 1. *SuperDraco* engine produced with EOS metal 3D printer and made of *Inconel* superalloy.<sup>2</sup>

<sup>1</sup> Reference [14]

<sup>2</sup> SpaceX, [www.spacex.com](http://www.spacex.com)

Printing layer by layer offer many advantages with respect to traditional manufacturing like CNC machining:

- **Speed.** Complex design can be printed in just a few hours from the CAD model. This advantage makes additive manufacturing the easiest and faster solution for prototyping and production of small series.
- **One step manufacture.** 3D printing allows to produce most of the parts in just a single step. Moreover, in many cases, if more parts are printed at the same time, and they are part of the same assembly, they can be printed already assembled.

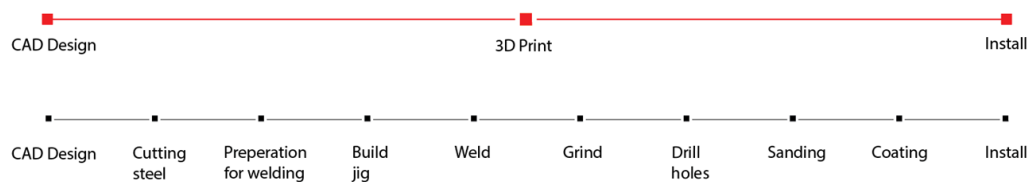


Figure 2. 3D printing process compared to traditional manufacturing process<sup>3</sup>

- **Cost.** The low 3D printer energy consumption (comparable to a PC) and the faster production, means more efficiency lower cost than CNC machines. Material cost vary considerably among different additive manufacturing technologies from 20\$ to more the 150\$ per kilo.<sup>4</sup> Labour work is cheaper, because parts do not need much post processes and machine are easy to use. This explain why 3D printers are not suitable for large production series, but are perfect for prototyping and small series.

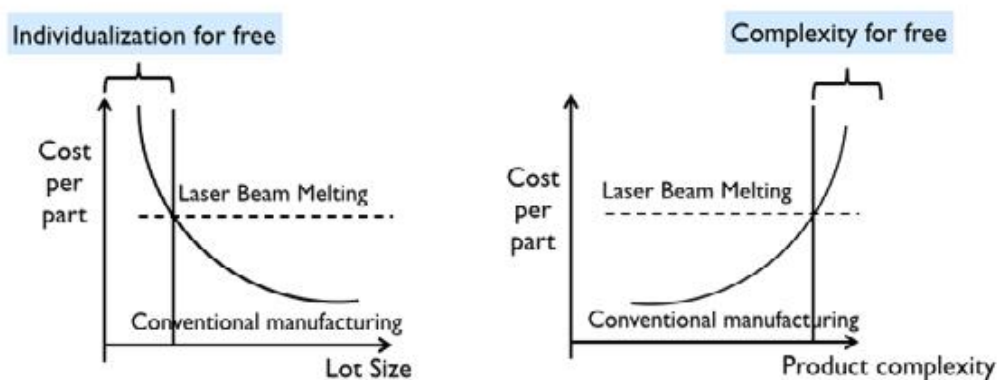


Figure 3. Comparison between AM and conventional manufacturing. Laser beam Melting is one of the AM main technologies. The same pattern is valid for the other AM technologies.

<sup>3</sup> Image from Ref. [12]

<sup>4</sup> Data from Ref. [12]

- **Risk mitigation.** Faulty prototype or machine affects just the current print. The file can be modified or the machine adjusted without losing time and money.
- **Complexity and design freedom.** Printing layer by layer allows for much more freedom than standard manufacturing.



Figure 4. Example of complex 3D printed geometry

- **Sustainability.** Additive manufacturing, generally, uses just the material of the final part. The only material loss is that needed for occasional support structure. CNC machining instead is a basically a subtractive manufacturing process which obtain the final part by removing material form a material block.

If from one side many advantages have been shown, additive manufacturing introduces some limitation:

- **Part size.** Printer build plate is usually limited in dimension. Large build plate machines are available but require a huge investment. Therefore, object produced by AM are usually small in dimensions.
- **Production series.** For the cost/part graph in Fig. 3 it is clear that Additive Manufacturing is not suitable for mass production, although in recent years the development of new AM technologies and materials have improved productivity, and make larger production series more feasible.
- **Not complete shape freedom.** Even if AM increase the possibility of producing complex shapes, some manufacturing constraints are still to consider (e.g. minimum member thickness, and maximum overhang angle).
- **Anisotropy.** Most parts produced with AM technology shows anisotropy on the printing direction

## 1.1 Additive Manufacturing Technologies<sup>5</sup>

In the previous section, we introduced what is Additive Manufacturing and shown what are the main advantages and disadvantages.

With the term Additive manufacturing we are including all these technologies based on the production of a part by overlapping a layer of material over another layer of material. In this category of manufacturing technique, a large variety of 3D printers and materials are available. They differ on work principle, melting energy source or adhesive system, materials, functionality given to the part, quality and accuracy of the print, and for sure costs.

Today's machines in the market can be divide in mainly seven categories, summarized in Fig. 5 in the next page.

---

<sup>5</sup> Data and figures from Reference [13]

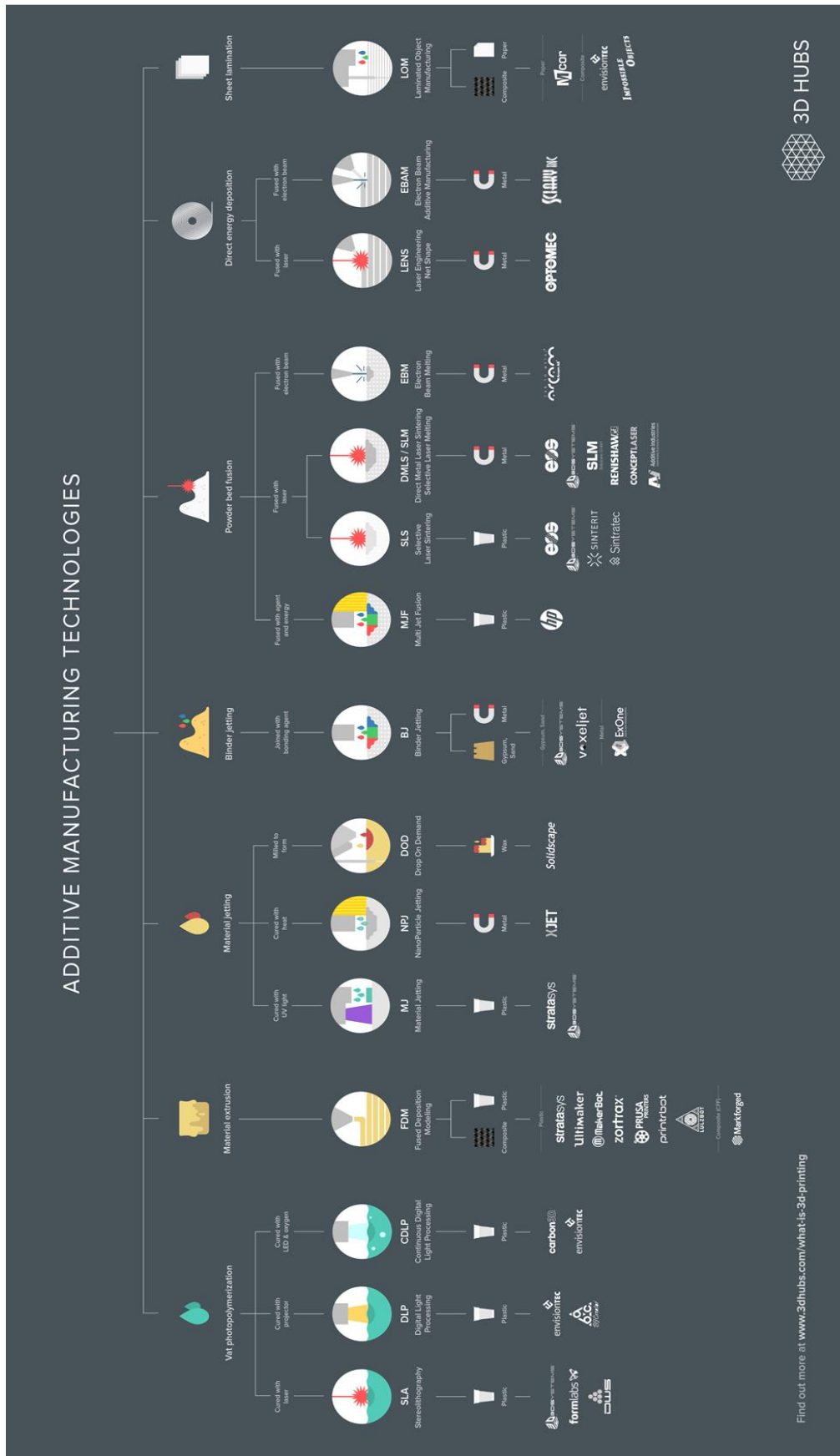


Figure 5. Resume of the main 3D printing technologies. Image from Ref. [12]

### 1.1.1 Vat Photopolymerization

The material used in this type of machines is a special resin which is subjected to a specific light source that transform the liquid material to solid material. In this category we find Stereolithography (SLA), Direct Light Processing (DLP), Continuous DLP (CDLP). They are all based on the same concept, and they differ just in the way they are exposed to the light source.

The parts are produced upside down and they are attached to the bed with external supports (see Fig. 6).

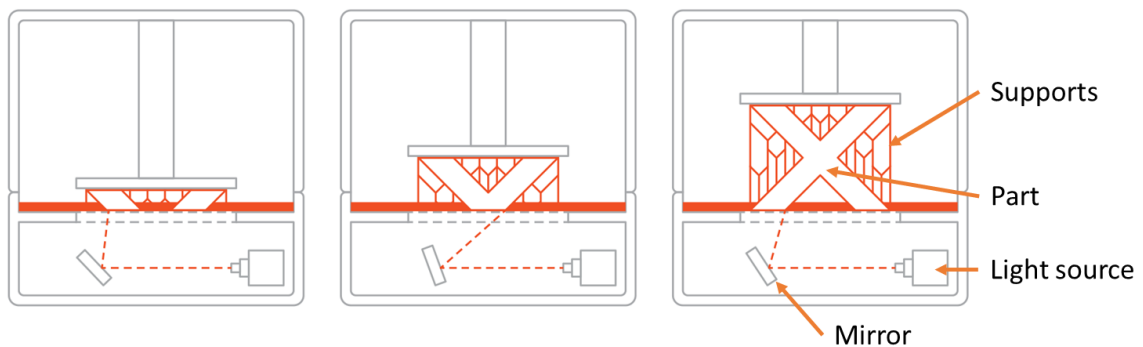


Figure 6. Typical scheme of an SLA machine. Image from Ref. [12].

Usually parts produced in this way are full solid because void regions inside the parts could trap part of the liquid resin difficult to drain out in post-process. The external finish is smooth and post processing is always needed to eliminate support material.

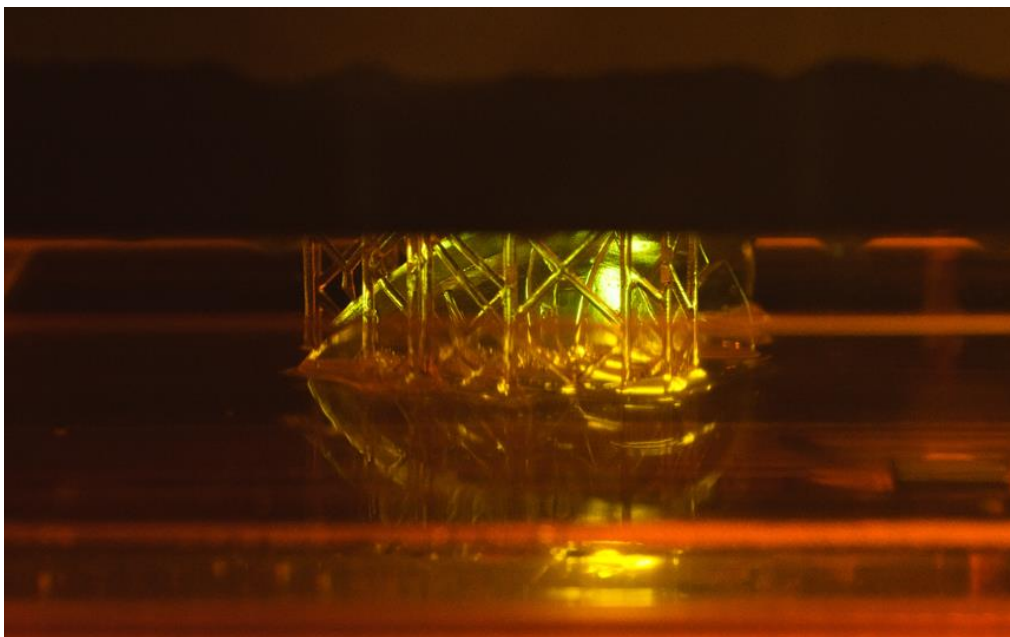


Figure 7. A part being printed with SLA technology. Image from Ref. [12].

### 1.1.2 Powder Bed Fusion (PBF)

The machines in this category make use of a metallic or plastic powder bed. An energy source heat, or melt, particles on the surface of this bed. The melted particles bond together and layer by layer a solid part is produced. This methodology includes, Selective Laser Sintering (SLS), Selective Laser Melting (SLM) and Direct Metal Laser Sintering (DMLS), Electron Beam Melting (EBM) and Multi Jet Fusion (MJF). All these sub groups differ on the heating source (electron beam, laser, IR energy source), on how the particle are bonded together (for example if it completely melts the particles or reach condition close to melting), and the powder material. (See Reference [13] for full details).

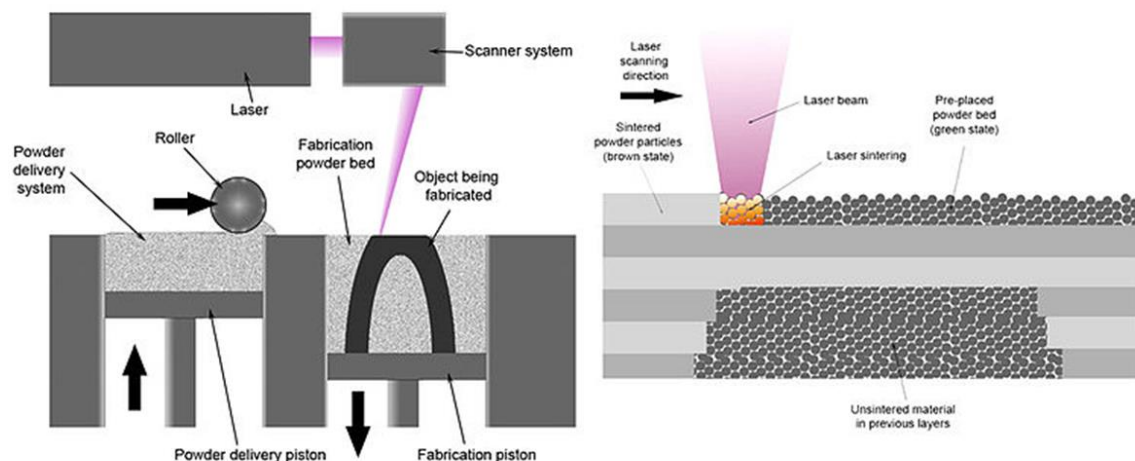


Figure 8. Typical scheme of a SLS printer<sup>6</sup>

This additive manufacturing technology produce parts very strong, good for structural functions. SLS can print without the need of support material (the powder is the support material itself), while DMLS and SLM due to the high temperature needed for metal to melt, they need support material. All part produced with Powder bed machines come out completely encapsulated in powder. For this reason, once they are extracted they need to be cleaned. Closed shapes with void regions inside are not suitable for this technology because the powder would remain closed into the solid part unless we drill some holes to let it escape.

<sup>6</sup> Image from <http://3dinsider.com/3d-printer-types/>



Figure 9. A general SLS printer in action.

### 1.1.3 Material Extrusion

This category that mainly include just Fused Deposition Modelling (FDM) printers, represents nowadays the most common and cheap solution for 3D printing. A filament of plastic or metal material is heated and pushed into a nozzle where it melts. The nozzle moves over the build plate extruding layer by layer the piece.

The design of parts produced with this technology need some attention. In fact, FDM machine cannot print in-air. This means that when exceeding certain inclination angle, support material will be needed in order to make the part printable.

Anyway, the cost-effectiveness of these type of machines makes them use widespread in many sector and at many levels. Moreover, the freedom of the filament material allows to give to the part peculiar characteristic (elasticity, food safe, heat and chemical resistance as examples).

The drawback of this technology is mainly due to the low dimensional accuracy compared to other additive manufacturing technology.

Figure 10 shows a general scheme of an FDM. In this case the machine is given two nozzles with two different filaments: one for the part material itself, and one for the support material. This solution allows a faster printing and an easier post processing of the part to detach the support material from the part. In Figure 11 an example of a part printed in FDM is shown.

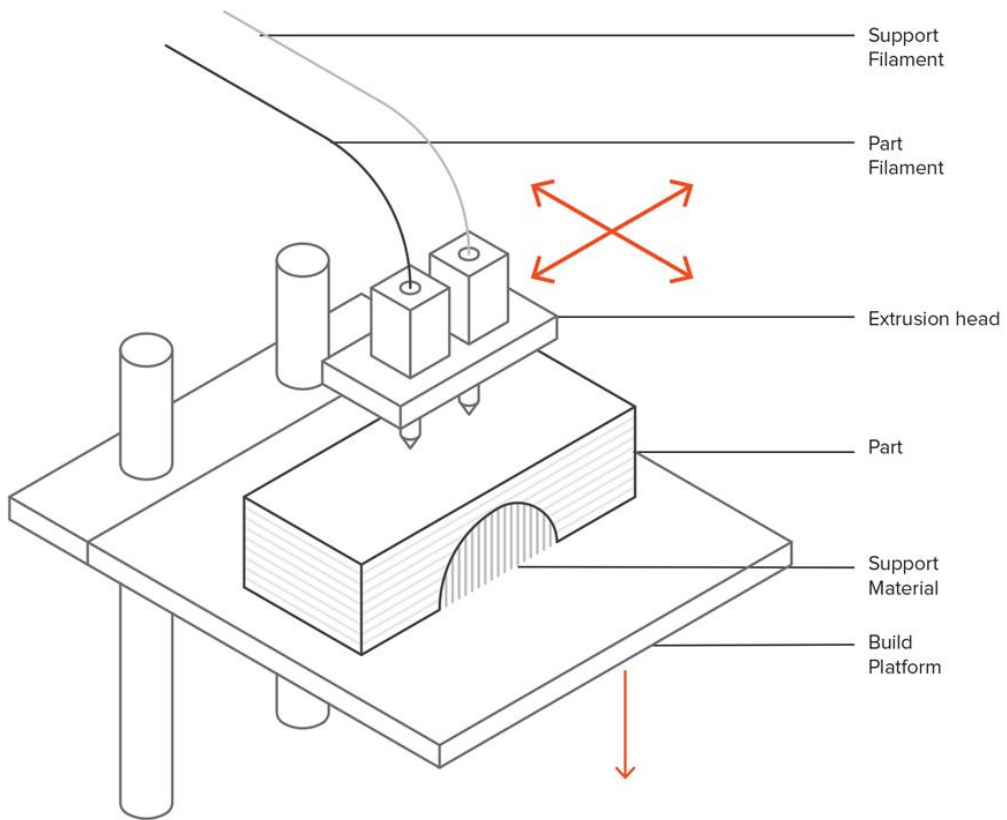


Figure 10. Scheme of a 3D double nozzle FDM printer. Image from Ref. [12].

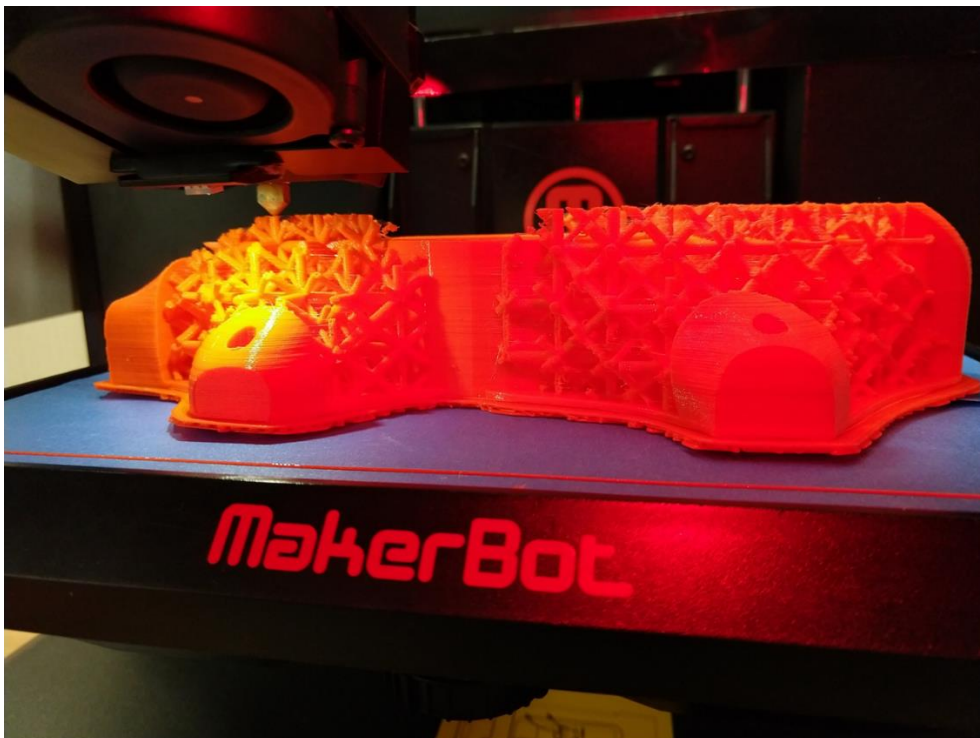


Figure 11. FDM printer in action to print one of the practical example of this thesis.

### 1.1.4 Material Jetting

This technology is often compared to 2D printers. In fact, layer by layer a similar printhead of ink 2D printers distributes droplets of photosensitive material which react to UV lights. It can drop droplet of different material allowing to produce solid parts made of different colour and support material soluble. The work scheme is shown in Fig. 12

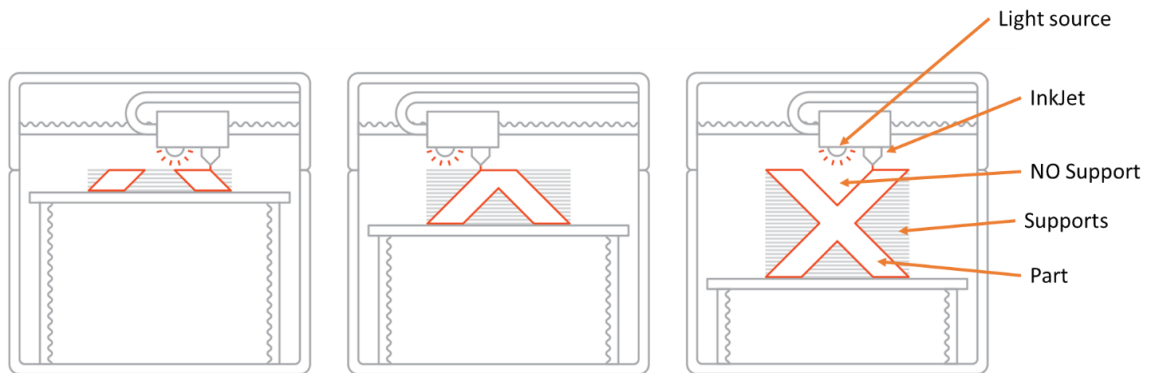


Figure 12. Working scheme of a Material Jetting machine. Image from Ref. [12].

Note that the support material is placed only when it is needed (i.e. when solid parts are supposed to be generated above).

Part produced with this technology result very good details and accuracy, but the cost of the printer is the main drawback.

Some example showing the potential of this machine are shown below.



Figure 13. An example of part produced with Material Jetting. The white part is stiff, while the black part is made up of another material flexible. Image from Ref. [12].



Figure 14. Another example with a clear use of two different materials, one glossy and one matte. Image from Ref. [12].

### 1.1.5 Binder Jetting

This technology is based on the use of a binder agent layer by layer which solidifies a powder bed and bind each layer to the other to create the final solid model. It comprises features of the powder bed fusion printers and the droplets use like the material jetting printers but instead of a heat source use a binding agent.

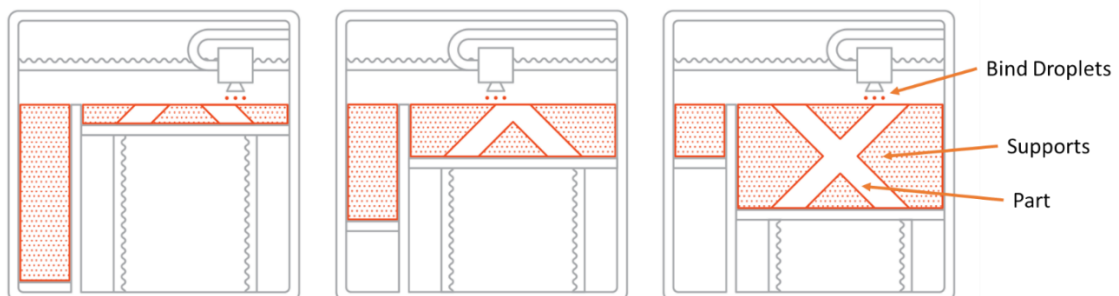


Figure 15. Working scheme of a binder jetting printer

With Binder Jetting machines it is possible to use ceramic powder bed which produce parts with a pretty smooth surface, but brittle. Instead, using metallic powder is possible to use part produced in this way for functional use.

In Figure 16 is possible to see that, as with material jetting machines, here it is possible to produce parts with different colour during the same print.



Figure 16. Example of a multicolour part produced with Binder jetting technology

### 1.1.6 Direct Energy Deposition (DED)

In this family of printers, an energy source is used to melt a metal powder in the same moments it is spread. No powder bed is used in this case. Technologies in this family are Laser Engineered Net Shape (LENS) and Electron Beam Additive Manufacture (EBAM). They are based on the same idea shown in Fig. 17 but they differ on the heat source: the former uses a laser, the latter an Electron Beam.

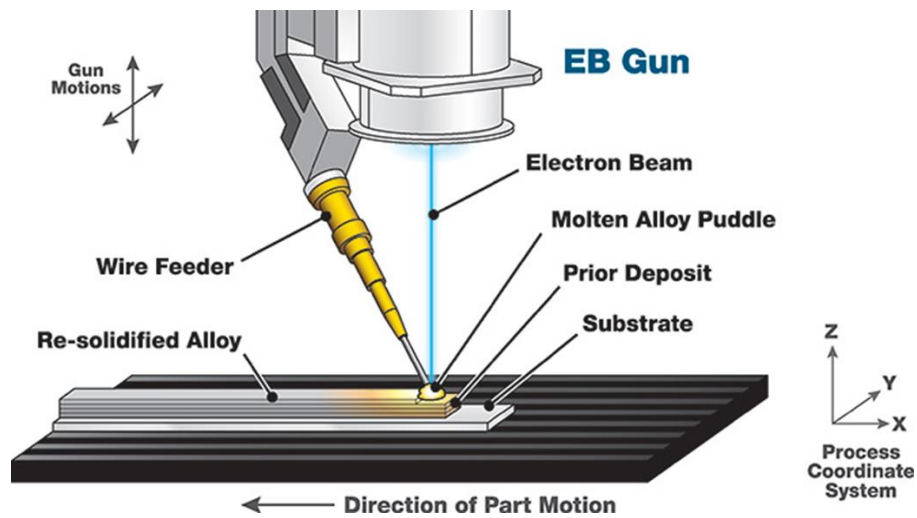


Figure 17. Working scheme of an EBAM machine. <sup>7</sup>

This technology is interesting cause it can be used to repair parts. The laser (or the electron beam) can heat the surface of the broken part and the nozzle can spread powder to melt with the original part and fix it.



Figure 18. LENS system in action. <sup>8</sup>

<sup>7</sup> Image courtesy of [www.sciaky.com](http://www.sciaky.com)

<sup>8</sup> Image curtesy of [www.sculpteo.com](http://www.sculpteo.com)

### 1.1.7 Sheet Lamination

This Additive Manufacturing technology is pretty different from the other shown before. In this case both Additive manufacturing a CNC machining are used to generate a part. Thin sheets of metal are over imposed and attached one on the other through ultrasonic welding. Then, a CNC machining system get rid of the superfluous material layer-by-layer and give the shape of the sections of the part. A scheme of this machine is shown in Fig. 19. The part produced in this way are full solid material

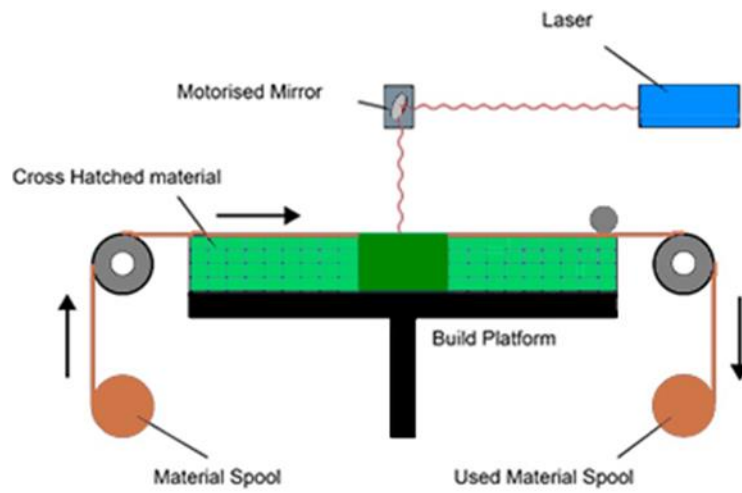


Figure 19. Scheme of a typical Sheet Lamination machine.<sup>9</sup>

This technology is useful also to combine more materials in the same print and weld them together, like in Fig. 20.

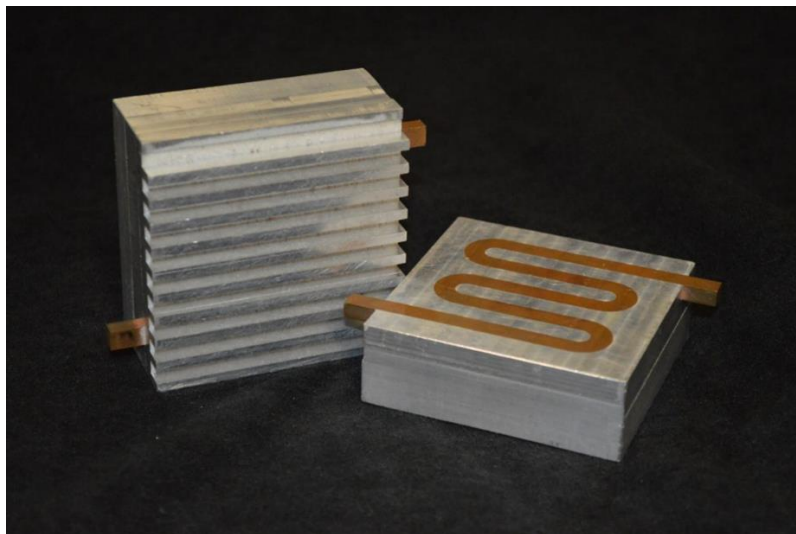


Figure 20. Example of multi-material (copper and aluminium) part printed with Sheet Lamination.<sup>10</sup>

<sup>9</sup> Image courtesy of [www.engineersgarage.com](http://www.engineersgarage.com)

<sup>10</sup> Image courtesy of <http://www.3diligent.com>

The same machine can also be used with paper sheet instead of metal sheet. In this case adhesive material substitutes ultrasonic welding and full colour spectrum can be achieved by adding an inkjet to the machine.

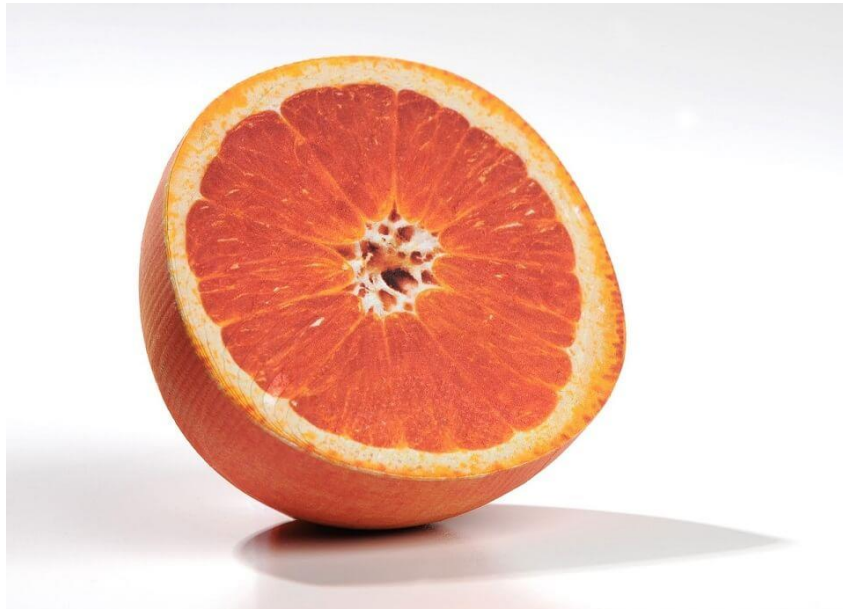


Figure 21. Example of full colour print object printed with Sheet Lamination.<sup>11</sup>

---

<sup>11</sup> Image courtesy of <http://www.3diligent.com>

## 2 Topology Optimization in Additive Manufacturing

Topology optimization is a method of main interest, and widely used, when weight reduction is an important factor in the design of a part. Given a design domain, and given loads and constraints, this method allows to define regions where the presence of material is less needed than others. In other words, it allows to reduce the weight keeping the same performance (i.e. same stiffness). Topology optimization can be applied in both standard manufacturing techniques (CNC machining) to remove elements of the part less supposed to stress, and to AM to fabricate parts with material just where it is needed.

In both CNC machining and additive manufacturing, topology optimization can be applied directly through a standard optimization problem. The design domain is meshed and design variables are the relative densities,  $d_i$ , of each mesh element  $i$ .

The objective function is, for example, the minimization of the overall compliance  $\hat{C}$  (that means maximization of the stiffness,  $\mathbf{K}$ ), subjected to a constraint over the total amount of material. One possibility to solve this problem is to use the penalized, proportional stiffness model (SIMP)<sup>12</sup>. Supposing the material to be isotropic, this approach assigns to each design variable  $d$  a material property  $E(d)$  that will affect the stiffness matrix, through the relation:

$$E(d) = d_i^p E_0 \quad (1)$$

Where  $E_0$  is the Young's Modulus of the solid material, and  $p$  is the penalization factor. In SIMP model, penalization factor is  $>1$  (usually  $p \geq 3$ ). In this way, intermediate densities will not appear because mid-densities elements will have very low mechanical properties and a scenario with just 0-1 relative densities will be more convenient from a mathematical point of view. This method will result in a sort of bi-colour map where elements can be solid void like in Fig 22.

---

<sup>12</sup> Reference [8]

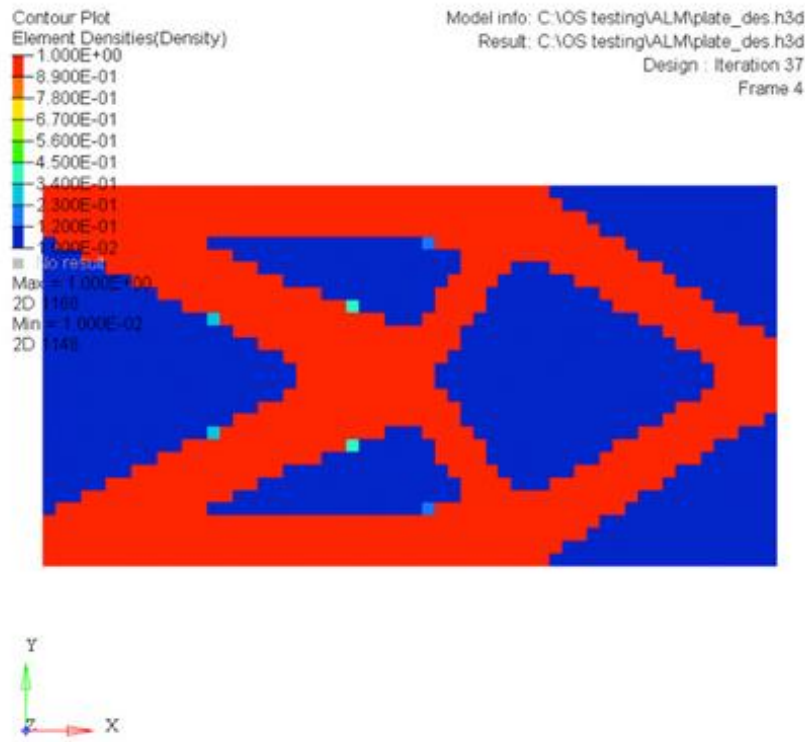


Figure 22. Result of a standard topology optimization with SIMP model for  $p \geq 3$ . Image from [10].

This bi-colour maps evidence zones of the design domain which we can get rid of without ruining the mechanical performance. It is evident the direct application of this to CNC machining to trim away those region from the part for a more lightweight design. The same result can also be used in Additive Manufacturing as it is and in many cases, AM allows to follow the result of the topology optimization more closely.

On the other hand, use a penalization factor which allows just solid or void regions means not exploiting the full potential of additive manufacturing. In fact, layer-by-layer manufacturing allows the creation of very intricate structures that cannot be treated as full solid or void region. For example, AM allows for the creation of small periodic cells that behave halfway between solid and void material. Introducing the possibility of mid-density elements, the binary condition 0-1 on the relative density of the elements has to be broken and the method to resolve the optimization problem has to be modified to include the possibility of mid-density elements. Using a different method (for example reducing the penalization factor or replacing the SIMP method) the result of the optimization is no more bi-colour, and become something like in Fig. 25.

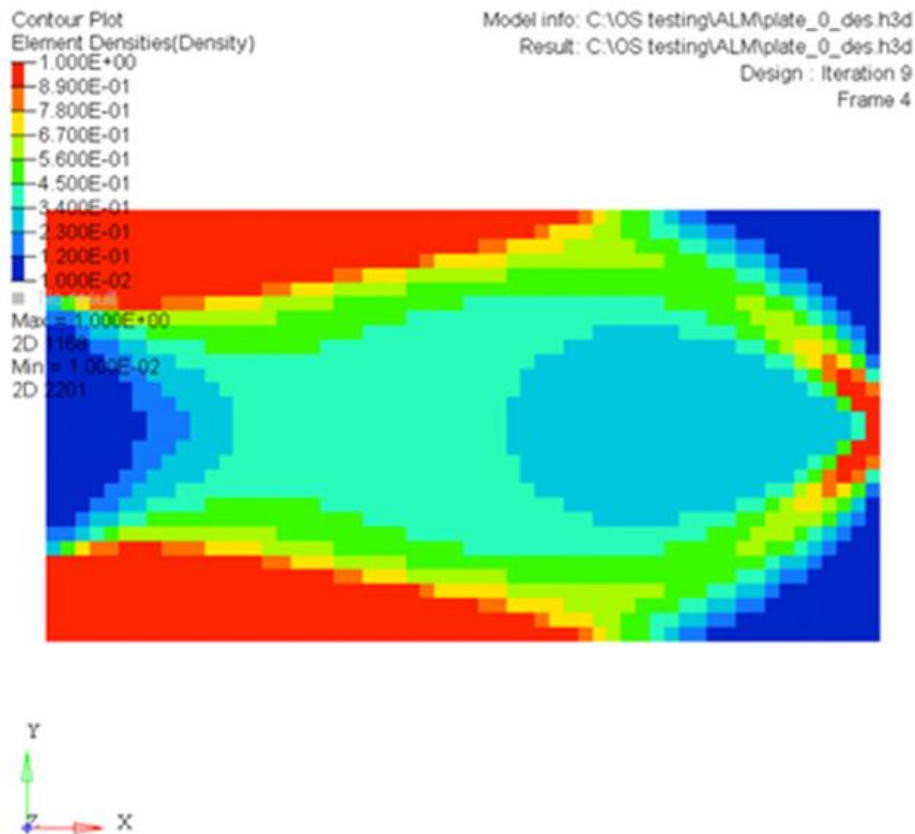


Figure 23. Result of the optimization problem allowing mid-densities elements.

The result shown above has then to be processed to obtain the microscale characteristic of the cell (topology, thicknesses, cell size, etc.) that gives the correspondent value of relative density.

Microstructures with different small-scale geometries and topology are often use in additive manufacturing to create mid-densities elements. Typically, every cell topology is characterized by certain dimensions (e.g. length and thickness of bars/plates in the cell). This is the so called *lattice infill*.

There has been considerable research on how these dimensions affect mechanical properties both in 2D and 3D. For instance, Ref. [2,4,5,6], discuss different lattices, considering isotropy and the relation between effective cell density and stiffness. Some examples of cells for 2D and 3D applications are shown in the next figures.

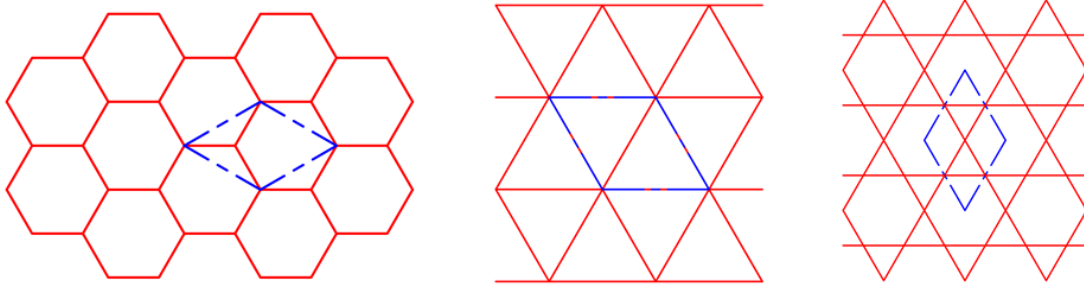


Figure 24. Typical 2D cells. From the left: Honeycomb cell, Triangular cell, Kagome cell.

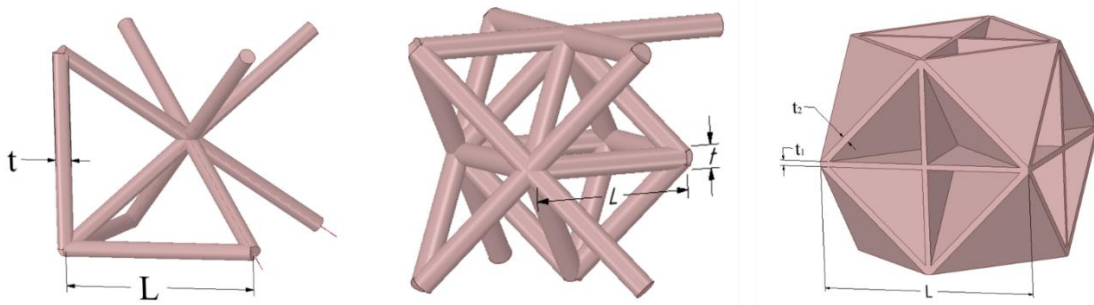


Figure 25. Some of the 3D cells. From the left BCC cell, Octet-truss cell, cubic-octet foam.

## 2.1 2D Optimization Examples

The idea of optimizing the distribution of lattice material within a design domain is not new.

In the methodology presented in Ref. [3], applied to extruded (2.5D) objects the authors present an implicit slicing formulation based on the definition of a function  $H(x)$ , that describes the toolpath that the nozzle has to follow in order to generate the optimum material distribution. The nozzle follows a continuous trajectory. This means that the geometry produced contains a series of walls and not cell-type infill. An example, taken from Ref. [3], is shown in Fig. 26. Here a spanner wrench is optimized. Given loads and constraints, a FEM simulation gives the result shown in Fig 26a. From this contour plot, a few regions of very low stresses are detected and eliminated from the design domain (Fig. 26b). From the distribution of stresses, the Function  $H(x)$  define the black lines in Fig 26c and 26d that are to be consider the toolpath of subsequent layers. This means that one layer follows the path defined by 26c, the next layer follows 26d (that is just a  $90^\circ$  rotation over the around the printing direction). The superposition of the two, gives the final shape in Fig. 26e and 26f shows the part extruded and printed.

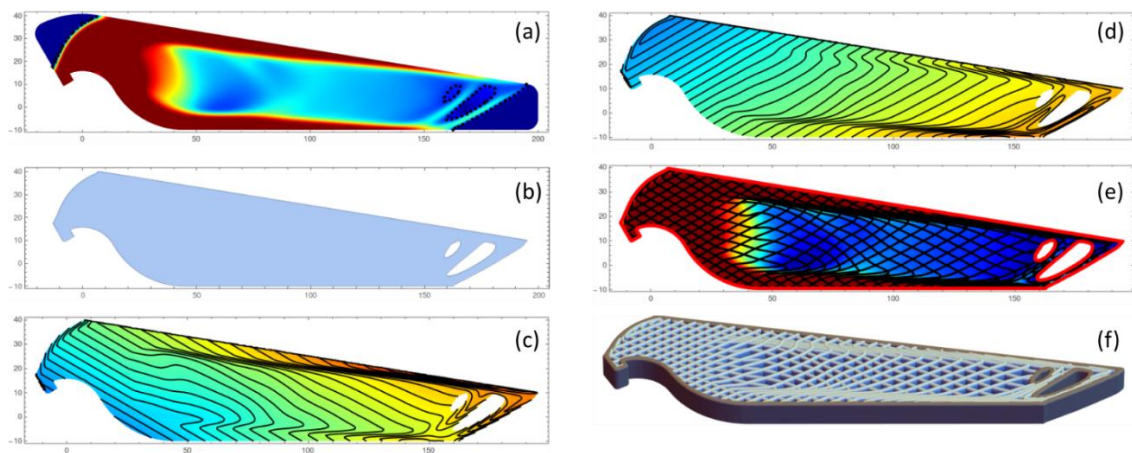


Figure 26. Optimization procedure presented in Ref [2]. First Fem simulation to get rid of very useless part of the domain (a); new design domain (b); toolpath of even layers (c); toolpath of odd layers (d); final aspect (e); printed object (f)

This methodology has the great advantage of having the density changing smoothly within the domain and it can be applied easily in 2D. Instead, its application in general 3D problems with geometries not just extruded, is difficult. In fact, the function  $H(x)$  should change for each slice, and to make the part printable,  $H(x)$  should take in

consideration also other slices (at least the one before). Therefore  $H(x)$  should be history dependent and have a control over subsequent layer to guarantee that the layer below gives enough support to print the current layer. Several attempts of doing so have been tried, without achieving any good result.

Another approach, Ref. [1], has been presented last here by Campagna Francesco, and Professor Alejandro R Diaz, for extruded 2.5D shape objects. It is an example of optimization using periodic cells distribution as infill.

Here a smart choice of walls, prior to optimization, subdivides the design domain into regions that shares same topology, cell size, thicknesses, and consequently effective density. The subdivisions were made based on a standard topology optimization process that gave struts that was conveniently dividing the domain. Kagome cells, shown in Fig. 27, were used to fill each subdomain.

From the literature, a relation between the geometric characteristics of the Kagome cell and its mechanical behaviour was given. Then the optimization problem with using that function was solved, and resulted on a material distribution over the subdomains. From the values of the relative density for each subdomain, the minimum number of cells per region, the minimum printable thickness and the maximum aspect ratio  $t/L$ , the cell characteristics per subdomain were extracted.

The result of this methodology is shown in Fig. 27, while Fig. 28 shows the same part been printed with FDM technology.

Many complications arise when trying to apply this procedure to real 3D applications. As the object is no longer a simple extrusion, printability becomes a crucial factor and partitioning the design domain based on a standard topology optimization, becomes impractical or outright impossible except in very specific situations.

The methodology presented within this thesis have some ideas in common with Ref. [1] that we will see in the Chapter 3.

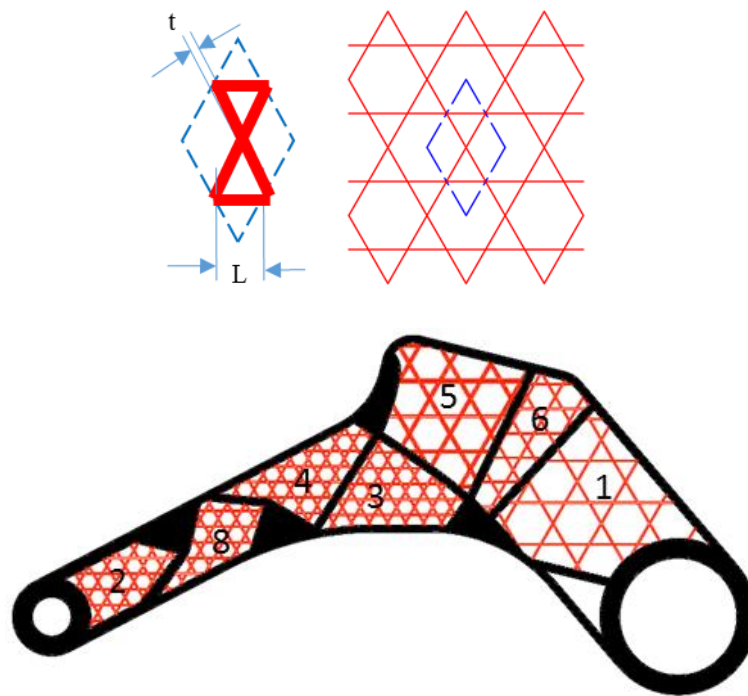


Figure 27. Kagome cell dimension, and result of the optimization presented in Ref [1].



Figure 28. Real 2.5D part of Ref [1] printed.

## 2.2 3D Optimization Examples

On the very last few years some software houses presented new procedures to optimize the lattice infill in real 3D object. For example, Altair Optistruct (Ref. [10]) use the edges of a tetrahedral mesh to define a lattice pattern. relying thus on the finite element mesh to define the microstructure. The edges of this mesh are then given a section area that become the design variable in the optimization problem. Making the section area variable and finite element mesh as lattice pattern, is a way to avoid using cells and achieve a continuous density variation. The result of the application of this optimization is shown in Fig. 29 and 30.

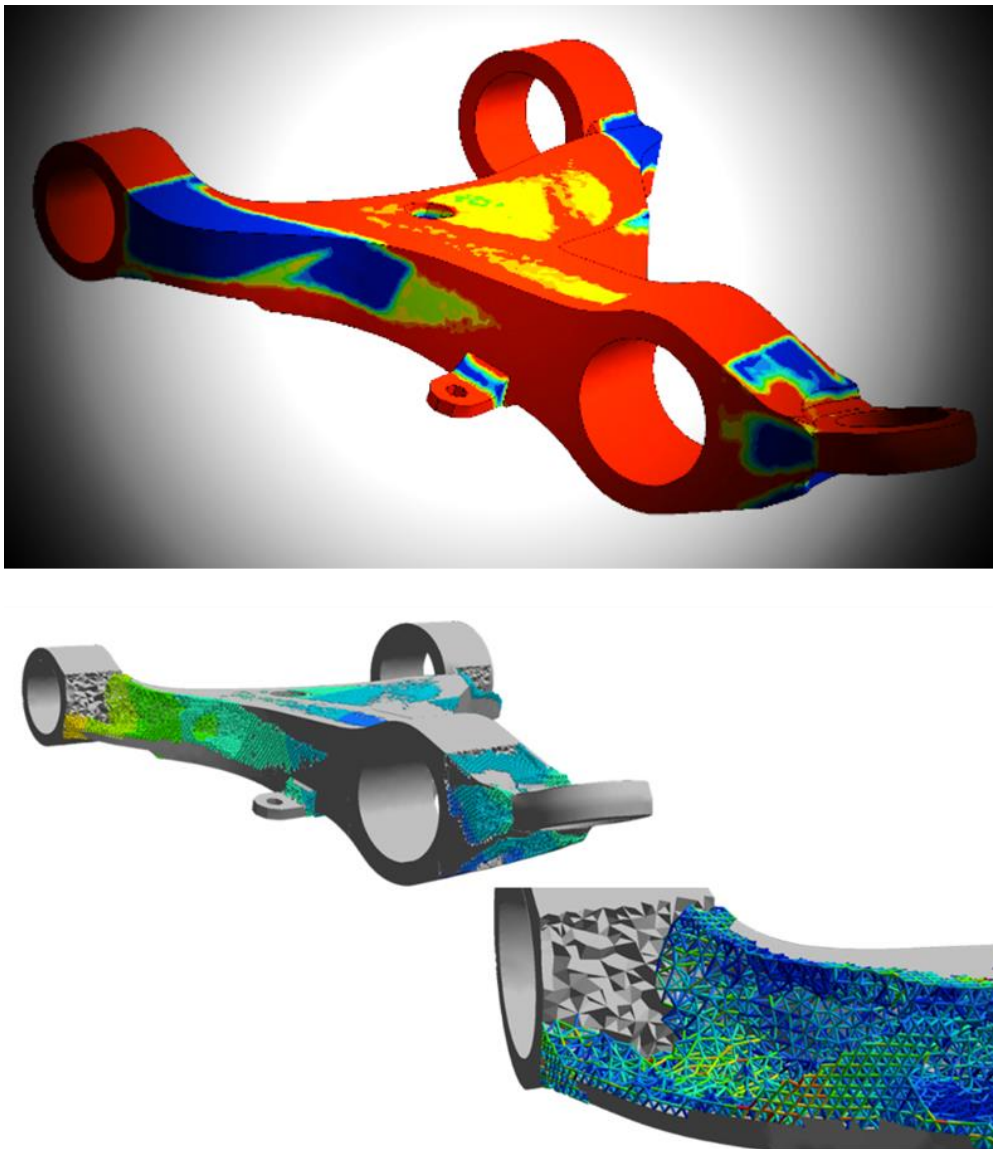


Figure 29. Bracket optimized through Altair Optistruct (Ref. [10]).

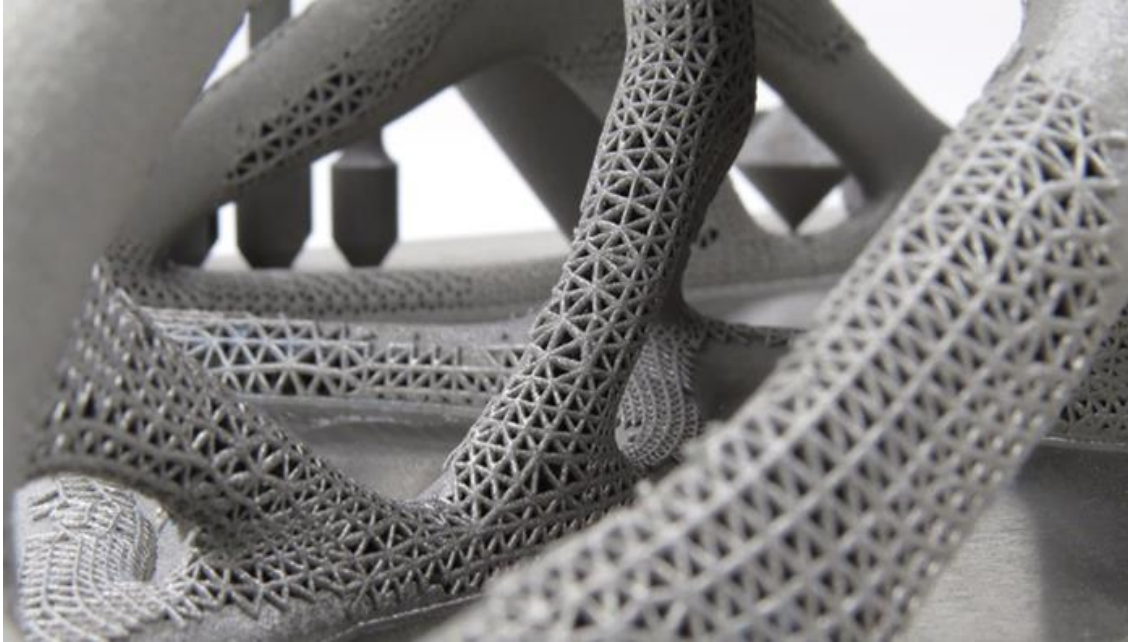


Figure 30. Titanium 3D printed structural object optimized with Optistruct.

First, some regions very less used (coloured blue in Fig. 29 are removed) are removed. The rest becomes the design domain. The section area of the infill is then optimized. This will have a hybrid aspect, being made of solid parts as well as tetrahedral structure with variable thicknesses.

The disadvantages of this approach are firstly that manufacturability constraints are not typically considered while generating finite element meshes, and secondly one cannot choose a lattice microstructure geometry that may be best suited to the application. Thus, this methodology is applicable to a problem just for some printing technologies, that do not need support structures (like SLS). Typically, these solutions are very expensive and not affordable by many.

### 3 Design Process

#### 3.1 Starting Point and Objective

In Chapter 1, an overview of Additive Manufacturing and its technologies have been presented. In Chapter 2, topology optimization theory has been introduced, and some examples of the application of it to Additive Manufacturing for both 2D and 3D have been shown.

Cause SLS and other powder bed technologies can use Altair Optistruct, or other similar software, to optimize lattice infill distribution, the purpose of this thesis is to introduce a new methodology to optimize the lattice infill inside real 3D parts dealing with the manufacturing constraints imposed by FDM manufacturing, or others which shares similar constraints.

Every part to be printed is different. Additive Manufacturing offer a wide range of technologies and materials. Choose the right one considering its shape, functions and requirements is the first step to efficiently design a part. The overall design is affected by the technology that is going to be used. In this case we just focus on the internal structure. The following flowchart resume the design process form the idea of the part to be produced to the actual print.

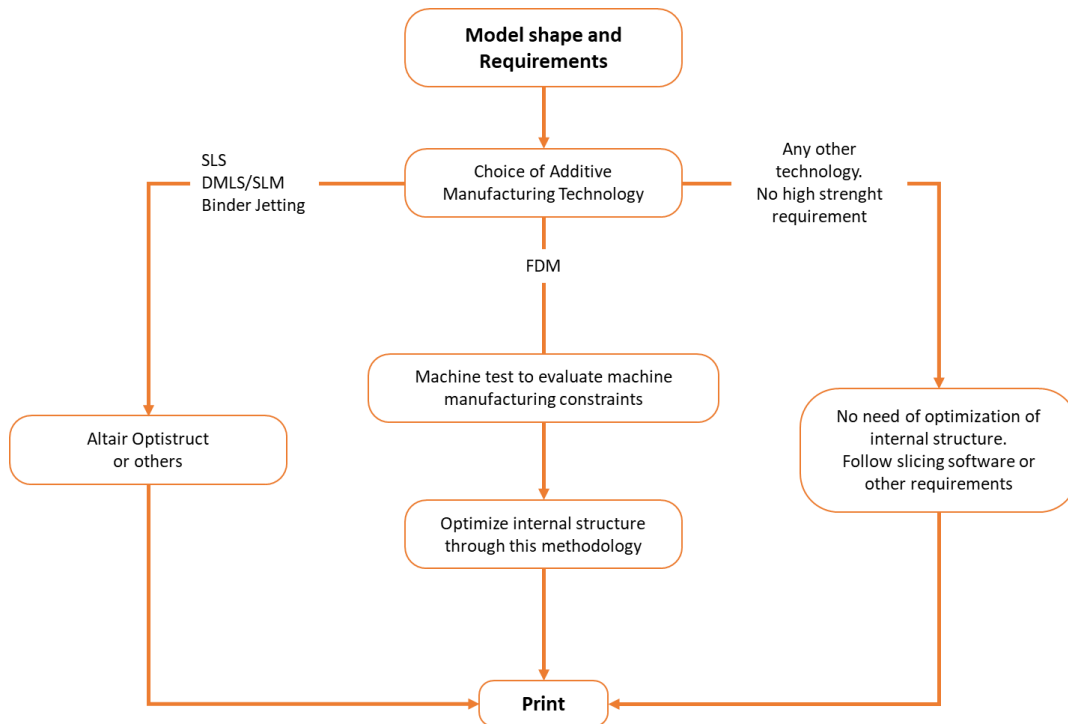


Figure 31. Design process for additively manufactured parts.

### 3.2 Choice of Additive Manufacturing Technology

In Section 1.1 most of the currently additive manufacturing technologies in the market have been presented. It is evident that the same part exhibits different characteristics if produced by such a variety of technologies and materials.

Moreover, if from one side 3D printing allows the production of parts impossible to produce any other way, on the other side each technology has its own manufacturing constraints that can differ radically one to another.

For this reason, before design the part, it is necessary to decide which AM technology will be used to produce it. In order to make the right choice factors to be considered are: function of the part, machines already available or the investment to buy new printers and materials. Figure 32 groups 3D printing technologies based on the function of the part being printed.

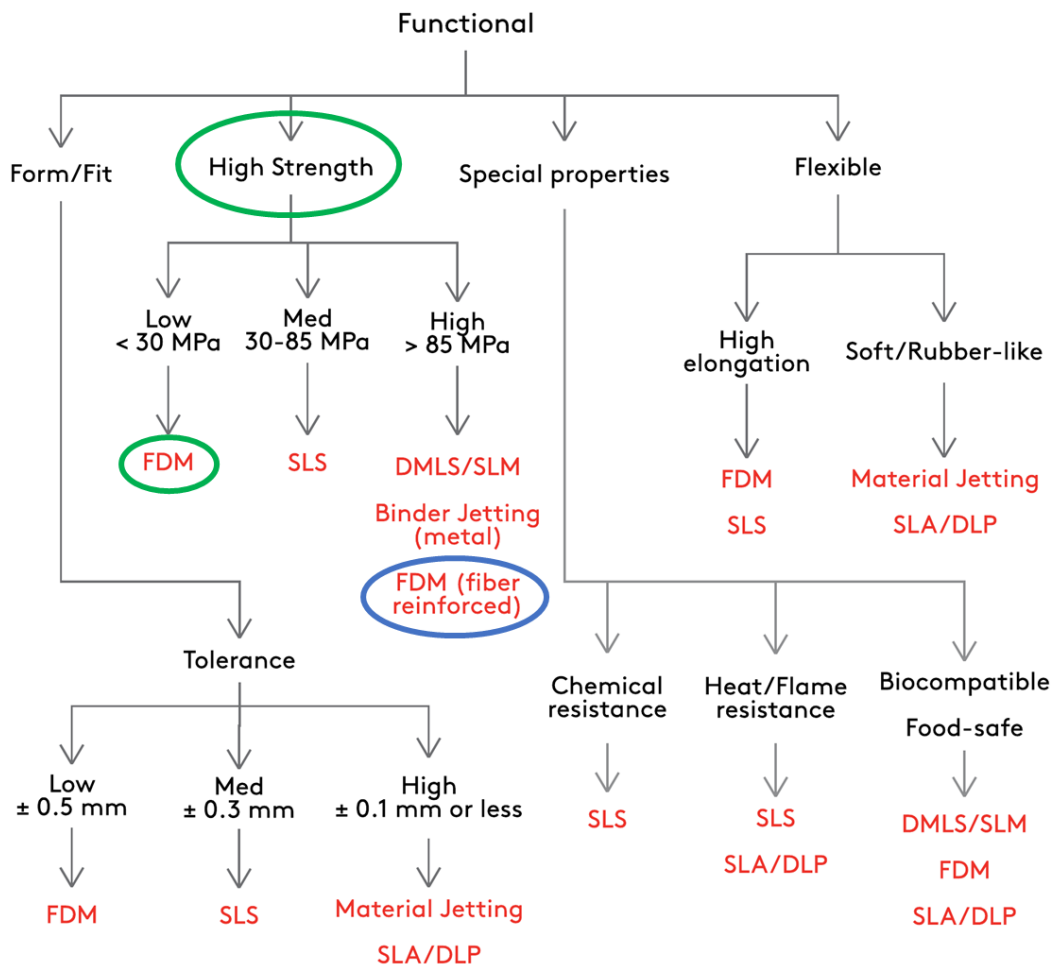


Figure 32. Resume of the additive manufacturing technologies grouped by the function of the printed part.

In the application of this thesis, we are looking for a maximization of the stiffness of the part. Thus, it is clear that the function of the part is high strength.

Considering high strength, the range of additive manufacturing technologies we can choose is limited to mainly three families: Extrusion (FDM), Powder Bed Fusion (SLS, DMLS, SLM) and Binder Jetting. Between them Table 1, in the next page, resume the main characteristics.

Note that Binder Jetting has been excluded from the table because, the mechanical characteristics are actually similar or worse than DMLS and SLM and the manufacturing constraints were very similar and also reliable data was not easily available and there were not such machines available in labs. Thus, the comparison regards just FDM and SLS and DMLS/SLM.

	FDM	SLS	DMLS/SLM
<b>Material</b>	ABS, PLA, Nylon	Nylon, Alumides, Carbon-fiber filled nylon, PEEK, TPU.	Aluminum, titanium, stainless steel, nickel alloys, cobalt-chrome, Maraging Steel.
<b>Achievable quality</b>	Low to Medium	High	High
<b>Layer thickness</b>	0.5 to 0.127 mm	0.05 to 0.01 mm	0.05 to 0.01 mm
<b>Minimum wall thickness</b>	1 mm	0.8 mm	0.4 mm
<b>Surface texture</b>	Rough (“staircase” effect) but can be polished	Slightly rough but can be polished	Slightly rough but can be polished
<b>Colors (without post-process)</b>	Opaque and translucent. All colors.	Opaque White, Gray and Black.	Depend on the material
<b>Support (complex designs)</b>	Required	Not required	Required
<b>Mechanically</b>	Variable (can be strong or flexible). Possibility of using reinforced fibers to make very stiff prints	Pretty strong and flexible	High Strength and flexible
<b>Mechanical failure</b>	Gradual deformation until fracture	Gradual deformation until fracture	Gradual deformation until fracture
<b>Abrasion resistance</b>	Variable	Superior	Superior
<b>Post-process</b>	Polishing, Painting, Sealing, Smoothing (with acetone vapor)	Polishing, Smoothing Nickel plating, Varnishing, Dyeing, Painting	Heat treatment, Machining, Support removal, Surface treatment
<b>Food compatibility</b>	Leakage due to micro-gaps	Yes	Yes
<b>Chemicals compatibility</b>	Leakage due to micro-gaps	Highly resistant (Nylon)	Highly resistant (Nylon)
<b>Cost</b>	Printers inexpensive. Material inexpensive (reinforced fiber more expensive)	Printers very expensive, Material inexpensive	Printers very expensive, Material very expensive

Table 1. Characteristic of additive manufacturing technologies for high strength prints.<sup>13</sup>

<sup>13</sup> Data from [www.sculpteo.com](http://www.sculpteo.com) and Ref. [12].

At this point the choice really depends on the goal and the requirements of the object to be printed. SLS has the useful feature of producing a very complex part without support material and without strict manufacturing constraints. The only constraints (that also apply to DMLS and SLM) is that closed shell bodies can be produced but the powder is trapped inside, unless one drill a hole big enough to allow the powder to escape. SLM and DMLS require support material even if it is based on a powder bed fusion technology because of the high temperature needed to melt metal powder. Anyway, support material is very easy to remove and small bars are possible to print easily.

FDM instead have the advantages of being easy accessible; machines and material are cheap (for an ideal investment is more affordable than SLS), but the design process has to deal with printability issues that means manufacturing constraints to take in consideration. For SLS, SLM and DMLS some lattice optimization methodology already exists, like Altair Optistruct (Ref. [10]) that allows for optimization without introducing printability as a requirement for the design.

Due to the accessibility of FDM machines, the lower cost the absence of an optimization criteria for this technology, and the acceptable strength (with the possibility of increasing it with the use of a reinforced filament), made us to choose FDM technology to develop this new methodology accepting the challenge of dealing with manufacturing constraints, and exploiting it to create closed solid bodies filled by infill (not easy to produce with SLS).

### 3.3 FDM Manufacturing constraints

In Section 1.1.3 the FDM technology has been presented. In section 2.2 it has been explained why it was chosen for this methodology. It is now necessary to show what are the manufacturing constraints, what are the general rules for the design, how to evaluate the actual constraints, and what make an object printable.

#### 3.3.1 Bridging

Bridging issue arise when the machine is required to print a flat, horizontal element between two anchor point without support. That means the printer will print mid-air to fill the gap left by two solid elements already printed (called *pillars*).

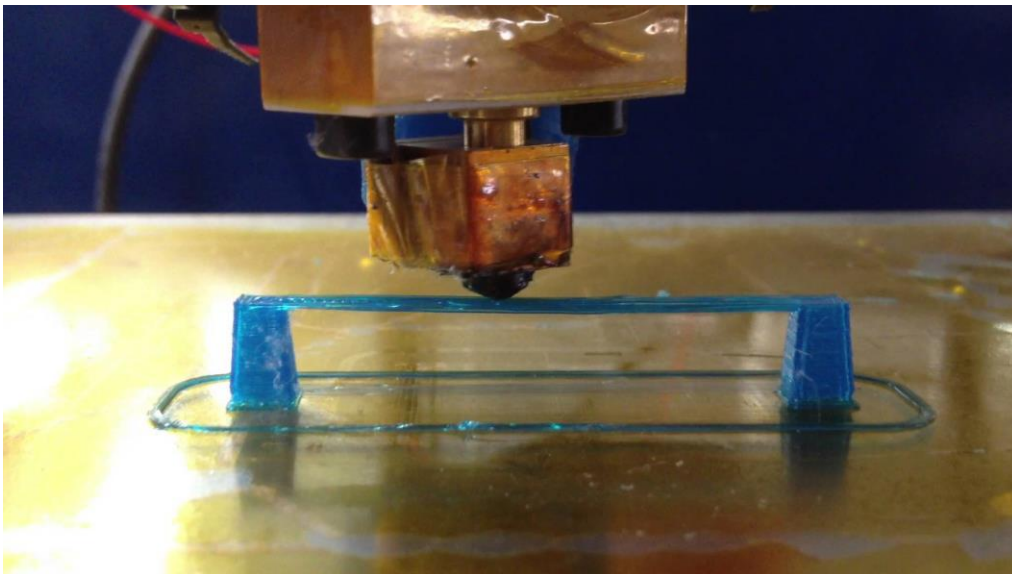


Figure 33. Attempt by the 3D printer to make a bridge.

Bridging depends a lot on a few factors. For example, the printing direction is the most influent: when designing a part, printing direction should be chosen in a way that it minimizes both support material and bridging length. Moreover, print speed should be chosen to let the filament stick on the pillars: if the plate moves too fast the nozzle could drag the filament all around without sticking it to the pillar and causing the failure of the printing. Temperature is another important factor: if too cold, the filament will not extrude easily; if too hot the material is more liquid and easier to string. Finally, it is important that the fans are at high speed. Cooling down the filament after being extruded guarantee better result in printing. Figure 34 in the next page, shows the difference between a good and bad bridging.



Figure 34. Effect of bridging handled in a bad way (top) and a good way (bottom).

### 3.3.2 Overhang Angle

Exceeding the maximum overhang angle, is one of the most common cause of bad printing quality.

We define the overhang angle as the angle between the printing direction and the face of the object, as shown in Fig. 35, where  $\alpha_1$ ,  $\alpha_2$ , and  $\alpha_3$  are two overhang angles. Typically, the maximum overhang angle is around  $45^\circ$ . Once this value is exceeded, if no support material is provided the print quality will decrease, or it might also fail for very high angles. It is obvious that angles  $>90^\circ$  are not printable at all without support material. So, in Fig. 35 the overhang in the right side will be printable without any problem, while the one on the left will present a bad surface quality, or in some cases also fail.

In order to improve the performance of overhang one could act on mainly two factors: increasing the cooling by increasing the speed of the fans, and decrease the nozzle temperature to make the filament less liquid (consider the same range for bridging).

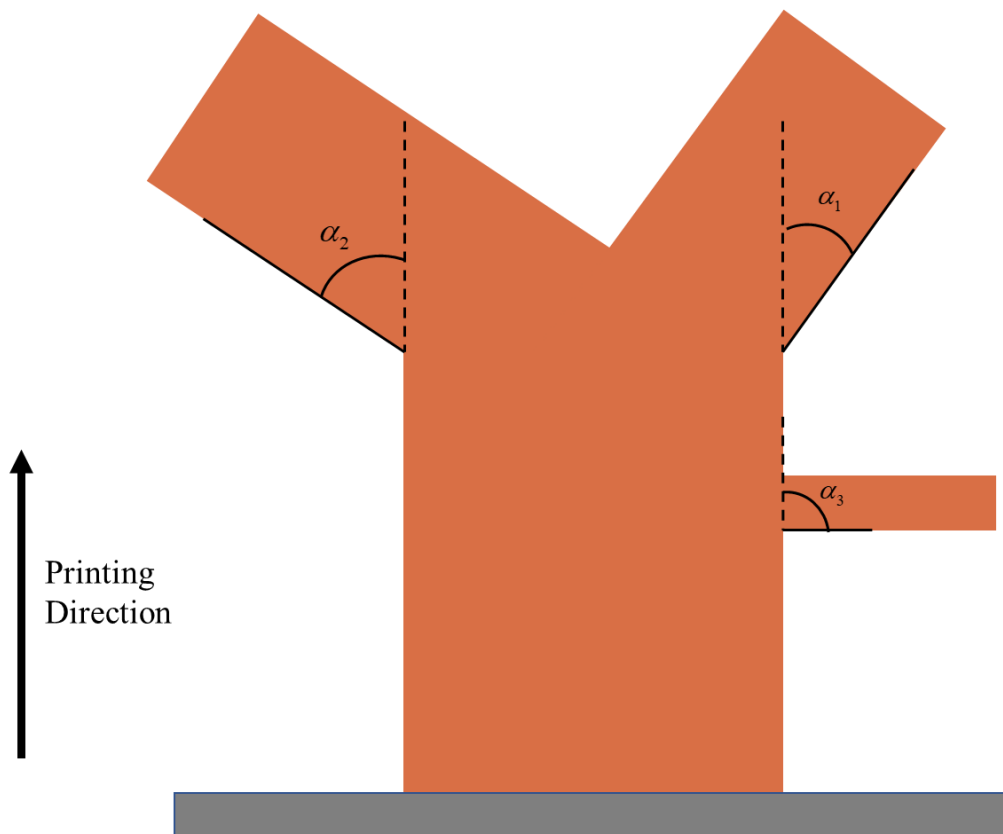


Figure 35. Definition of overhang angle.  $\alpha_1$  is printable.  $\alpha_2$  might be printable worse quality,  $\alpha_3$  is not printable.

### 3.3.3 Wall Thickness

Every printing technology has a minimum wall thickness depending on the way it works and the material used. In the case FDM, the minimum thickness is determined by the diameter of the nozzle. Generally, the diameter is 0.4mm wide but in other common cases the diameter can be 0.5mm for larger prints paying a bit of quality, and 0.2mm that requires more time to print a part but guarantee overall a better quality. It is worth noting that having a nozzle of 0.4mm does not mean that every shape 0.4mm thick is printable. In fact, for example, a shell sphere could collapse under its weight if the thickness is too small, as shown in Fig. 36. Same thing could happen if very thin walls are not connected to other walls. In that case the thickness should be increased to avoid a sawtooth shape.

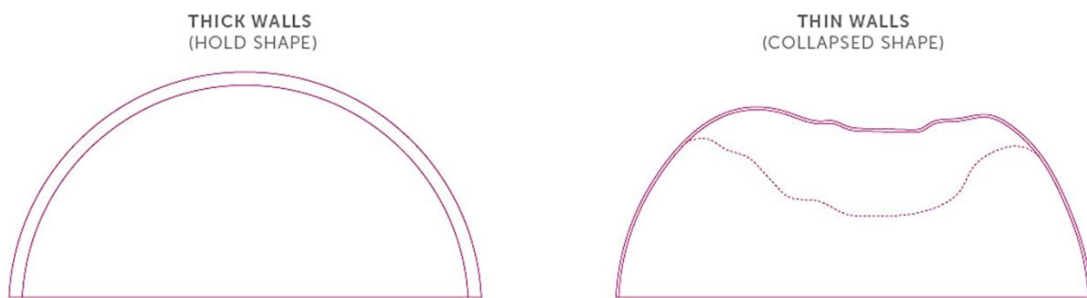


Figure 36. Sphere printed without support. A thin wall could cause the collapse of the shape caused by its own weight<sup>14</sup>

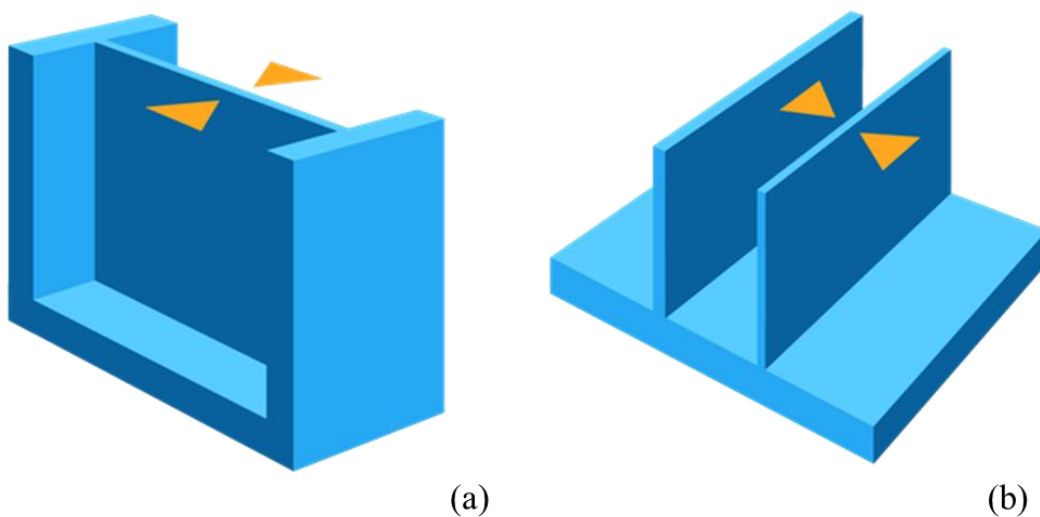


Figure 37. Wall attached to other two walls (a). Minimum wall thickness can be used (generally 0.4mm)  
Wall not attached to any other wall. Minimum thickness should be increased.<sup>15</sup>

<sup>14</sup> Image from [www.fictiv.com](http://www.fictiv.com)

<sup>15</sup> Image from [www.formlabs.com](http://www.formlabs.com)

### 3.3.4 Minimum Cylinder Diameter

Print a cylinder is not the same to print a wall. For instance, it is not possible to print a cylinder with a diameter equal to that of the nozzle. That would mean that the nozzle should print a point over a point, that it is not feasible practically for more than a few millimetres. To print a cylinder, the nozzle should draw a circle on its trajectory. Thus, in theory, any printer should be able to print a cylinder with the diameter of at least twice the diameter of the nozzle. In practical cases, usually printers are not so precise and the general rule say to not print cylinder with a diameter shorter than 4 times the diameter of the nozzle. This topic became even more complicated to deal with, if the cylinder axis is not parallel to the printing direction and if the cylinder is long. In these cases, there are no general rules, but its feasibility depends a lot on the printer and on the slicing software used.

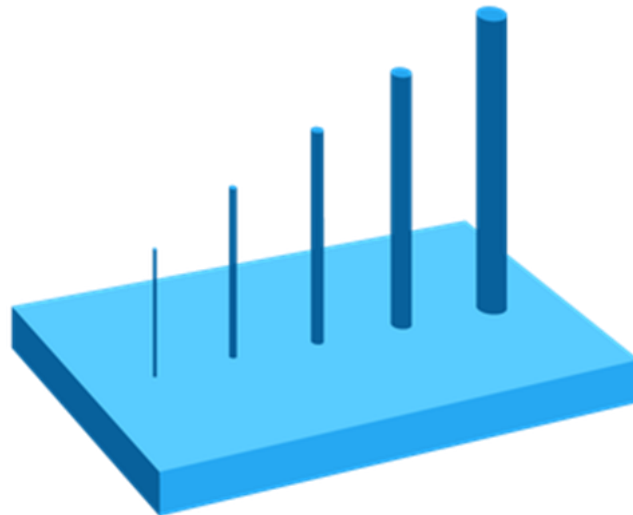


Figure 38. Cylinders of different diameters, without any support material.  
The thicker the longer can be printed.

### 3.3.5 Estimate of actual manufacturing constraints

General rules have been presented in the previous paragraph for every manufacturing constraints. Anyway, the great variety of machines available in the market corresponds to a wide variety of actual constraints. The evolution of this technology on the last decade has made possible that many of the more expensive and best performant machines would break the general rules limits and made printings, unfeasible before, feasible.

For this reason, before starting to design any part, it is important to test the machine available, in order to estimate the actual manufacturing constraints that will have an essential role in the procedure shown in this thesis. In our case the machine we are going to test is the MakerBot Replicator+ (5<sup>th</sup> generation).

The first test run is the bridging test in which the STL file of Fig. 34 is sent to the printer as it is. The printing temperature speed and resolution are left as the printer manufacturer suggests being the best setting (temperature 215 °C, resolution 0.2 mm, speed 30 mm/s). The result of this test is shown in the picture below. It shows that just the two longer elements show visible deflection. Thus, we can assume that:

$$L_{bridge}^{max} = 45mm \quad (2)$$



Figure 39. Result of the bridging test on the machine used in this thesis.

The next test to run is the overhang test. It is basically an element like that shown in Fig 35 with overhang elements of growing angle, from 5° to 90° with step of 5°. The result is shown in Figure 40.

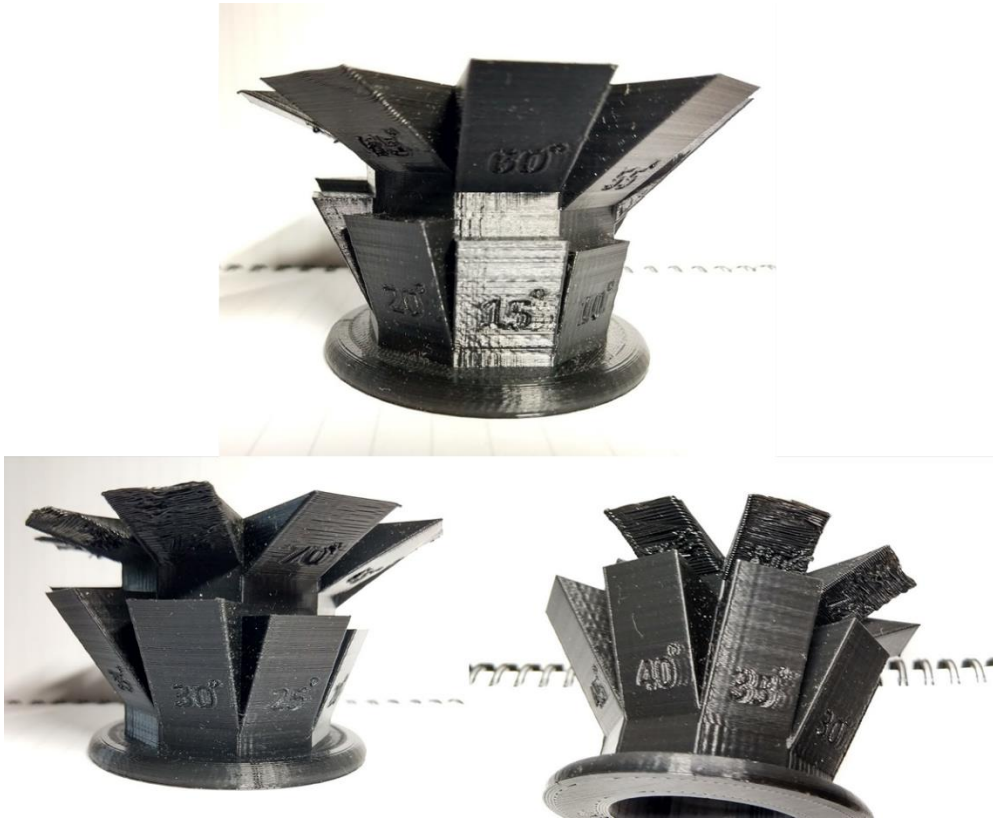


Figure 40. Result of the overhang angle test on the machine used in this thesis.

Here it is possible to analyse the results:

- Overhangs elements with angle till the general rule of 45° are printed perfectly and well defined.
- The aspect keeps being the same till 60° overhang angle
- At 65° first little deformation appears, but at 70° seems to disappear.
- From 75 to 90 the surface is badly deformed. It is interesting to see that even at 90 degree the printer can print something even if deformed.

From the consideration above and considering that other layout of the part, with less straight shapes could be more difficult to print, we decided to be more conservative and choose the maximum angle as the one before first deformations appear. Therefore:

$$\alpha_{overhang}^{max} = 60^{\circ} \quad (3)$$

Next test is the minimum wall thickness. Due to the type of parts we are going to print, the walls are always going to be connected to other walls, so the test that we are more interested regards walls connected to other walls. For this test the machine result to work very well for both vertical and inclined wall, so that reported here are just the latter one. The result is shown in Fig. 41 and shows that even the thinnest one (0.4 mm) is printable.

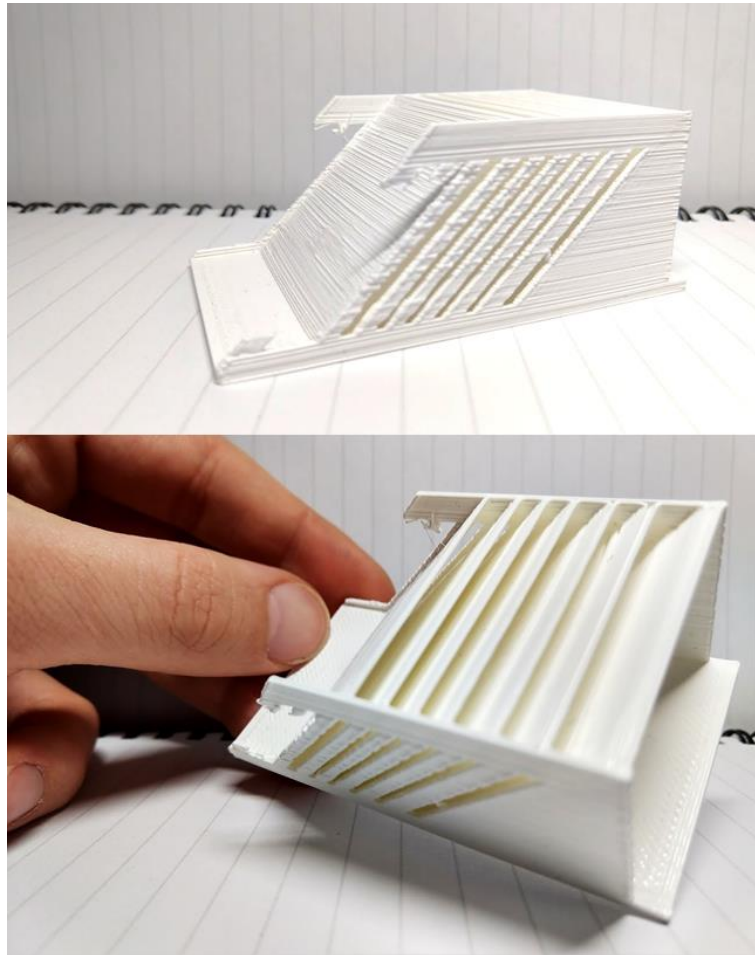


Figure 41. Result of the thin wall test on the machine used in this thesis.

The parts that seems to fail regard walls even thinner than 0.4mm that we wanted to try to see how the printer would handle them. The result is that the software gets rid of parts so thin and the printer does not even see those thin walls.

Therefore, the test demonstrates that for thin walls linked to other walls, the minimum thickness is:

$$w_{wall}^{\min} = 0.4mm \quad (4)$$

Last test to do allows to get the minimum diameter of printable cylinders. One way of doing it is shown by Ref. [13]. Here cylinders of increasing diameter are printed. For bigger diameter, the smaller hole in the middle is also measured. The scheme is the one shown below.

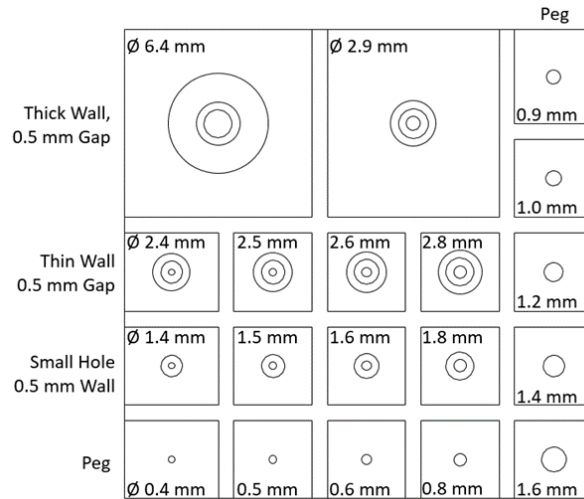


Figure 42. Scheme of the cylinder test in Ref. [13].

The result of this test shows that cylinders are printable starting from 1 mm diameter. Holes instead are visible from diameter greater than 2. Full table result and aspect of the print is shown below.

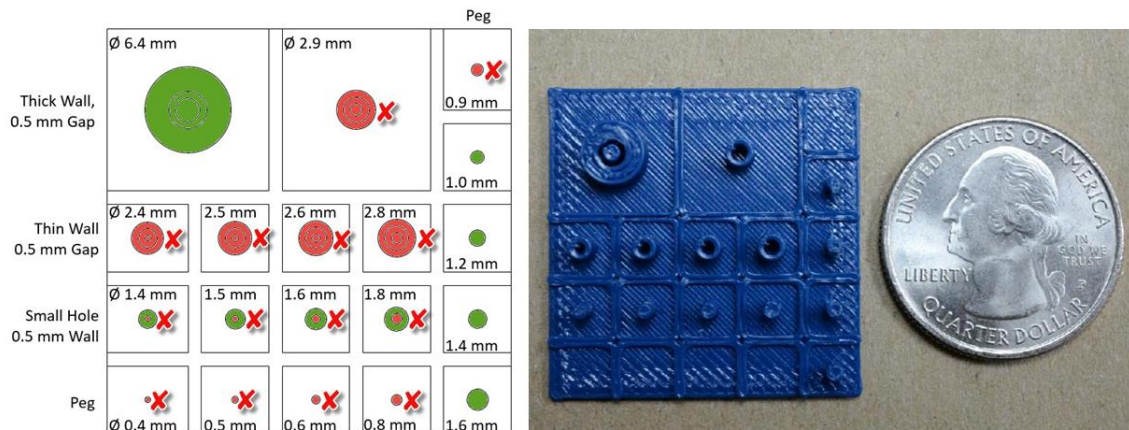


Figure 43. Result of cylinder test in Ref [13].

This result is valid just for cylinder with the axis on the printing direction. If instead the same test is repeated with inclined cylinder the result does not shows encouraging result. After several attempts we found out that the problems with such a test was probably related to the failure of the first cylinders because the nozzle was still extruding material

and carrying it all around. Once we find it out, we used another approach. Knowing already the geometry of the cell we wanted to use, we created a pattern of the cell keeping the thickness of the bar constant.

By creating pattern of different thicknesses, we find out which one was the thinnest bar printable without fail. In this way we also demonstrate that the cell used is always printable (for that machine) without support material.

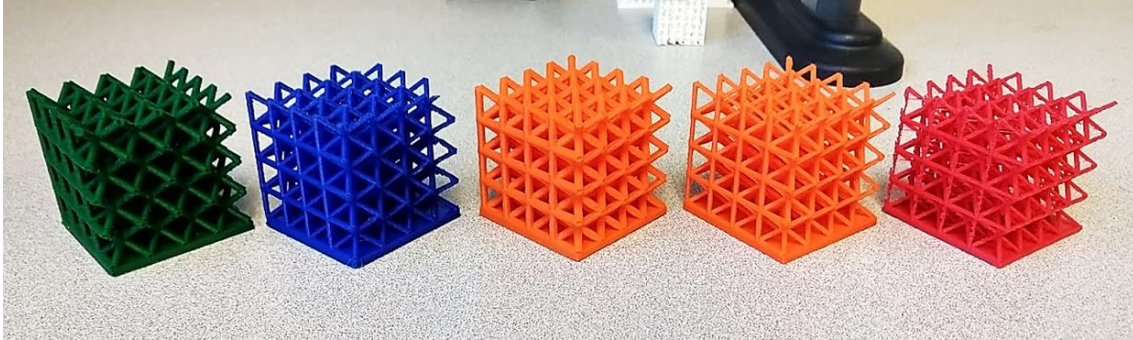


Figure 44. Five cell patterns of different thicknesses.

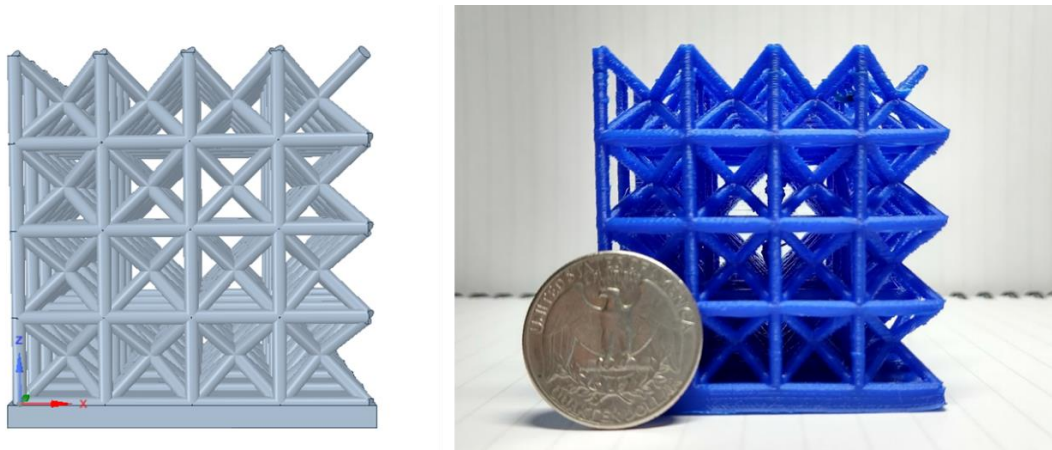


Figure 45. Zoom on one of the pattern (2 mm diameter bars) and comparison to the CAD model.

The red pattern has bar diameter equal to 1.7mm. Pattern with lower diameters have resulted unprintable, failing few layers after the cell pattern begun. For this reason, we deduce that the minimum diameter for the cylinders is:

$$t_{cyl}^{\min} = 1.5mm \quad (5)$$

### 3.4 Outline of the methodology proposed to enhance lattice infill distribution

After having introduced the state of art of Additive Manufacturing, explained the choice of FDM technology to develop this methodology, introduced the concept of *printability* and to assure it, calculated the manufacturing constraint for the machine used in the lab, it is now time to show the methodology conceived in this thesis.

The “dogbone” geometry shown in Fig. 46 is used to introduce notation and illustrate the procedure. In the figure,  $\Omega$  refers to the entire *dogbone* body. It is initially split into two non-overlapping regions,  $\Omega_B$  and  $\Omega_D$ .

The region  $\Omega_B$ , shown in light blue, is called “skin”. It is a region of prescribed shape and thickness

that bounds  $\Omega$ . By extension,  $\Omega_B$  includes any region whose shape is prescribed, e.g., as required to support loads or constraints, or prescribed internal boundaries.  $\Omega_B$  is not subject of optimization. Some portions of the skin may be assigned zero thickness, in order to identify a geometric boundary for the inner core without build an actual solid element.

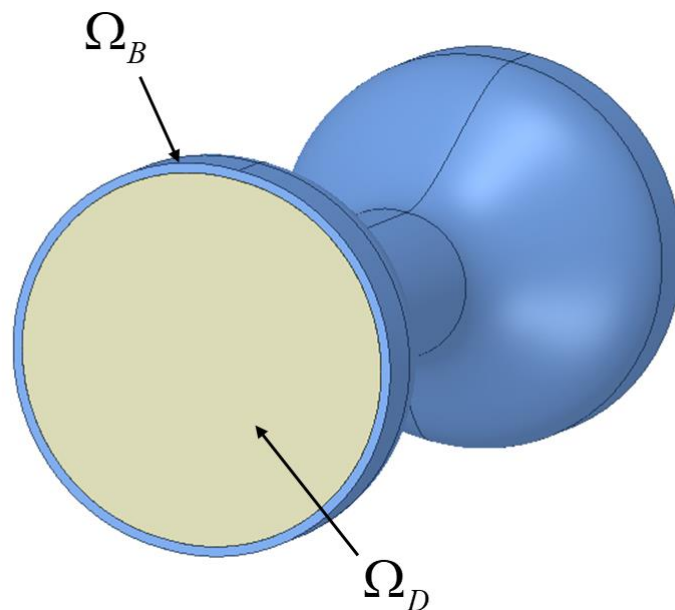


Figure 46. Component used for illustration.  $\Omega_B$  is the “skin”, of prescribed shape.  $\Omega_D$  is the design domain to be optimized.

The region  $\Omega_D$ , shown in yellow in Fig. 46, identifies the design domain, a region in the interior of  $\Omega$ . The goal of the procedure is to find the optimum way to distribute lattice material inside  $\Omega_D$ . The design domain is divided into subdomains by physical walls of prescribed thickness as shown in Fig. 47. We will refer to each subdomain as  $\Omega_i \in \Omega_D$  where  $i = 1, \dots, N_\Omega$  and  $N_\Omega$  is the number of subdomains.

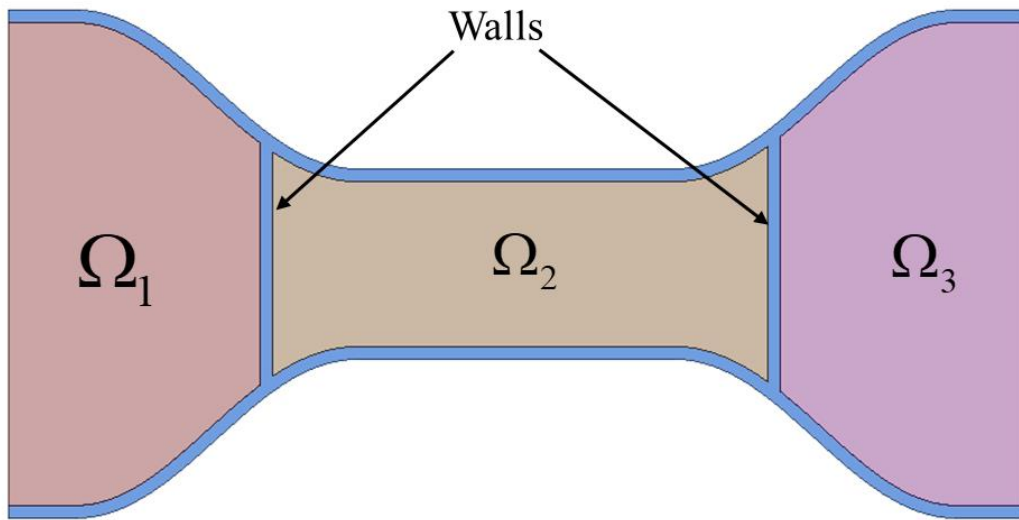


Figure 47. Possible division of the internal domain through two internal walls.  $\Omega_i \in \Omega_D$  are filled with lattice infill.

Thus, having introduced the notation used from now on, the design procedure discussed here can be outlined here. It consists of several steps. Each step is described in detail in the following chapters but they are introduced here as a guide to the organization of the rest of the thesis.

1. The body  $\Omega \in R^3$  being designed is first partitioned into separate subdomains  $\Omega_B$  and  $\Omega_D$ , already shown in Fig. 46. The thickness of the external wall, can be a requirement or can be chosen by the designer taking in consideration the minimum wall thickness printable.
2.  $\Omega_D$  identifies the design domain to be filled by lattice. The topology of the lattice is characterized by the spatial repetition of a characteristic cell. Only pure translations of this cell are allowed, i.e., a spatial variation of the orientation of the cell is, in principle, not allowed. This restriction is imposed to ensure that the lattice is printable from a single print direction. The use of different cell topologies in separated subdomains is in theory allowed, but this potential feature is not exploited in this thesis. The choice of the cell should guarantee first-hand the printability of the cell all over the domain, and second-hand the best stiffness and wider range possible. Analysing many researches treating period cell structure and its mechanical characteristic we decided to use the Body Centred Cell shown in Fig. 48 which shows isotropic behaviour and have a small mass/volume ratio which guarantee a wide density range. All this will be explained in detail in the next chapter.

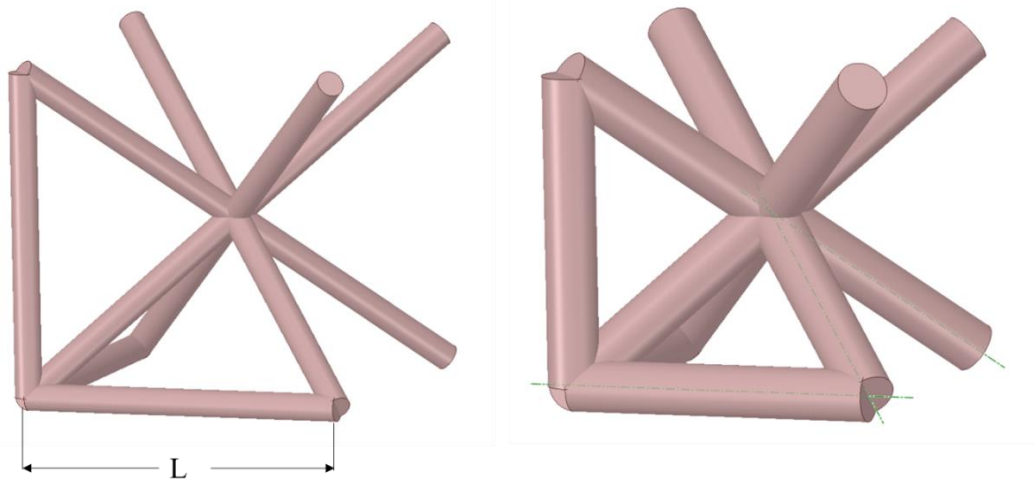


Figure 48. Body Centred Cell (BCC) used as infill.  
Two setups with same cell size but different bar thickness

3. The design domain is itself partitioned into subdomains  $\Omega_1, \dots, \Omega_{N_\Omega}$ , separated by solid walls (as shown in Fig. 47), initially chosen considering the dimensions of the design domain and refined (if necessary) after the step 4a below. Within each subdomain  $\Omega_i$  the topology and lattice cell size are constant. This is a fundamental constraint in our formulation.

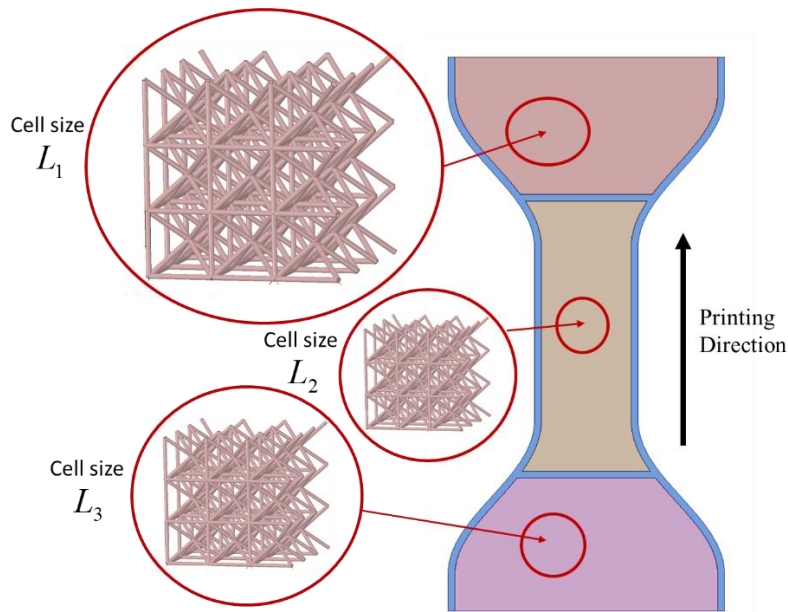


Figure 49. Each subdomain contains cells of same topology and size. Thicknesses of the bars may change.

4. The effective material density can vary within each subdomain to accommodate a more efficient utilization of material. This is accomplished by allowing a spatial variation of lattice section properties (e.g., thickness), leading to two optimization problems, performed in sequence:
  - a) *Optimization Problem 1.* Design variables control the spatial variation of lattice effective densities within each subdomain. This means that the behaviour of the cells is approximated by a function which relates the microstructure of the cell to the effective mechanical properties of a fictitious material. The body is so meshed with tetrahedral elements which effective properties are corresponding to some average values of the dimensions of the cell inside each tetrahedra. Tetrahedral masses (or relative densities) become

the design variables of the optimization problem. These hypotheses considerably simplify the problem, from a computational point of view.

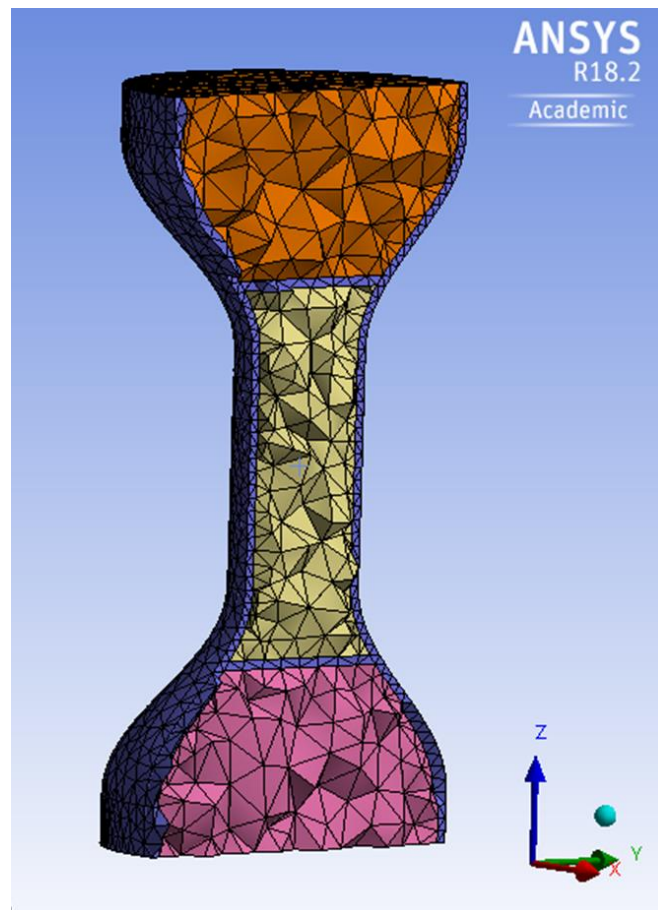


Figure 50. Dogbone mesh for Optimization Problem 1. Each tetrahedra is an element of the optimization. Mechanical properties are given to each element by averaging the microscopic dimensions of the cell.

Optimization Problem 1 results in an amount of material assignment throughout the domain which provides a rapid assessment of the expected optimal lattice distribution to be used inside each subdomain. This information can be used as a feedback to define new subdomains boundaries to leave (if possible) regions completely void.

- b) *Optimization Problem 2.* Design variables control the spatial distribution of section properties of the lattice within each subdomain. In other word, the body is now meshed with both tetrahedral (for skin and internal walls) and beam elements for the cell bars. Each beam section area is now a design variable. The result will be such that the material distribution in each subdomain is no more constant but variable as the section area of the bars.

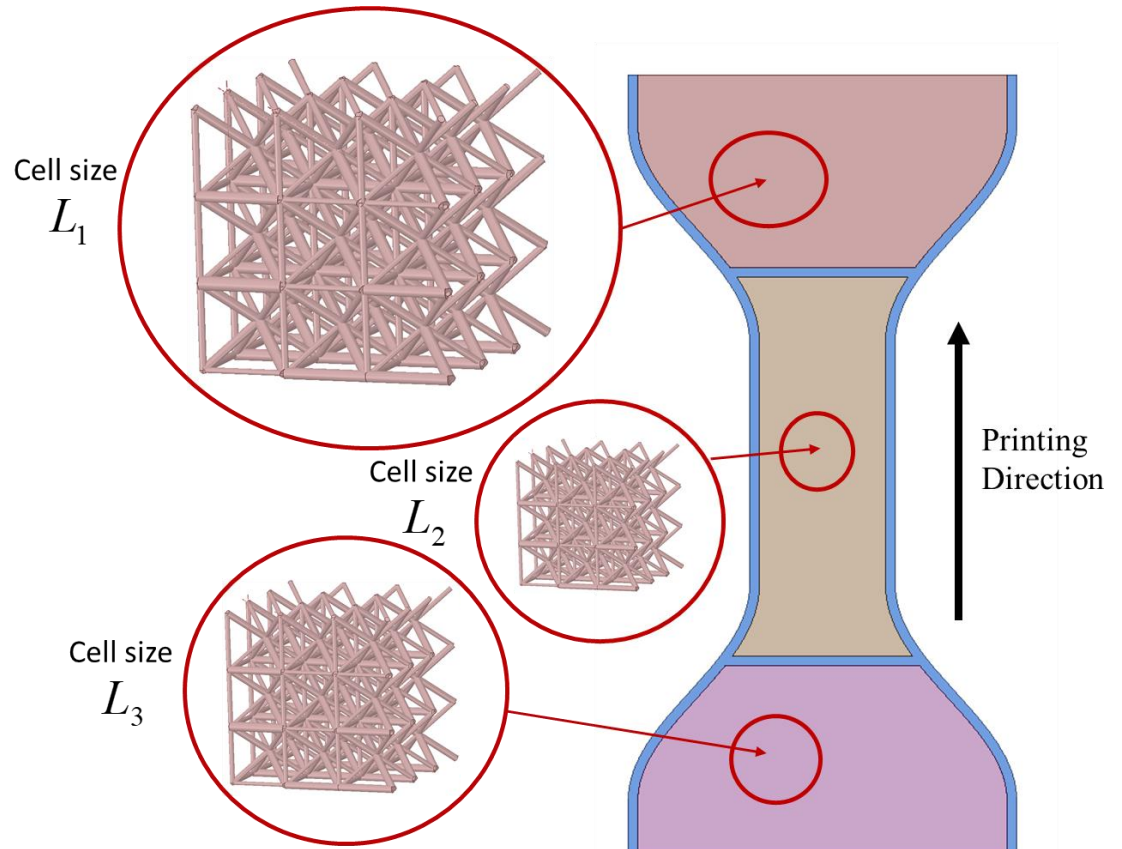


Figure 51. Body after Optimization Problem 2. Each subdomain  $\Omega_i$  is assigned to a lattice pattern of length  $L_i$ . Note that this time the cells have independent diameter.

5. Export of the STL file of the geometry and print with the machine tested like in the previous chapter.

The rest of the thesis discusses the infill optimization problem explaining in detail each step. The methodology is then illustrated through a couple of examples. Before getting in the details, a block scheme diagram of the methodology is shown to resume the steps explained before.

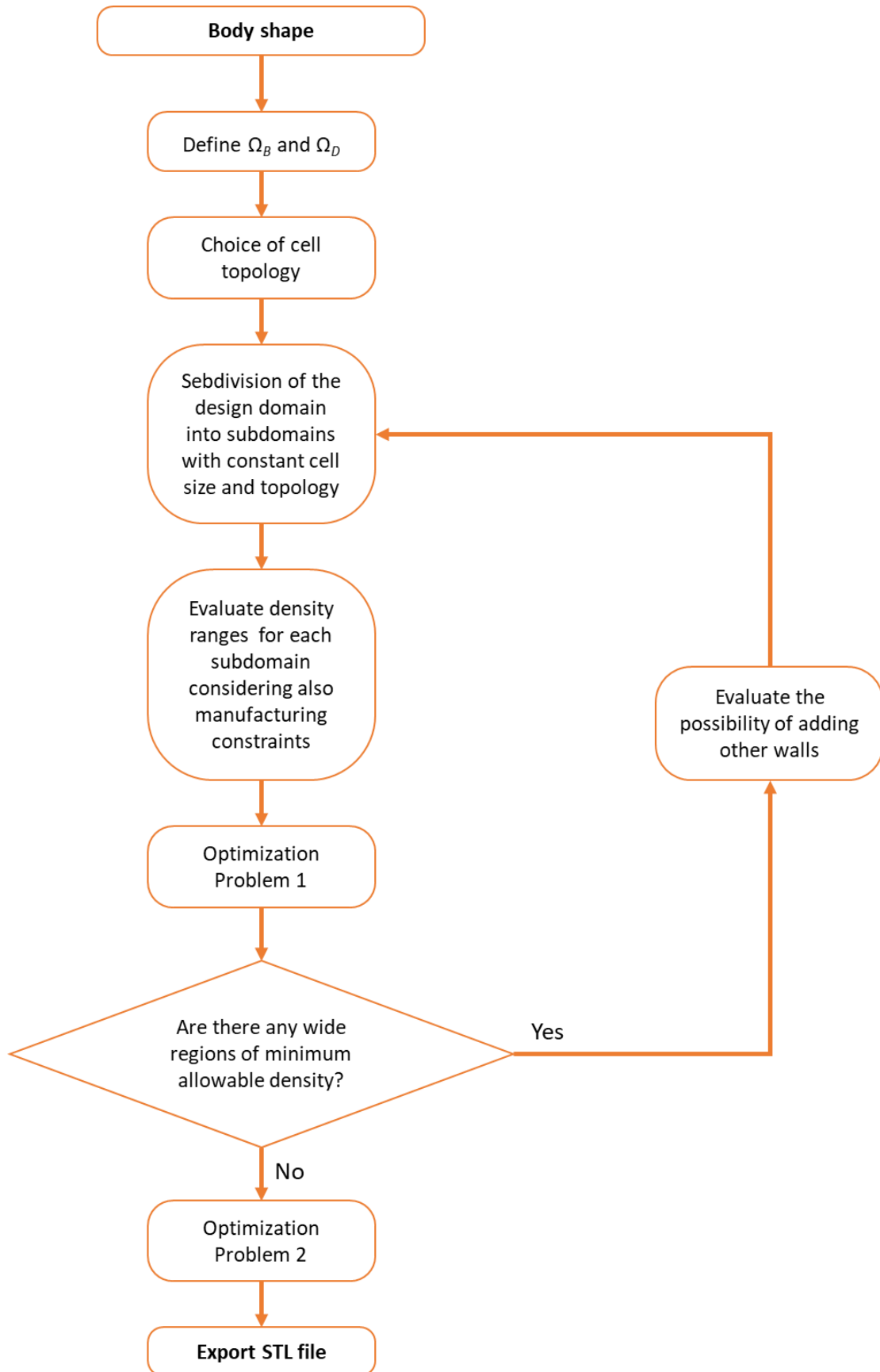


Figure 52. Flowchart of the methodology proposed.

## 4 Lattice Effective Properties

Optimization Problem 1, introduced in the previous chapter, use relative density of the elements mesh of the design domain as design variable. In order to solve the FEM problem, it is necessary to relate the relative density of the element to the correspondent mechanical properties. Relative density is a parameter just dependent on the geometry of the cell inside the element (topology, length size and section area of the bars). Therefore, have a relation between mechanical properties and relative density means also to relate microstructure characteristic of the cell to mesostructure characteristic of a group of cells by averaging. The mechanical properties so obtained are called *lattice effective properties*.

When the size of the object being designed is much larger than the size of the lattice cell, modelling every cell in detail is often computationally impractical or infeasible. Instead, a typical approach is to use these effective properties to “homogenize” the microscale behaviour of the structure and simplify considerably the complexity of the problem to obtain a fast but approximate result. Effective properties of typical 2D and 3D cells have been studied and tested in many researches like in Ref [2,4,5,6].

### 4.1 Effective properties from literature

Most results discussed in the literature estimate the effective elastic tensor  $\mathbf{D}$  associated with a lattice microstructure by an expression of the form

$$\mathbf{D}(d) = f(d) \mathbf{D}^0 \quad (6)$$

where  $d$  is the effective density of the lattice defined as  $d = \rho_c / \rho_0$  with  $\rho_0$  the density of the solid material, and  $\rho_c$  the density of the cell (i.e. the mass of a cell divided by its volume), and  $\mathbf{D}^0$  is the elastic tensor of a reference material. Typically, this approximation is more accurate for low effective densities and for aggregates of many cells.

Particularly interesting is the research done by Thomas Tancogne-Dejean and Dirk Mohr in Ref. [2] where they studied effective properties and isotropy of many cells. In particular they focused on cubic symmetric cells like those in the following picture.

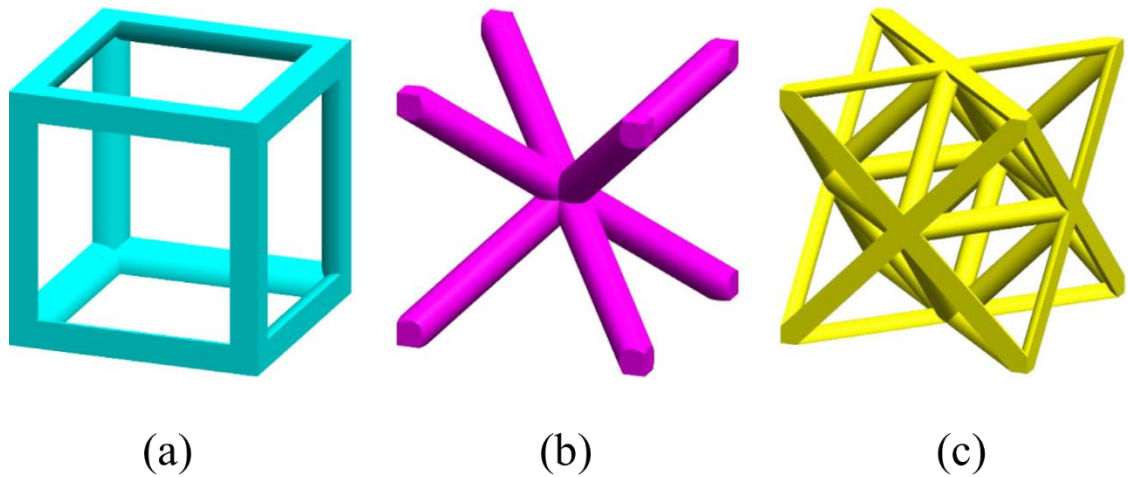


Figure 53. Elementary lattices with cubic symmetry. Simple Cubic (SC) (a); Body-Centred Cubic (BCC) (b); and Face-Centred Cubic (FCC) or Octet truss (c).

Cells shown in Fig. 53 are elementary cubic symmetric cells, in general anisotropic. In first-hand, in Ref 2, they have demonstrated that combination of this basic cells results in other cubic symmetry cell, isotropic. These cells are shown in Fig. 54.

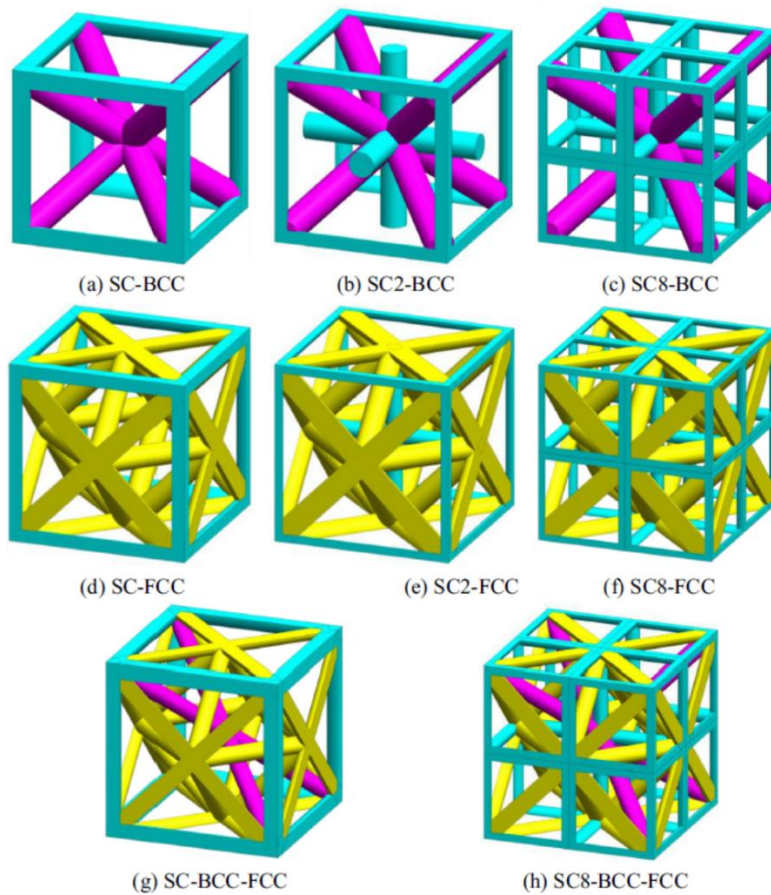


Figure 54. Isotropic cubic cells resulting from the combination of elementary cells in Fig. 53.

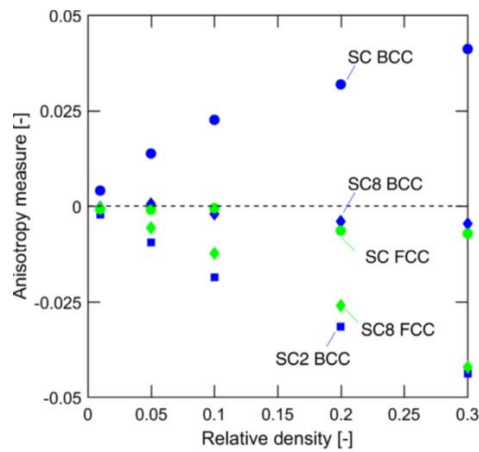
Moreover, the most interesting observation, is that for small values of relative densities, they all behave mechanically the same, so they all have the same effective properties.

This means that if the scaling factor  $f(d)$  relates the relative density  $d$  of the cell, and the elastic matrix of the whole cell,  $f(d)$  is the same for all the cells in Fig. 54. What change is the relation between the geometry of the cell (the topology in this case) and the relative density  $d$ .

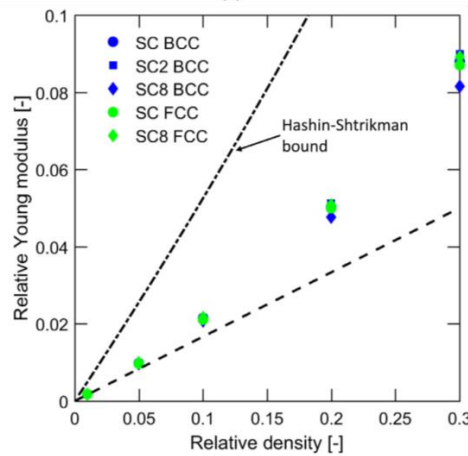
Thus, for the cells shown above:

$$f(d) = \frac{d}{6} \quad (7)$$

This result was obtained through theoretical formulation and verified with FEM simulation. Isotropy is shown to be good for a wide range of density, while the equation (7) seems to be valid for just a narrow range of relative density (<10%).



(a)



(b)

Figure 55. Numerical results of the simulation of cells in Fig. 54. Anisotropy analysis (a),  $f(d)$  that being isotropic cell is just the relative Young's Modulus (b)

Isotropic cells are not the only possibility to use periodic cells as infill. Anisotropic cells like Octet-truss cells have been object of many researches in the last years. This cell is shown in the following figure alone and in a pattern.

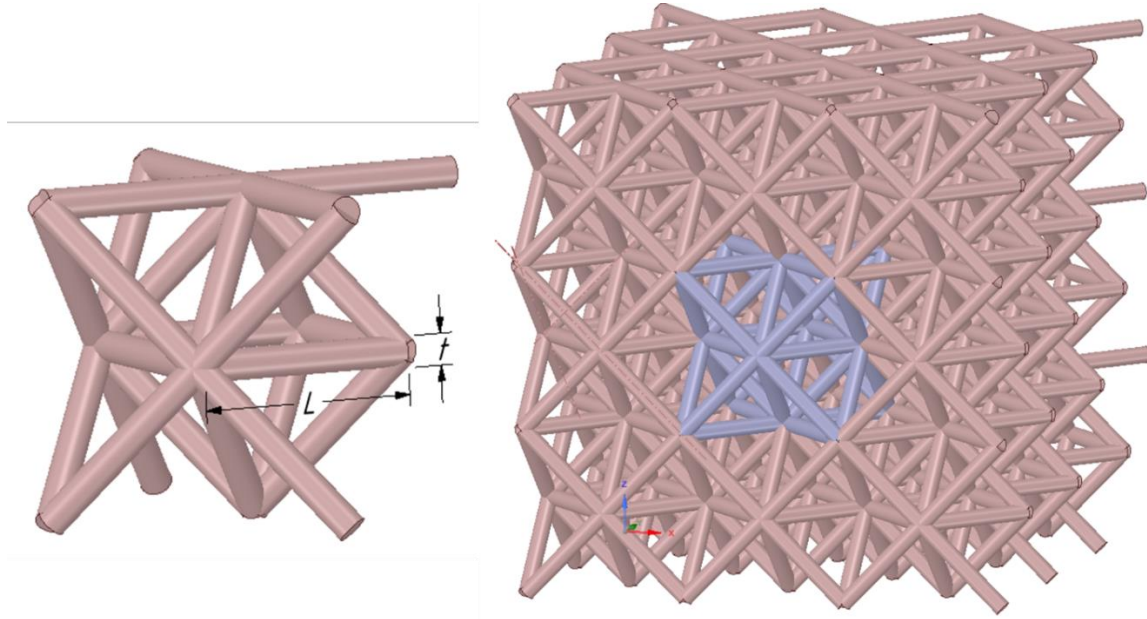


Figure 56. Octet truss cell, 3x3x3 Octet cell pattern

This cell is deeply studied by Vigliotti Andrea and Pasini Damiano in Ref. [6]. Here, through theory and FEM simulation they found a formulation of the stiffness matrix describing the octet truss in Fig. 56.

Thus, D become:

$$D_0 = \begin{bmatrix} \alpha & \beta & \beta & 0 & 0 & 0 \\ \beta & \alpha & \beta & 0 & 0 & 0 \\ \beta & \beta & \alpha & 0 & 0 & 0 \\ 0 & 0 & 0 & \gamma & 0 & 0 \\ 0 & 0 & 0 & 0 & \gamma & 0 \\ 0 & 0 & 0 & 0 & 0 & \gamma \end{bmatrix} \quad (8)$$

With  $\alpha, \beta, \gamma$  dependent on cell size and bar section area. It is interesting to note that, being no more isotropic,  $f(d)$  cannot be just a number, but it must be a matrix that modifies each entry of the matrix. In this case it will have three different values each  $\alpha, \beta, \gamma$ .

The last type of cell interesting to mention represent a different family of lattice infill: foam cells. These cells are made of plates instead of bars and shows in general higher stiffness performance. This type of cell is studied by Berger, JB; Wadley, HNG and McMeeking, RM in Ref. [5]. Many of this cell are anisotropic, but a combination of them make a very interesting isotropic cell, called Cubic-Octet Foam. The aspect of the cell is shown in the following picture and it can be noted that the geometry parameters are now three, instead of two for every truss cell.

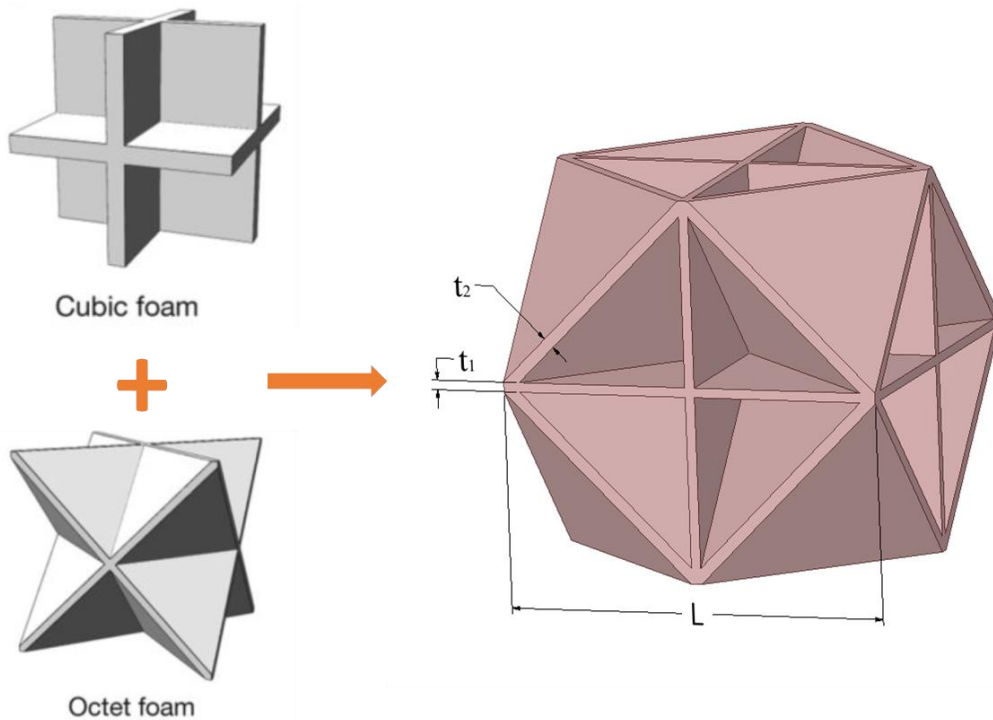


Figure 57. Cubic-Octet Foam cell

The reason why there is a new parameter is that the thicknesses of the plate that make the cell can be different for the cubic part and for the octet part. The ratio between them govern the anisotropy behaviour of the cell.

In particular, in [5] they demonstrate that the cell behaves as an isotropic material if:

$$\frac{t_{cubic}}{t_{octet}} = \frac{8\sqrt{3}}{9} = 1.54 \quad (9)$$

In this case  $f(d)$  is still a number, and become:

$$f(d) = \frac{d}{2} \quad (10)$$

Table 2 summarize the properties of the cells shown in the literature presented before. In the next chapter it will be clear why we chose BCC cell.

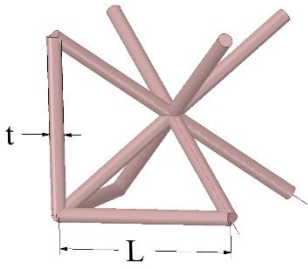
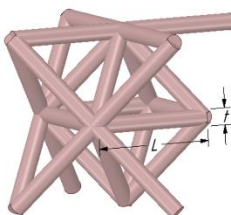
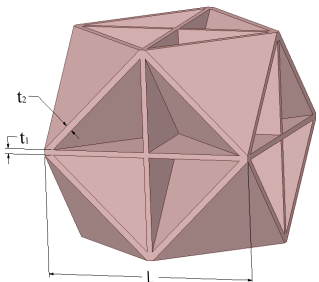
Cell topology	$d(t,L)$	$f(d)$	$\nu$
 <p>BCC cell</p>	$(3+4\sqrt{3})\frac{A}{L^2}$	$\frac{d}{6}$	constant
 <p>Octet truss cell</p>	$(6\sqrt{2})\frac{A}{L^2}$	Ref. [6]	constant
 <p>Octet-cubic foam</p>	$3\frac{t_1}{L} + 4\sqrt{3}\frac{t_2}{L}$	$\frac{d}{2}$	constant

Table 2. Resume of the geometrical characteristics and effective properties of the three cells of the literature.

#### 4.1.1 Choice of BCC cell for the methodology

In the previous sections a few members of the families of periodic cells have been presented. Now, it is worthy to explain the reason why we chose BCC isotropic cell as the cell to use for this methodology.

The Octet-truss, being anisotropic, shows the highest performance just in some orientations. This means that to optimize a structure made of this cell, one should reorient every cell in the main direction of the stress point by point. This issue brings two main problems on the feasibility of that structure.

- First, it is impossible to rapidly change the orientation of adjacent cells without the use of a wall so that some control over the maximum rotation should be added on the optimization problem, making it way more complex.
- Second, the cell is not printable in every direction, but just for a few orientations and for some ranges depending on the additive manufacturing technology.

Therefore, for these reasons we decided to exclude this and in general anisotropy cells from the methodology. This does not mean that it is impossible to use anisotropic cell. One could consider using it anyway without reorienting it, ore find a way adding the orientation of the cell as a design variable and find a way for the printer to print it.

Foam cells show better effective properties than cell trusses, but considering that the minimum thickness of the walls, and the minimum aspect ratio, foam need way bigger cell size than truss cells for the same relative density  $d$ . For the dimension of the design domain in general printed with FDM and the need of having a minimum number of cell in each subdomain, the use of this type of cell is unfeasible.

By exclusion, use cells with cubic symmetry and isotropic seems to be the most reasonable choice. Between all cubic cells shown in Ref. [2], and considering that at same relative density  $d$ , they all behave the same, the choice fell on the cell which for the same bar section area, was showing the smallest relative density. In other word, the cell that contains the less possible number of bars. In this way we guarantee to have the wider possible relative density range. Among all cells in Ref. [2] the “lightest” one isotropic is the BCC cell shown in Fig.48

## 4.2 Effective properties of BCC cells through homogenization

In this section the homogenization process for the BCC cell in Fig. 58 is presented and it is then compared to the result from the literature. The intent is to find a relation of the BCC cell valid for a broader range of densities and to make sure that the number of cell in the coupon  $n \times n \times n$  does not influence the effective properties.

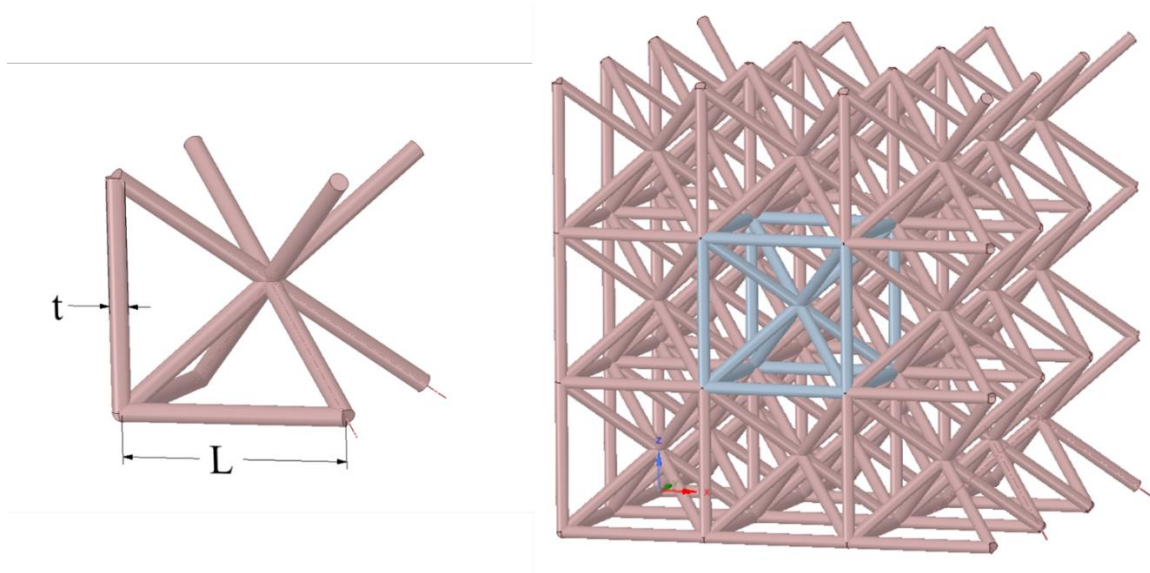


Figure 58. The BCC lattice cell topology with its parameters and a  $3 \times 3 \times 3$  coupon of the same cell.

Relevant geometric parameters are  $t$  (diameter of the bars) and  $L$  (length of the cell). The relative density of the cell is  $d = \rho_c / \rho_0$  where  $\rho_0$  is the density of the solid material, while  $\rho_c$  is the density of the cell (i.e. the mass of a cell divided by its volume). For each cell topology we will have a relation between  $d$ ,  $A$  and,  $L$  such as:

$$d = C_1 \left( \frac{A}{L^2} \right) \quad (11)$$

where  $A$  is the bar section area, and  $C_1$  is a value which depends only on the topology of the cell. Equation (11) does not take in consideration that the volume in the joints, where two bars are connected, is counted twice. This approximation holds for small values of  $d$ , for which these volumes are much smaller than the volume of the bars. Typically, a maximum recommended value  $d_{max}$  is chosen around 0.3. For the BCC cell in Fig. 58,

$$d = (3 + 4\sqrt{3}) \frac{A}{L^2} \quad (12)$$

According to [2, 5], the effective elastic tensor corresponding to this cell is essentially isotropic and

$$\mathbf{D}(d) = \left(\frac{d}{6}\right) \mathbf{D}^0 \quad (13)$$

where  $\mathbf{D}^0$  is the elastic tensor of the underling (isotropic) material. Poisson's ratio can be considered constant over the range of densities  $d$ .

The effective tensor  $\mathbf{D}$  in (6) can also be estimated using numerical homogenization. This can be useful for cells where an explicit result such as (13) is not available or, like in this case to estimate the effect of the number of cells in a coupon and the errors in the approximation.

Once defined  $d$ , the result of the homogenization will be a factor  $f(d)$  that determines the relation between elastic properties of the lattice and relative density of the cell, in the form (6):

$$\mathbf{D}(d) = f(d) \mathbf{D}^0$$

The method of Homogenization used is explained in detail in Ref. [7]. Consider a coupon of  $n \times n \times n$  cells of the topology chosen. We supposed this coupon to the perturbation procedure (activation of small displacements). Several small strains are applied one at a time in the boundaries of the coupon in the main directions of the cells. From FEM simulation, given the strain perturbation, we get the resultant stresses. From the obtained stresses, the perturbation strains and the relation,

$$\mathbf{D} = \boldsymbol{\sigma} \boldsymbol{\varepsilon}^{-1} \quad (14)$$

it is possible to obtain each component of  $\mathbf{D}$  and so, build up the matrix. Depending on the topology of the cell, the aspect of this tensor change. In the most general case of an anisotropy material, the elastic tensor is characterized by 21 parameters. By the way the cubic geometry, symmetry and periodicity allows to many simplifications. In particular, [2] and [5] agree to assert that the BCC cell in Fig.2, behave as an isotropic material with constant Poisson's ratio. Under this assumption the elasticity tensor  $\mathbf{D}_0$  and consequently  $\mathbf{D}$  become of the form:

$$D = \begin{bmatrix} D_{1111} & D_{1122} & D_{1122} & 0 & 0 & 0 \\ D_{1122} & D_{1111} & D_{1122} & 0 & 0 & 0 \\ D_{1122} & D_{1122} & D_{1111} & 0 & 0 & 0 \\ 0 & 0 & 0 & D_{1111} - D_{1122} & 0 & 0 \\ 0 & 0 & 0 & 0 & D_{1111} - D_{1122} & 0 \\ 0 & 0 & 0 & 0 & 0 & D_{1111} - D_{1122} \end{bmatrix} \quad (15)$$

Where the elements in the tensor are dependent on just two variables. According to [2] and [5], Poisson's ratio can be considered constant, so actually the tensor is dependent on just one variable: Young's Modulus  $E$ .

The results of applying numerical homogenization to an  $n \times n \times n$  coupon of BCC cells is summarized in Fig. 59. Numerical homogenization is applied to compute  $D_{1111}$  as a function of effective density  $d$  for patches of cells of different lengths  $L$ , thickness  $t$ , and coupon size  $n$ . The red dashed line corresponds to the nominal value  $f(d) = d/6$  from (13), while the deviations from this value are shown by the blue dots. Coupons of different size  $n$  are used.

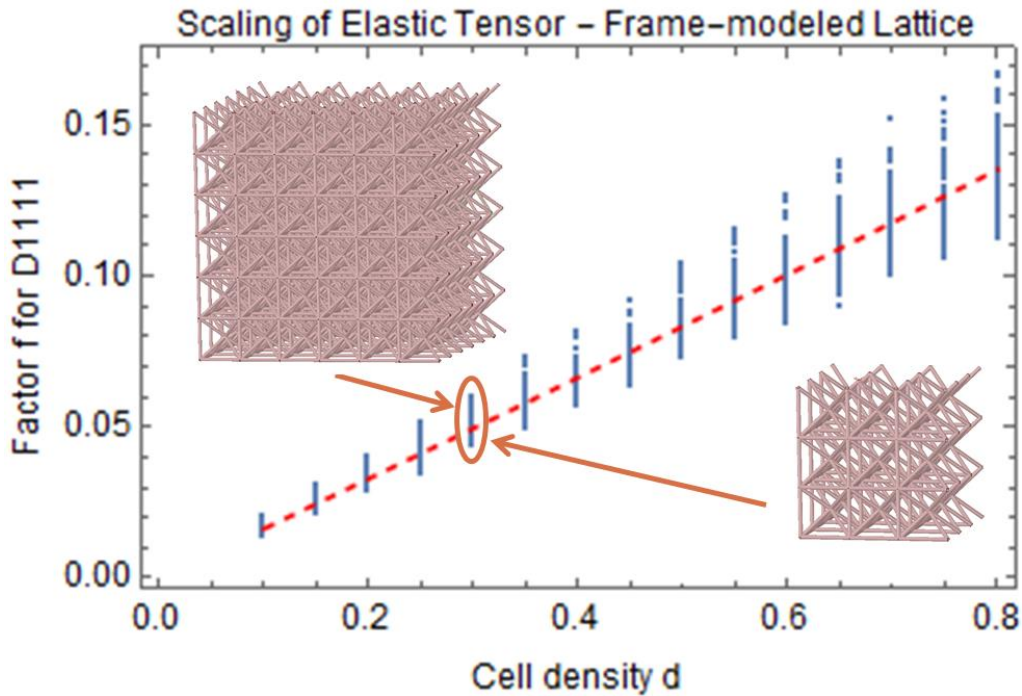


Figure 59. Result of the homogenization procedure for the BCC cell of different lengths  $L$ , thickness  $t$ , and coupon size  $n$ . Blue vertical lines represent the deviations of the results, while the red dashed line follows (13).

As expected, the result of the homogenization shows closer agreement with the predicted value  $f(d) = d/6$  for lower densities. However, it should be noted that even though the disagreement appears to be more pronounced for higher densities, the *relative* error bounds remain approximately constant for a wide range of densities. Moreover, we included in the experiments also different coupon size, so that it is also verified that coupon size does not affect the results.

### 4.3 Limits given by FDM manufacturing constraints

The homogenization process has been run for density ranges from  $0.1 \leq d \leq 0.8$  assuming that for  $d \leq 0.1$  the result of the literature is always true. Anyway, not all densities are possible to consider in the optimization. In fact, very low densities are impossible to produce for the manufacturing constraint of minimum member size imposed by every additive manufacturing technology. High density will behave differently than expected one. Every approximation we have made is based on the assumption of slender beam for which the section diameter is way smaller than the length of the beam.

Figure 60 shows the contour plot of the relative densities of the BCC cell as a function of thickness  $t$  and cell size  $L$  (from (12)). This plot is used to establish bounds on the feasible values of the parameters, to be used later in the optimization problem. Such bounds result from the following manufacturing constraints:

- Minimum printable thickness,  $t_{\min}$ , depends on the printing technology, printing machine, and material used. (tested in Section 3.2.5)
- Beam slenderness limits the maximum aspect ratio of the beams, generally  $L/t \geq 5$ . From this relation we can calculate the maximum acceptable thickness,  $t_{\max} = L/5$ , and the minimum cell length as  $L_{\min} = 5t_{\min}$
- Maximum cell size  $L_{\max}$  determined by the dimension of the cell to guarantee a certain minimum number of cells inside the design domain (or subdomain). (see next Chapter to understand how to calculate  $L_{\max}$ )

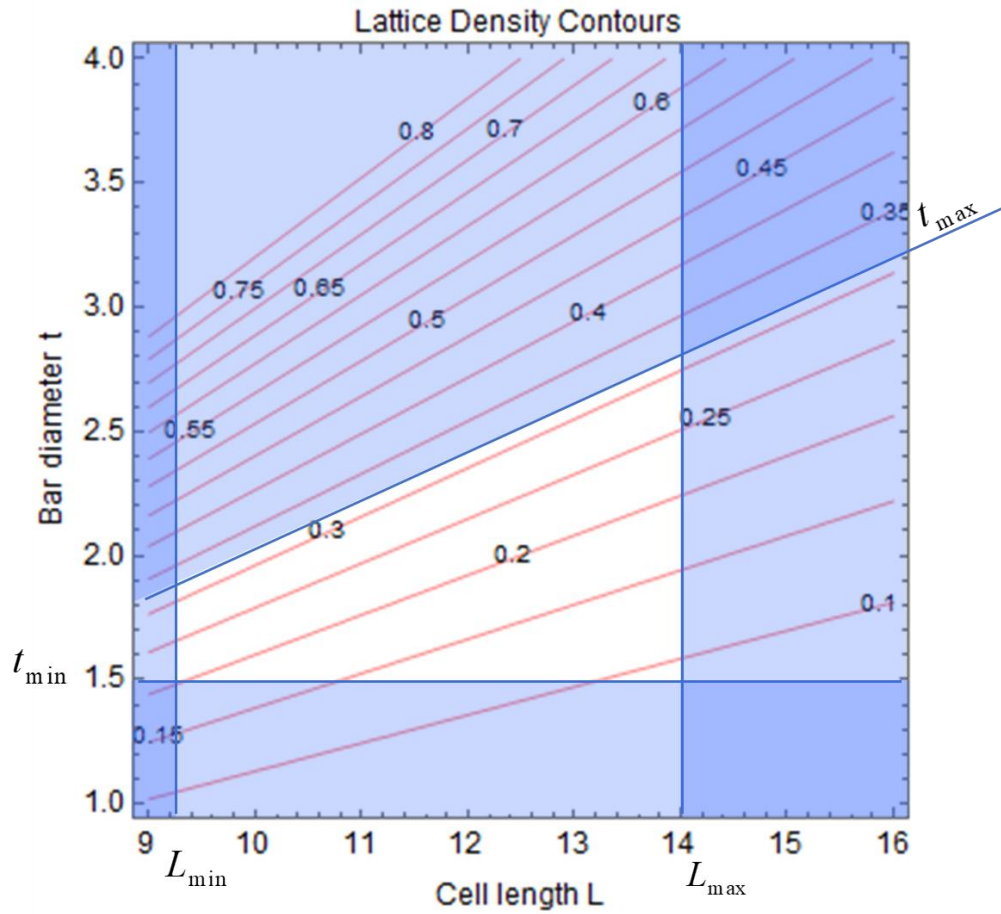


Figure 60. Contour plot of the relative densities as a function of the cell length  $L$  and bar thickness  $t$ . The plot is bounded by the manufacturing constraints, and shows the range of possible densities. (Dimensions  $t$  and  $L$  in mm)

Incorporating the bounds on the contour plot in Fig. 60 results in bounds on the effective density for a given cell size. For instance, for a subdomain where a cell size  $L=12\text{mm}$  is used, the effective density should be bound within (roughly)  $d=0.15$  and  $d=0.30$

## 5 Partition into Subdomains of Constant Lattice Cell Size

After Chapter 4, we have the model shape and requirements, the manufacturing technology that will be used, the manufacturing constraints, the cell that will be used and the density ranges for each cell size. In Chapter 5 the subdivision of the design domain is explained. As a resume, we remember that every subdomain is isolated to the others through solid walls. This is necessary to connect lattice cells of different size (or eventually, different topologies). It is so clear that find the division scheme and where to put internal walls, means finding regions that require similar cell size.

In order to achieve such a subdivision, many ways have been tried.

- Using FEM software like ANSYS we tried to internal structure with the shape of a wall to isolate part of the domain. It was the attempt of applying the same methodology used in Ref [1]. Unfortunately, the result of the optimization was not satisfying even using convenient loads, different amount of material, manufacturing constraints in the analysis settings, and other models. The result was that in general not usable internal structure appear, when a standard topology optimization is run on a real 3D model. Just as an example, it is shown an output of the optimization for the *Dogbone* model.

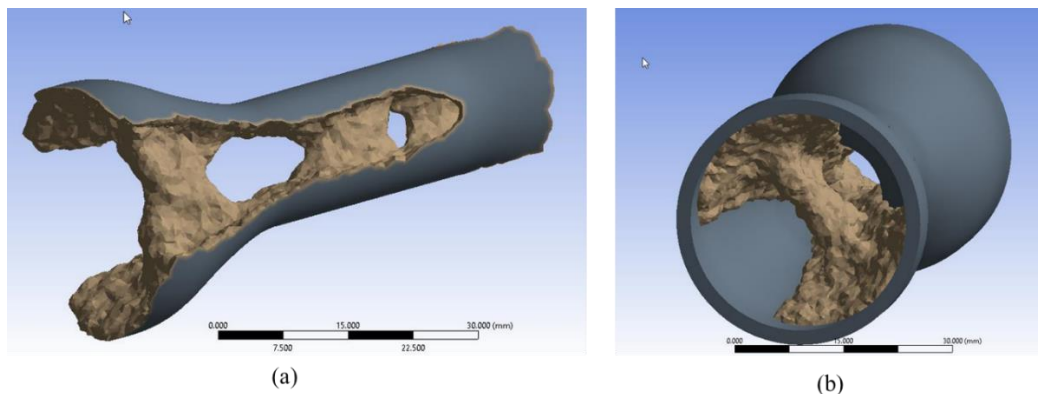


Figure 61. Result of standard topology optimization on Dogbone geometry.  
(a) Just internal material, (b) internal material and external skin.

- Another way is to run a topology optimization with a low penalization factor, or with some solving criteria which allows mid-density elements. In this case we could group elements with similar relative density and obtain a sort of 3D contour plot. Also this problem was dropped because of many reason: subdomains were in general overlapping, one intersecting the others; no printability constraints

could have been set (for example walls over void regions are not printable if exceed the maximum overhang angle); and finally, regions so obtained could contain both narrow and hefty region that require to use very small cell that have a small range of densities and less freedom for optimization.

Given that for 3D problems, topology optimization is not a convenient methodology to define internal walls, we decided to change point of view. We defined a new method that is the one that we finally implemented in the methodology. The new assumption now is that internal walls do not derive directly from an optimization but are a result of geometry consideration with a refinement after the first optimization result. It is a sort of iterative procedure were the designer, once seen the result of the first optimization can decide to apply some modification to the internal wall design and run the optimization again.

Thus, the final method of subdivision result of two steps: the first based just on the geometry of the part, and the second based on the feedback from the first optimization problem.

## 5.1 Geometry Partition

The initial partition of the design domain into subdomains is determined by the geometry of the problem. Being the part to optimize a real 3D model, it is intended to accommodate parts with varying overall thickness, e.g., parts with large volumes as well as narrow channels. Such geometries impose limitations on the cell dimensions that are feasible within each subdomain. In essence, the aim of the subdivision should be to try to keep hefty regions of the design domain separated from narrow regions so that bigger cells can be used, if appropriate. In fact, as see in Fig. 60, larger cells allow wider ranges of possible densities, thus a more efficient optimization.

The partition scheme used here is relatively straight forward, and it is defined implicitly by the criterion

$$meas(\Omega_i) > D_i \tag{16}$$

where  $D_i$  is a prescribed dimension and  $meas(\Omega_i)$  is a characteristic dimension of  $\Omega_i$ , e.g., a representative diameter of  $\Omega_i$ . The constraint (16) guarantees that subdomain  $\Omega_i$  can contain a sphere of diameter  $D_i$ . This is illustrated in Fig. 62, which shows walls that split  $\Omega$  into three subdomains, each one containing a sphere of different diameter,  $D_i$ .

If each sphere is required to be large enough to contain a patch of  $n \times n \times n$  cells of length  $L_i$ . Thus, the cell size inside subdomain  $\Omega_i$  must satisfy

$$L_i < D_i/n \quad (17)$$

ensuring (roughly!) that  $\Omega_i$  is large enough to contain the patch.

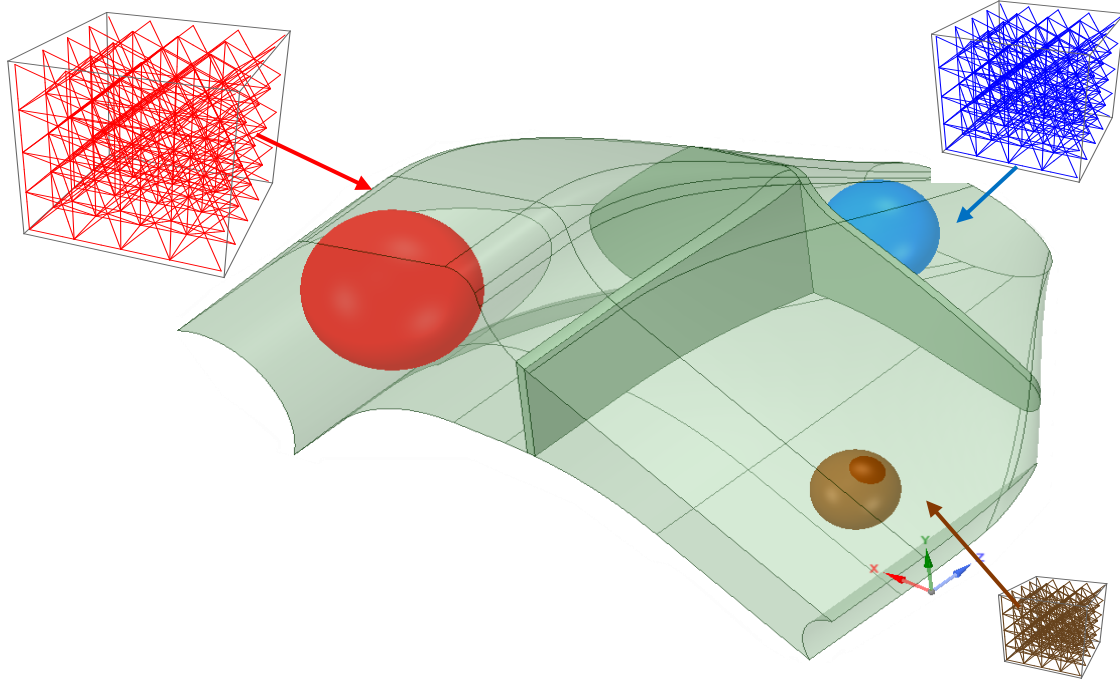


Figure 62. Subdivision of the design domain based on constraint (16). Three spheres of different diameters show the need of different cell dimensions and walls to separate them.

Constraint (16) does not consider possible internal features or support/load regions which could require a smaller cell dimension. Small internal features may require smaller cells than predicted by (16). Figure 63 shows such scenarios. A sphere of the size  $\hat{D}_i$  of the feature (blue disks in the figure) is replicated inside the domain (red disks). Setting:

$$L_i \leq \hat{D}_i / n \quad (18)$$

makes sure that about  $n$  lattice cells connect to the feature. Adding more internal walls can isolate regions of small features.

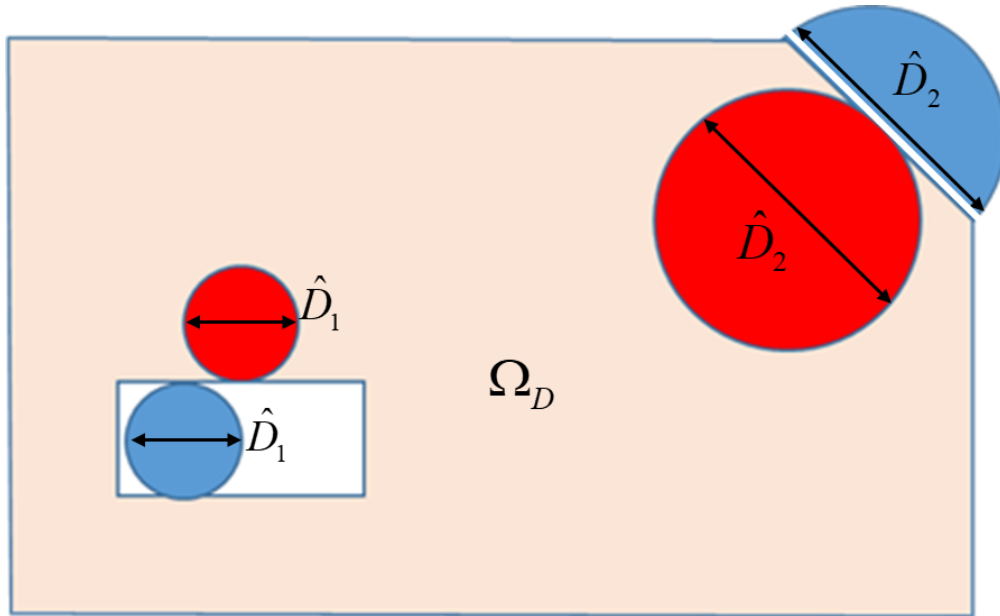


Figure 63. Possible scenarios where small features impose restrictions on cell size.

It should be taken into consideration that walls are not object of optimization. So, every wall we add “consume” material that would be assigned to the lattice. Thus, the two aims of the partition, is to isolate narrow region to let hefty regions use large cell, but use the minimum possible number of walls.

## 5.2 Optional subdivision from feedback of Optimization problem 1.

A second, optional step in the partitioning of the domain involves feedback from Optimization Problem 1, discussed in the next chapter. Problem 1 determines an optimal spatial distribution of effective density within each subdomain. This information can be used to assess the suitability of a second partition. For instance, areas of very low density may not require infill and a wall separating these areas from the rest of the domain may result in better use of material. In general, separating areas that call for low lattice densities from the rest of the domain allows more variation in the lattice length scales across the whole body. In this way, an iterative procedure is started like it is shown in the next figure. When a region of low density is detected one should consider using the material of the region to set void to build the wall to separate that region. If the infill eliminated is enough to build a wall (consider minimum wall thickness printable) and this does not bring any printability issue, then the wall can be set. Instead, if the wall would require more material than the one eliminated is maybe better to keep the lattice, because

adding such a wall would mean to “consume” material from the optimization of the infill and add it to a not optimized part.

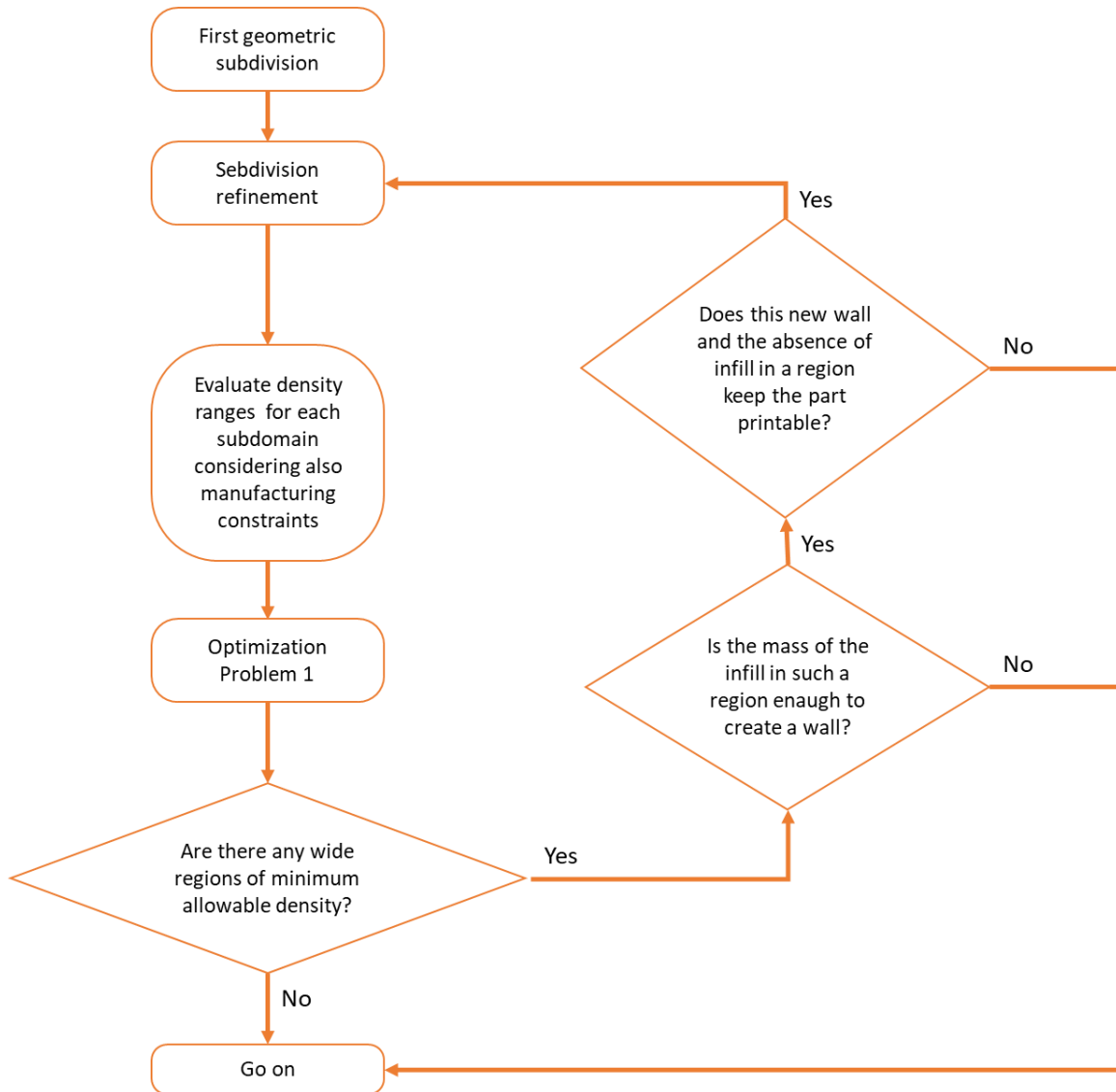


Figure 64. Iterative procedure of design domain subdivision.

## 6 Optimization Problems

At this point the model is already subdivided (maybe just the first geometry subdivision) and the cell sizes and topologies for each subdomain are fixed.

From Fig. 60 and relative formulas, it is possible to define the ranges of relative density and section area for each subdomain. Details and actual ranges will be shown in the formulation of each optimization problem in the following.

The optimization procedure is made up of two optimization steps, as already briefly explained in Chapter 3. The first optimization problem makes an efficient use of lattice effective properties to obtain an approximate map of the mass distribution over the design domain. The solution of Problem 1 is particularly useful because it gives a fast analysis of the effectiveness of the internal walls, and give the possibility of design refinement without losing much time.

Once the subdivision is completely defined, the model for Optimization problem 2 has to be prepared. A cell pattern with the correct dimension must fit every subdomain. This procedure must be carried out very carefully and the method of trimming the cell pattern with internal walls and external skin is shown in Chapter 6.2. Once the model is ready the model is meshed with a hybrid beam tetra model. The structure is then optimized with a FEM Matlab script which minimize compliance by changing the section area of each beam independently keeping a certain amount of total mass fixed.

Note that the trimming procedure is a pretty long procedure, on the order of 4-8 hours (depending on the complexity of the model). Having Optimization Problem 1 allow us to make this model just once and same a big amount of time.

Both optimization problems are solved using the method of moving asymptotes (MMA) [9].

## 6.1 Optimization Problem 1

Optimization Problem 1 is performed to obtain the spatial variation of lattice densities inside each subdomain. The problem involves a classical compliance minimization, imposing a constraint on the total amount of material. The body  $\Omega$  is discretized using standard 3D finite elements (tetrahedral elements are used in this thesis). The mesh is then imported in a FEM Matlab script that assign to each element an effective density  $d_e$  like shown in Fig.65. The correct operation of the Matlab Script has been verified comparing the values of compliance given by the script and ANSYS for simple examples (not shown here). Some consideration on the mesh preparation should be outlined. The Matlab script we used, was able to process only linear elements, and the nodes in the contact region between infill regions, internal walls and external skin must appear just once. This is possible to achieve exploiting some functionality of CAD software used (enable Share Topology in SpaceClaim in this thesis), and adjusting the properties of the mesh generator (ANSYS in this case).

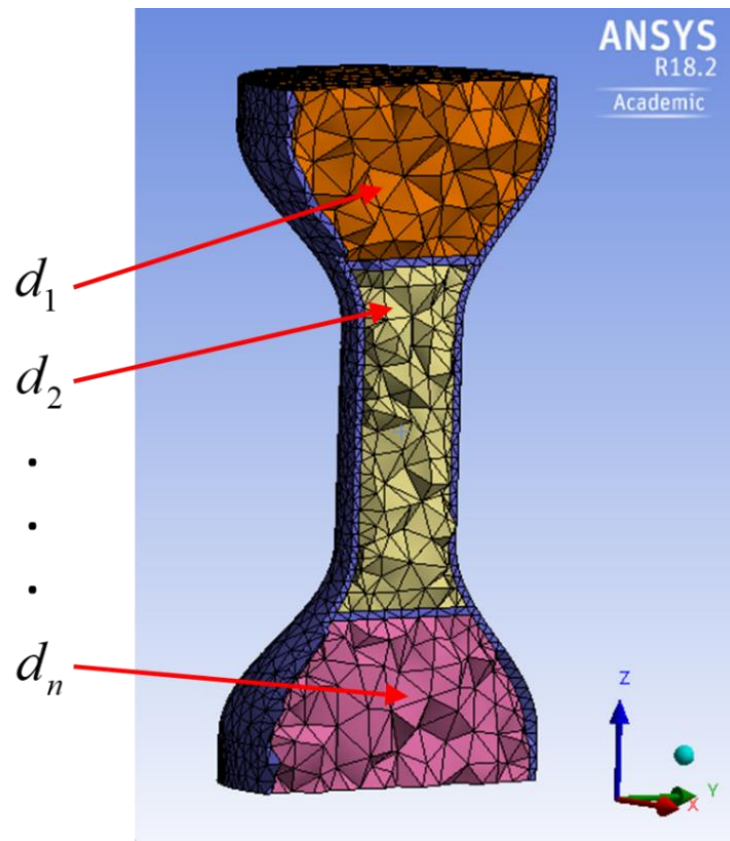


Figure 65. Tetrahedral mesh of the model. Each tetrahedra has different relative density and consequently different effective properties.

The elastic tensor assigned to each element is of the form (6)

$$\mathbf{D}(d) = f(d) \mathbf{D}^0$$

where  $f(d)$  depends on the cell topology selected for the problem:  $f(d) = 1$  if  $e \in \Omega_B$ , i.e., element  $e$  is not designable (solid). This is the case of the element of the external skin and internal walls. The optimization problem is then:

**Problem 1:** Find  $d_1, d_2, \dots, d_N$  that

$$\text{minimize: } \hat{C} = \mathbf{U}^T \mathbf{F}$$

$$\text{subject to: } \sum_e^N d_e V_e = v_1 V \quad (19)$$

$$\mathbf{K}\mathbf{U} = \mathbf{F}$$

$$0 < d_{i,\min} \leq d_e \leq d_{i,\max} < 1 \quad \text{if } e \in \Omega_i$$

$$d_e = 1 \quad \text{if } e \in \Omega_B$$

Here  $d_e$  is the relative density of element  $e$  and  $V_e$  is the volume of the element.  $v_1$  is a prescribed volume fraction of  $V$ , the total volume of  $\Omega$ . Also,  $\mathbf{U}$  and  $\mathbf{F}$  are, respectively, the global displacement and force vectors;  $\mathbf{K}$  is the global stiffness matrix,  $N$  is the number of design variables, one per finite element.

Length scales  $L_i$  are assigned to each subdomain as discussed in Chapter 5. Upper and lower bounds of the density are computed as described in Chapter 4. For the BCC cell,  $d_{i,\min}$  and  $d_{i,\max}$  are calculated from

$$d_{i,\min} = (3 + 4\sqrt{3}) \frac{A_{\min}}{L_i^2} \quad (20)$$

$$d_{i,\max} = (3 + 4\sqrt{3}) \frac{A_{\max}}{L_i^2} \quad (21)$$

with  $A_{\min}$  and  $A_{\max}$  corresponding to the lower and upper bounds on thickness (see Fig. 60). For instance, assuming a circular cross section and  $t_{\min} = 1.5\text{mm}$  we obtain the density ranges in Table 3

Cell size $L_i$ (mm)	8	10	12	14	16
Min density $d_{i,\min}$ (mm)	0.27	0.18	0.12	0.09	0.07
Max density $d_{i,\max}$ (mm)	0.31	0.31	0.31	0.31	0.31

Table 3. Density ranges for various cell size  $L_i$

## 6.2 Optimization Problem 2

Optimization Problem 2 is performed to obtain the spatial variation of lattice section properties inside each subdomain. We assume a circular cross section and use bar areas as the independent variables. A lattice of prescribed topology and cell dimensions  $L_i$  is generated to fit inside each subdomain and trimmed to follow the prescribed boundaries. In this paper we have reported solutions using truss elements, although in this case beam and truss elements produce essentially indistinguishable results. Portions of the body in  $\Omega_B$  are modelled using tetrahedral elements. The mesh is then imported in a FEM Matlab script which includes linear truss elements. The correct operation of the Matlab Script has been verified comparing the values of compliance given by the script and ANSYS for simple examples (not shown here). Material properties correspond to  $\mathbf{D}^0$  throughout  $\Omega$ . The optimization problem is then:

**Problem 2:** Find  $A_1, A_2, \dots, A_N$  that

$$\text{minimize } \hat{C} = \mathbf{U}^T \mathbf{F}$$

$$\text{subject to } \sum_e^N A_e \ell_e = v_2 V \quad (22)$$

$$\mathbf{K}\mathbf{U} = \mathbf{F}$$

$$0 < A_{i,\min} \leq A_e \leq A_{i,\max} \quad \text{if } e \in \Omega_i$$

Here  $A_e$  is the section area of bar  $e$ ,  $\ell_e$  is the length of the bar, and  $N$  is now the number of bars. Area upper and lower bounds are constant within each subdomain but may change when the cell size changes, as follows for BCC cells:

- $A_{i,\min} = \text{constant}$  (depends only on  $t_{\min}$ )
- $A_{i,\max} = \frac{d_{i,\max} L_i^2}{(3 + 4\sqrt{3})}$  (23)

Assuming a circular cross section and  $t_{\min} = 1.5\text{mm}$  we obtain the area ranges in Table 4.

Cell size $L_i$ (mm)	8	10	12	14	16
Min area $A_{i,\min}$ (mm <sup>2</sup> )	1.77	1.77	1.77	1.77	1.77
Max area $A_{i,\max}$ (mm <sup>2</sup> )	2.01	3.14	4.52	6.16	8.04

Table 4. Area ranges for various cell sizes  $L_i$

### 6.2.1 Cell Trimming Techniques

One of the main difficulties of Optimization Problem 2 is the trimming of the cells to make the lattice fit inside the subdomains. In fact, the mesh to be created has some strictly requirements to be read in the FEM script by Matlab:

1. Truss elements on the boundary and tetra elements must match. Every bar in the boundary must end on a node shared with the tetrahedral elements of the skin or the internal wall. In other words, bars that stick out or floats are not allowed

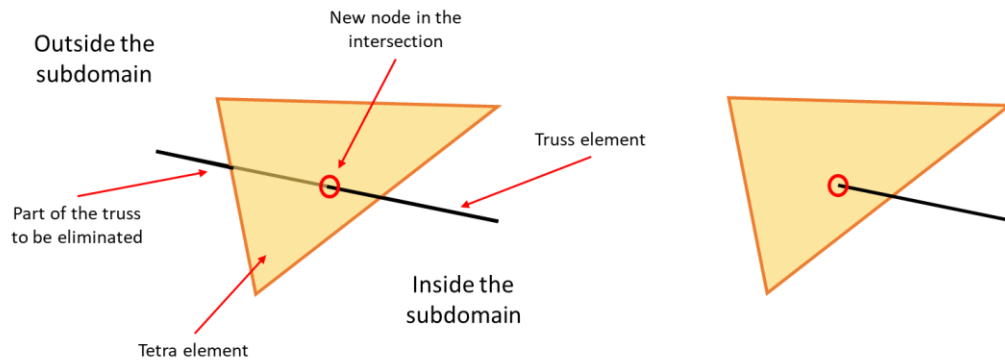


Figure 66. Typical condition at the boundary of each subdomain, where truss elements cross tetra elements.

2. Truss elements must contain just 2 nodes: its ends. No middle nodes are acceptable, so truss elements need to be meshed without middle nodes
3. Every node need to have connectivity  $>3$ . That is saying that situations like two truss pins jointed and not connected to any other truss or tetra elements are not allowable.

This trimming procedure seem to be possible to automatize through programming, but actually, it is a very challenging problem discussed a lot nowadays. Because of the absence of this automatism, it is still needed to make the trim manually, and make sure that the three conditions above are satisfied.

In this thesis Ansys SpaceClaim has been used to trim the lattice. Here it is shown the procedure used applied to the first practical example discussed in the next chapter.

Figure 67 shows the subdomain region in red and the lattice in green. The lattice has prescribed length  $L_i$ . Section area is not important now. All bars are modelled as solid cylinders. Figure 67a shows the starting point, with the lattice to be trimmed. Figure 67b shows the infill after splitting and trimming of the external bars.

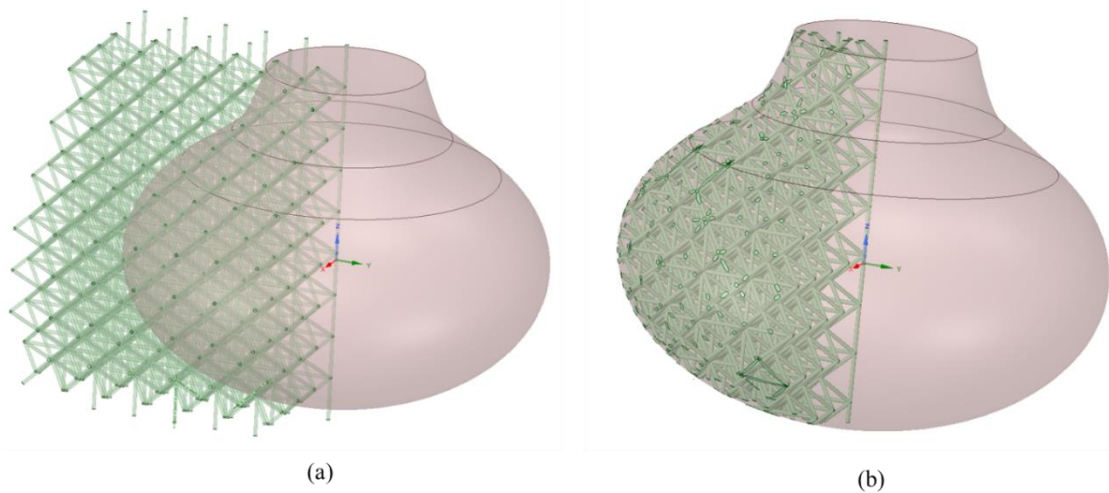


Figure 67. Lattice infill trim starting point (a), after trimming (b)

The trimmed cylinders are now transformed in truss elements through the command Extract. The result is shown below.

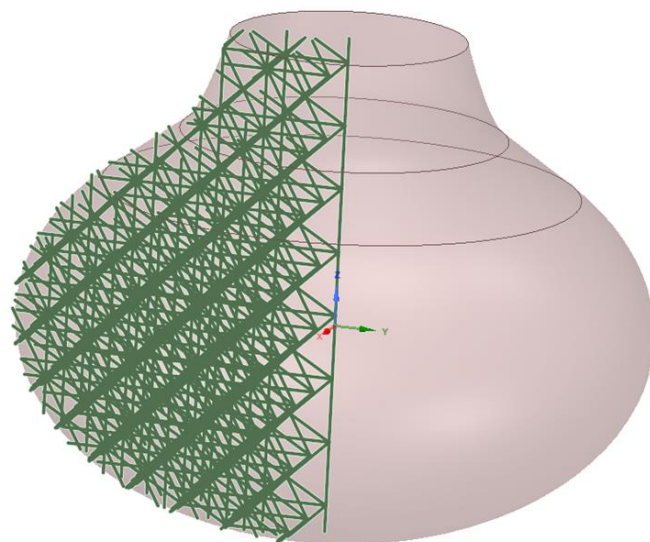


Figure 68. Lattice infill after transformation from solid to truss elements

The transformation generates all beam elements which stick a bit out of the infill subdomain. This situation is clear in Fig. 69a where blue dots shows intersecting point while red dots are sticking out bars. This model has then to be cleaned of all sticking out bars. To do such a thing, the truss bars need to be split again, but this time with the internal surface of the skin (or the walls). In this way all the sticking out bars will be separated and can then be eliminated to clean the whole model. The aspect of a clean model is that one shown in Figure 69b.

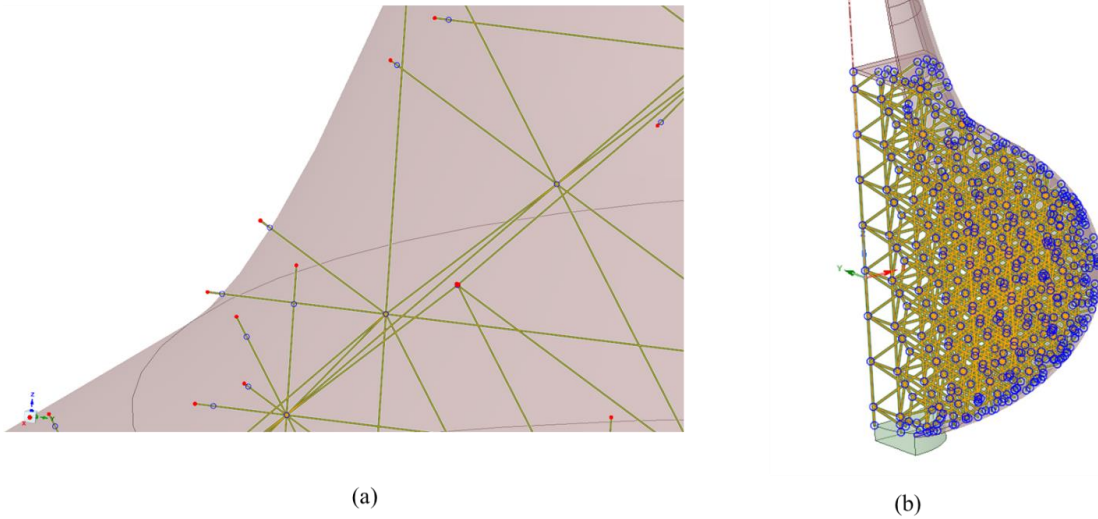


Figure 69. Aspect of the model after conversion from solid to truss full of sticking out bars (a)  
Aspect after cleaning the model (b)

Note that all sticking out bars had to be trimmed away manually, and the task should be carried out very carefully. One truss bar that do not respect the three conditions introduced above will give errors in the FEM simulation. This whole process cause to spend hours in cleaning up the model. It is clear that, an automatized process would greatly speed up the process.

Anyway, if no other ways are possible, manually trimming the lattice is probably the best way. Thanks to the presence of Optimization Problem 1, it is required to trim the lattice just once, in theory. If errors arise during the simulation for some bars, it is possible to individuate which are the problematic one. In fact, with another simple Matlab script it is possible to see which node appear twice in the connectivity list. These bars will be the one which need to be corrected, without starting everything over again.

## 7 Practical Applications

The methodology defined in the previous chapters is illustrated using two examples. The first is a test object with a “bottle” shape, useful to highlight each step and re-visit the notation. The second is an automotive application: a FSAE double wishbone upright has been re-designed taking in consideration the enhanced shape flexibility, and the possibility of using lattice infill, given by additive manufacturing and optimized through this methodology.

In all problems the goal is to minimize mean compliance.

Problems are set up and scaled as follows: if multiple loads are present, the corresponding compliances are added, contributing equally to the objective function,  $\hat{C}$ . Different weights for each load case are allowed but they need to be justified. Loads are scaled so that  $\hat{C}=1$  when a lattice of constant effective density is used throughout the design domain and the amount of material constraints (19) and (22) are active. To allow comparison of the models used in Problems 1 and 2, loads are scaled only once (i.e., the same scaling is used for both problems). Bounds  $v_1$  and  $v_2$  in (19) and (22) are consistent, representing in both cases the same amount of material.

## 7.1 Bottle Test Piece

The shape of the test piece is shown in Fig. 70, along with basic dimensions, forces and constraints. It is subjected to two load cases corresponding to forces  $F_1$  and  $F_2$ , applied separately, on the upper surface (see Fig. 70). The piece is fixed at the bottom surface. The shape considered are not a clear physical meaning, but was chosen because it allows a clear review of all passages of the methodology presented here.

The body  $\Omega$  is divided into three regions, shown in Fig. 70b.  $\Omega_B$  is the skin, excluded from the optimization process and considered solid;  $\Omega_1, \Omega_2 \in \Omega_D$  are the two subdomains to be filled by lattice. Because of their different dimensions, they are separated by a wall included in  $\Omega_B$  and considered solid. To set the position of the wall and to determine the cell size, the sphere method scheme in Chapter 5.1 has been used. One sphere is drawn in each subdomain, its diameter is chosen so that the sphere fits essentially everywhere in the subdomain. These spheres determine the cell sizes  $L_1$  and  $L_2$ , used in  $\Omega_1$  and  $\Omega_2$ , respectively, as described in Sec. 4. Note that using larger cell diameters allows a broader range of effective densities. Cell size were so calculated:  $L_1=8\text{mm}$  and  $L_2=12\text{mm}$ .

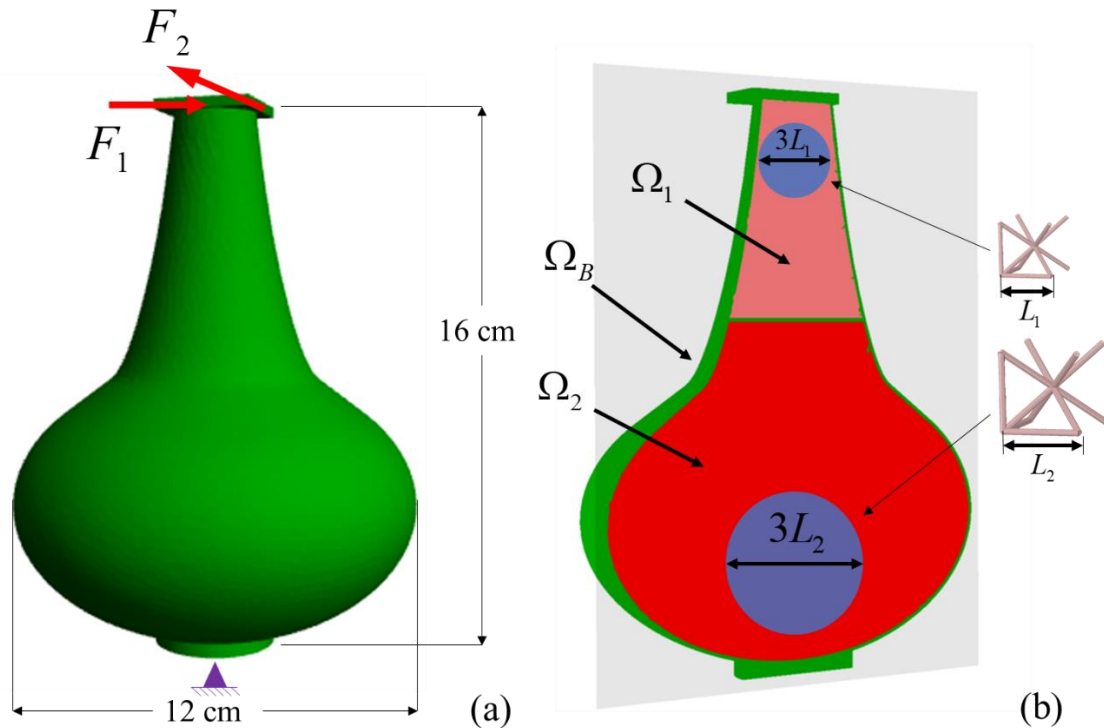


Figure 70. Test piece. External shape with forces and constraints (a). Mid-section with the three regions defined (b). A wall is placed to allow the connection between lattices of different scale lengths, defined by the blue spheres, from (17) with  $n=3$ .

### 7.1.1 Optimization Problem 1 on Bottle test piece

The result of the optimization 1 is shown in Fig. 71. From the values of cell size, the manufacturing constraints for the minimum bar thickness (so the minimum bar section area) and given the minimum slenderness, it is possible to calculate the ranges of relative densities through (20) and (21):

$$d_{i,\min} = (3 + 4\sqrt{3}) \frac{A_{\min}}{L_i^2}$$

$$d_{i,\max} = (3 + 4\sqrt{3}) \frac{A_{\max}}{L_i^2}$$

From these relations we have the following density ranges:

$$0 < 0.27 \leq d_e \leq 0.31 < 1 \quad \text{if } e \in \Omega_1 ;$$

$$0 < 0.12 \leq d_e \leq 0.31 < 1 \quad \text{if } e \in \Omega_2 .$$

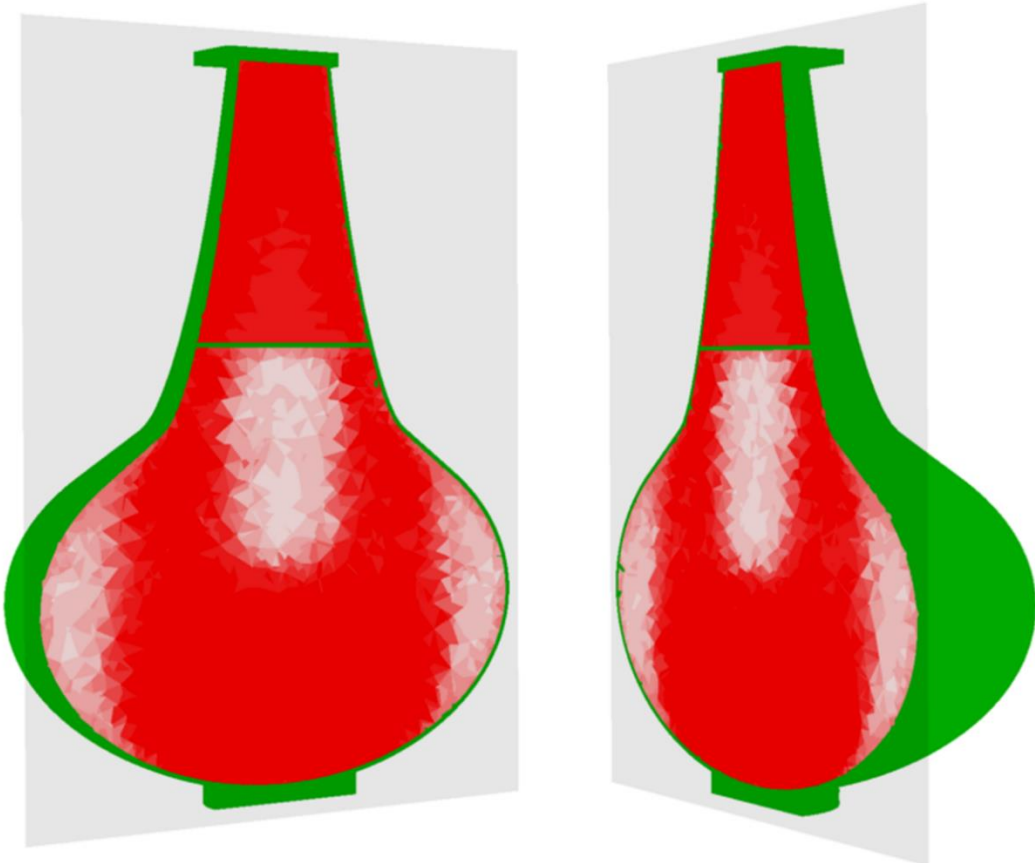


Figure 71. Result of Optimization Problem 1 for the “bottle” test piece.

Darker red areas show regions where the maximum possible density ( $d_{i,\max}$ ) is assigned, while the colour becomes lighter as the assigned density decreases. It is possible to see that regions on the sides and on the centre, are less dense.

At this point one could consider leaving the subdivision of the internal region as it is, or make some modifications adding a wall, based on the density distribution.

### 7.1.2 Subdivision Refinement

We now consider a new scenario, where the results of Optimization Problem 1 are used to change the partition of the bottle into subdomains. Based on the results suggested by Fig. 71, we partition the bottom part of the body into three subdomains by adding two vertical walls (in correspondence of the black lines in Fig. 72a), and exclude the left and right subdomains from the optimization, as shown in Fig. 72. These two regions (labelled  $\Omega_{\text{void}}$ ) will not be filled with lattice.

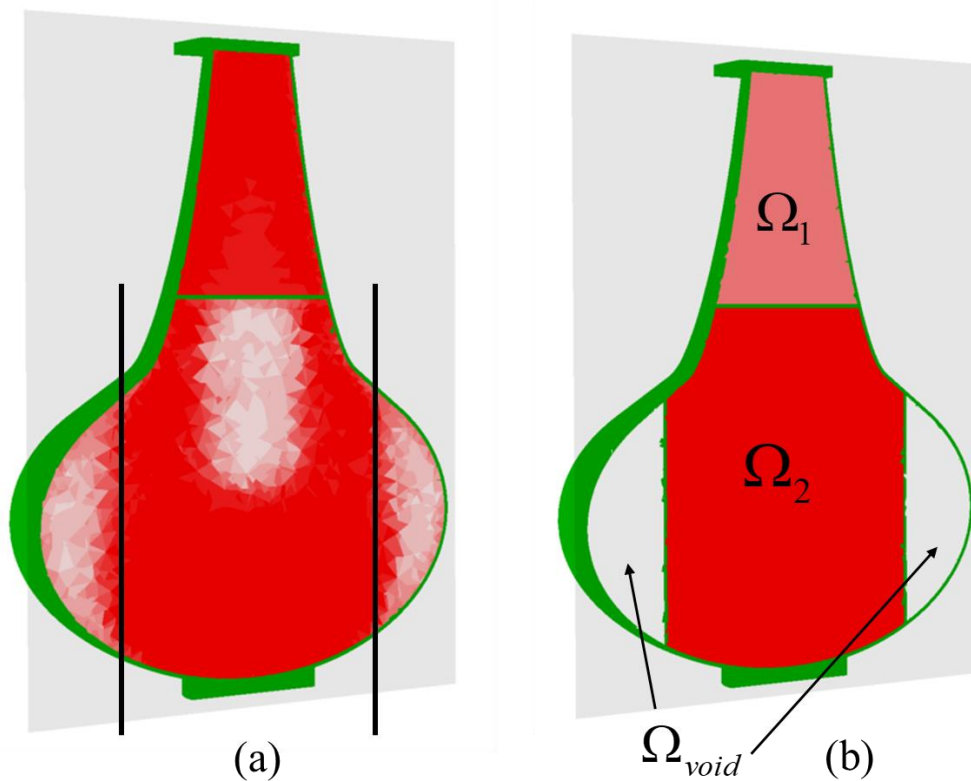


Figure 72. Choice of the position of the new internal walls (a). Modified subdivision and new labels (b).

As explained already in Chapter 5.2, we need to be sure that the amount of lattice material eliminated is more or at least equal to the material needed to build the wall, and be sure that the new subdivision will not bring any printability issue.

Through the software SpaceClaim it is possible to calculate the volume of the new walls  $V_{walls}$  and the overall length of the truss bar eliminated  $L_{overall}$ . Considering that the minimum thickness of printable wall increases if the wall is wide and connected to other walls just at the boundaries, we selected as thickness of the walls,  $t_{wall} = 1mm$ . The bars that are going to be eliminated are characterized by minimum thickness, so  $t_{min}^{bar} = 1.5mm$ . With these hypotheses, the volume of material eliminate and the volume of the walls are respectively:

$$V_{bars} = L_{overall} \left( \frac{t_{min}^2}{4} \pi \right) = 11469mm^3 \qquad V_{walls} = 8806mm^3$$

This means that creating these walls and keeping the same final mass, more material can be assigned to the lattice infill. Thus, running again Optimization Problem 1 for the updated version, the results shows that more material has gone to fill the central part as shown in Fig. 73. Please note that on the other section (parallel to the walls) no remarkable difference are observed.

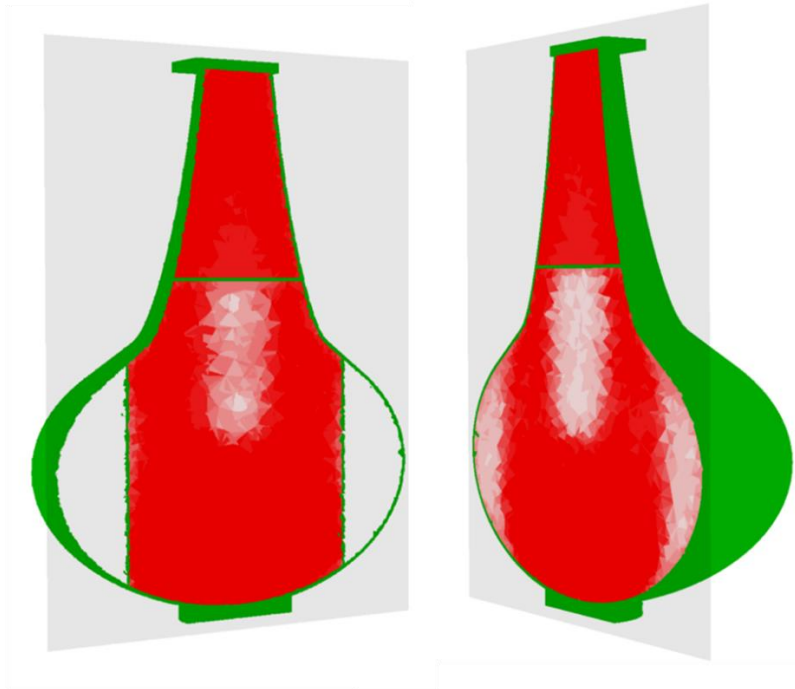


Figure 73. Result of the Optimization Problem 1 for the new subdivision of the design domain.

### 7.1.3 Optimization Problem 2 on Bottle test piece

For completeness, just for this test piece, we run the Optimization Problem 2 for both the original and the refined subdivisions.

For both partitions, a lattice mesh with the prescribed cell dimensions is trimmed inside each subdomain as shown in chapter 6.2.1, setting the stage for Optimization Problem 2. The solution to that problem is shown in Fig. 74. In this case the colour scheme is proportional to the area of the bars and the colour range is different, which explains why the top part of the bottle is no longer red.

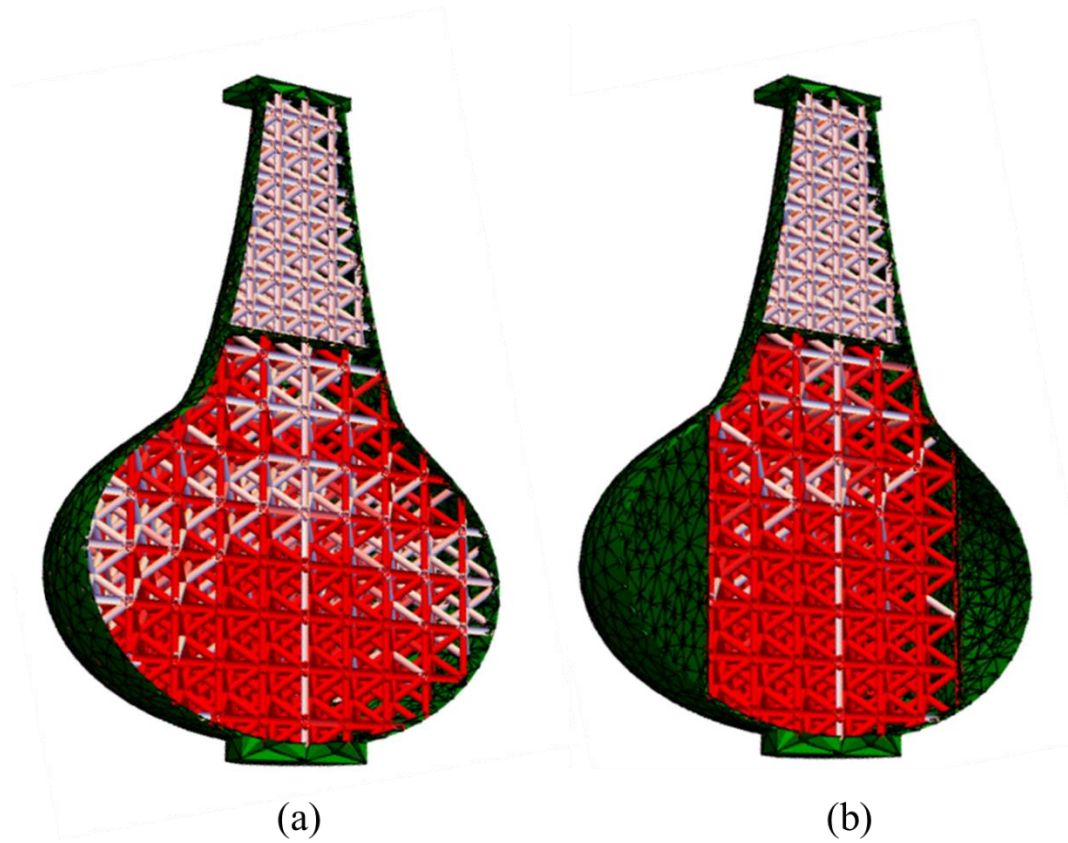


Figure 74. Result of Optimization Problem 2 for both partitions set.

Bounds on areas are selected from Table 4 and its relative formulas for each subdomain. Thus:

$$A_{i,\min} = \text{constant} = 1.77 \text{ mm}^2 \text{ (with } t_{\min} = 1.5 \text{ mm)}$$

$$A_{1,\max} = \frac{d_{1,\max} L_1^2}{(3 + 4\sqrt{3})} = 2.01 \text{ mm}^2$$

$$A_{2,\max} = \frac{d_{2,\max} L_2^2}{(3 + 4\sqrt{3})} = 4.52 \text{ mm}^2$$

Note that solution of optimization problem 2 agree with the distribution of material approximated by optimization problem 1. This shows that the approximation made by the effective properties is not so rough and it could be a reliable way to detect region of less usage.

#### 7.1.4 Results

The results in terms of compliance and stiffness increment are reported in Table 5. The loads have been scaled in order to have compliance  $\hat{C}=1$  for the model with uniform density distribution (or constant bar section area). Therefore, the stiffness increment is considered with respect to the model for compliance  $\hat{C}=1$ .

Partition	Original Partition		Refined Partition	
	<i>Opt. Problem 1</i>	<i>Opt. Problem 2</i>	<i>Opt. Problem 1</i>	<i>Opt. Problem 2</i>
Optimization Problem				
Compliance	0.80	0.77	0.79	0.78
Stiffness increment	+20%	+23%	+21%	+22%

Table 5. Results of FEM simulation of the “bottle” test piece

Note that both solutions of the Optimization Problems 1 and 2 results in essentially the same mean compliance, validating once more, the model (13) for effective properties of the lattice. Overall, the optimization carried out on this part with the methodology we propose, achieves a modest improvement in stiffness of about 20% from a design with uniform lattice density.

The two new walls of the refined partition, carry some of the loads that previously was carried by the infill. Compared to the previous result, no significant stiffness improvement was achieved by adding the wall and removing the lattice. Arguably, there may be differences in manufacturing costs and time between the two solutions.

A prototype of solution in Fig. 74a, has been printed and it is displayed in Fig. 75.



Figure 75. A prototype of solution in Fig. 74 (half), as built.

## 7.2 Upright

The second example represent a possible application of the methodology to automotive industry. It is just showed as an example, many actual characteristic (like the mounts) are not considered in deep.

The object to be optimized is a Formula SAE double wishbone upright. The problem was originally presented in Ref. [11] and solved using a standard topology optimization procedure to size the connecting structures. We borrow it here simply to see how this domain would be filled if it were filled with a lattice (but we have no illusions that the lattice infill solution is better than the standard topology optimization solution suggested in Ref. [11]). Loads, fixed constraints, the position of the mounts and the design domain are reproduced from [11].

The part being optimized is the element that connect the tires to the suspension system. Therefore, it is subject to many and important loads and many load cases.

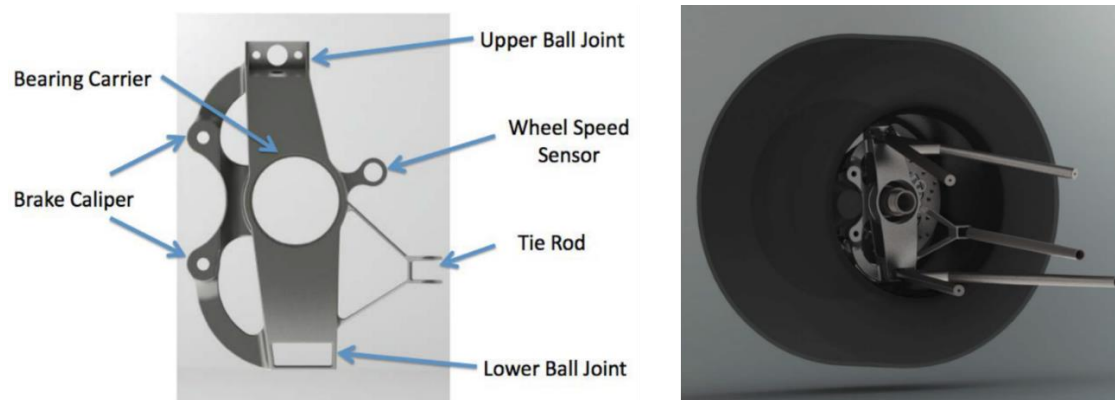


Figure 76. Upright designed with standard manufacturing technique and position in the assembly of the suspension.

The author supposes four load cases for four different driving conditions: outside and inside cornering, forward braking and rearward braking. With the data of the vehicle the equation of the dynamic of the vehicle and the direction of each suspension element, the author calculates the forces acting on the suspension elements (upper and lower wishbones, tie rod, pull rod braking calliper and bearing carrier) for each load case. The result is shown in the next Table 6

Inside Cornering	Outside Cornering
Upper Fore AA = -11.14 lbf Upper Aft AA = -31.36 lbf Pull Rod = 85.48 lbf Low Fore AA = 8.68 lbf Low Aft AA = 25.47 lbf Tie Rod Force = -11.79 lbf Bearing Lat Force = 132.2 lbf	Upper Fore AA = 29.39 lbf Upper Aft AA = 144.46 lbf Pull Rod = 430.3 lbf Low Fore AA = -389.81 lbf Low Aft AA = -589.57 lbf Tie Rod Force = 55.35 lbf Bearing Lat Force = -262.50 lbf
Forward Braking	Rearward Braking
Upper Fore AA = -547.32 lbf Upper Aft AA = 382.06 lbf Pull Rod = 485.23 lbf Low Fore AA = 1006.21 lbf Low Aft AA = -1457.35 lbf Tie Rod Force = 174.69 lbf Bearing Load = -448.6 lbf Brake Caliper Torque = 4082.54 lbf-in	Upper Fore AA = 86.27 lbf Upper Aft AA = -73.85 lbf Pull Rod = 80.47 lbf Low Fore AA = -227.68 lbf Low Aft AA = 175.54 lbf Tie Rod Force = -32.88 lbf Bearing Load = 77.80 lbf Brake Caliper Torque = -707.7 lbf-in

Table 6. Load cases

The author designed the part from just the suspension point, and the load cases. With the suspension pint he created the initial design domain like that in the Fig. 77a<sup>16</sup>. Then he run a standard topology obtaining the result in Fig. 77b.

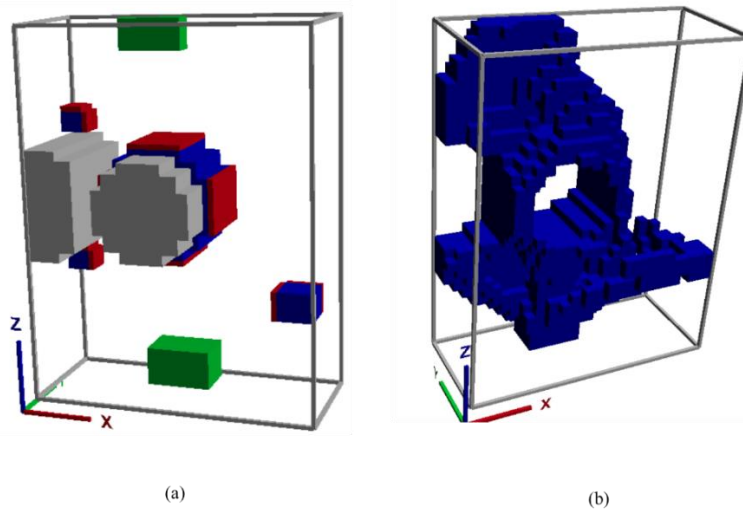


Figure 77. Design domain (a) and result of standard topology optimization (b) from Ref. [11].

Finally, the author interpreted the result and created the CAD model in Fig.76 trying to follow the result of the topology optimization.

<sup>16</sup> Grey, blue red and green regions are excluded from the design domain because of the presence of other mechanical component or because boundary conditions are applied on them.

### 7.2.1 Definition of the Design Domain and Subdomains

In our application we started from the same point. As the problem has no prescribed skin, we first use standard topology optimization to discard portions of the design domain in Fig. 78a where topology optimization predicts there will be no material. Whatever remains (Fig. 78b) form the external skin (Fig. 78c). While we recognize that this is arbitrary, it is sufficient to provide reasonable suggestions on how to get started.

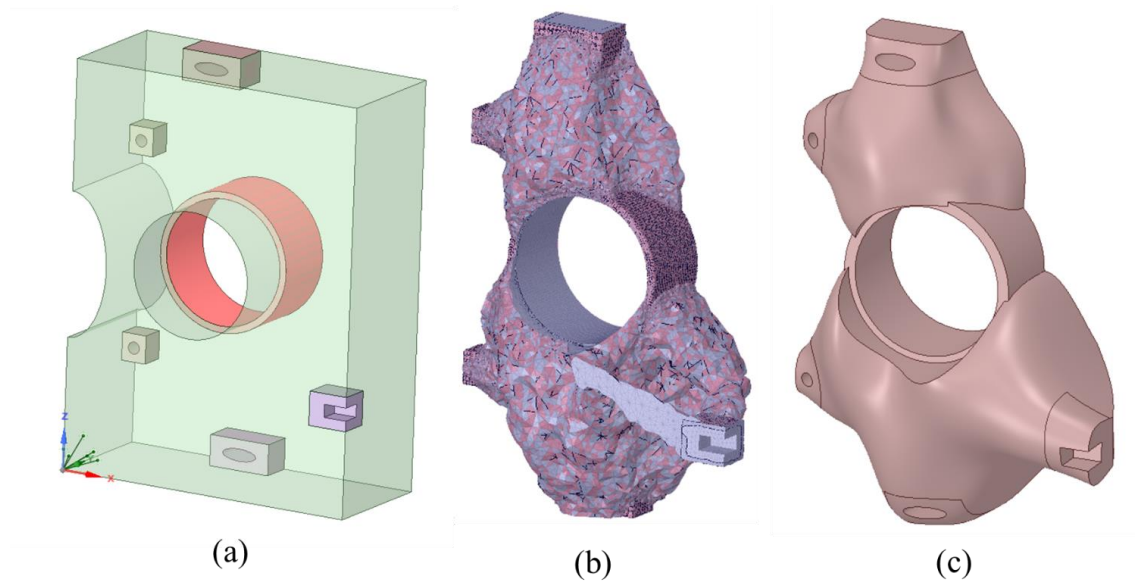


Figure 78. Problem set-up. Initial design domain given by [11] (a), result of the standard topology optimization (b), new design domain (c).

Note that, Additive Manufacturing technology allowed us to follow the shape of the topology optimization result very closely. We tried to avoid very narrow regions to let the internal subdivision simpler.

Having defined the external skin, and consequently the design domain, we can apply the lattice infill optimization procedure to this geometry. The setup is summarized in Fig. 79, which shows the overall shape of the skin (Fig. 79a), basic dimensions, forces, and constraints (all reproduced from [11]). The yellow areas are areas where boundary conditions are applied. Green areas indicate the outside skin, assumed, to be of thickness 2mm. The interior, shown in Fig. 79b, is the design domain that is going to be filled by lattice. It is naturally split into two subdomains by prescribed boundaries and requires no additional splitting.

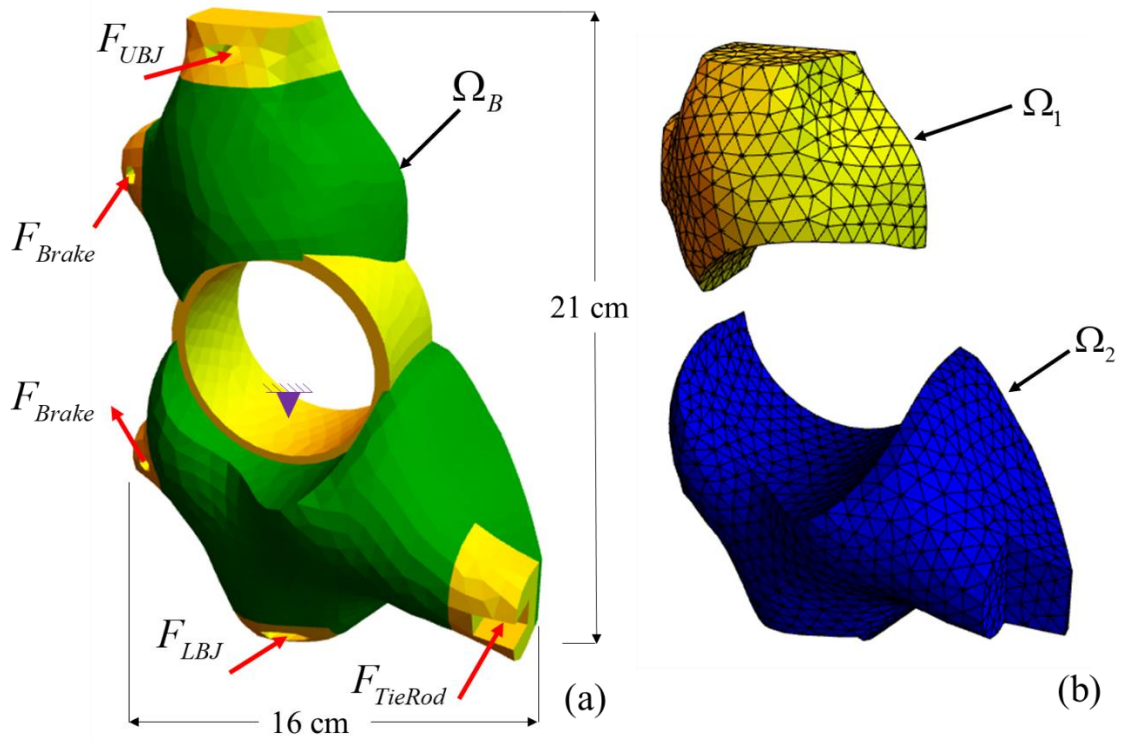


Figure 79. Upright geometry. External skin and mounts  $\Omega_B$  showing forces and constraints (a), Subdomains  $\Omega_1, \Omega_2$  to be filled by lattice (b).

Proceeding as in the previous example with the sphere method, we assigned a cell of length  $L=12\text{mm}$  to both subdomains, which meets constraint (17) and (18).

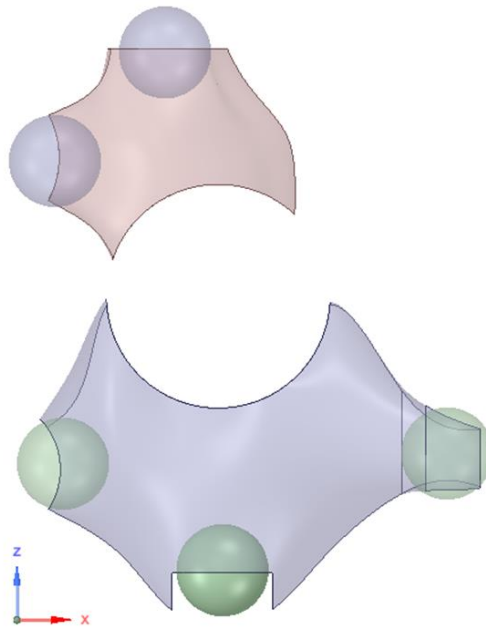


Figure 80. Sphere method to evaluate cell dimension. All spheres in the picture have diameter=36mm

### 7.2.2 Optimization Problem 1 – Upright

Once  $L_i = 12\text{mm}$  is defined for both infill subdomains, we can proceed as we did with the test piece. The density range for such a cell, is defined like in chapter 6, Table 3.

$$d_{\min} = 0.12$$

$$d_{\max} = 0.31$$

With these values it is possible to solve Optimization Problem 1 which result in the density shown in Fig. 81. Darker red areas show regions where the maximum possible density ( $d_{\max} = 0.31$ ) is assigned, while the colour becomes lighter as the assigned density decreases.

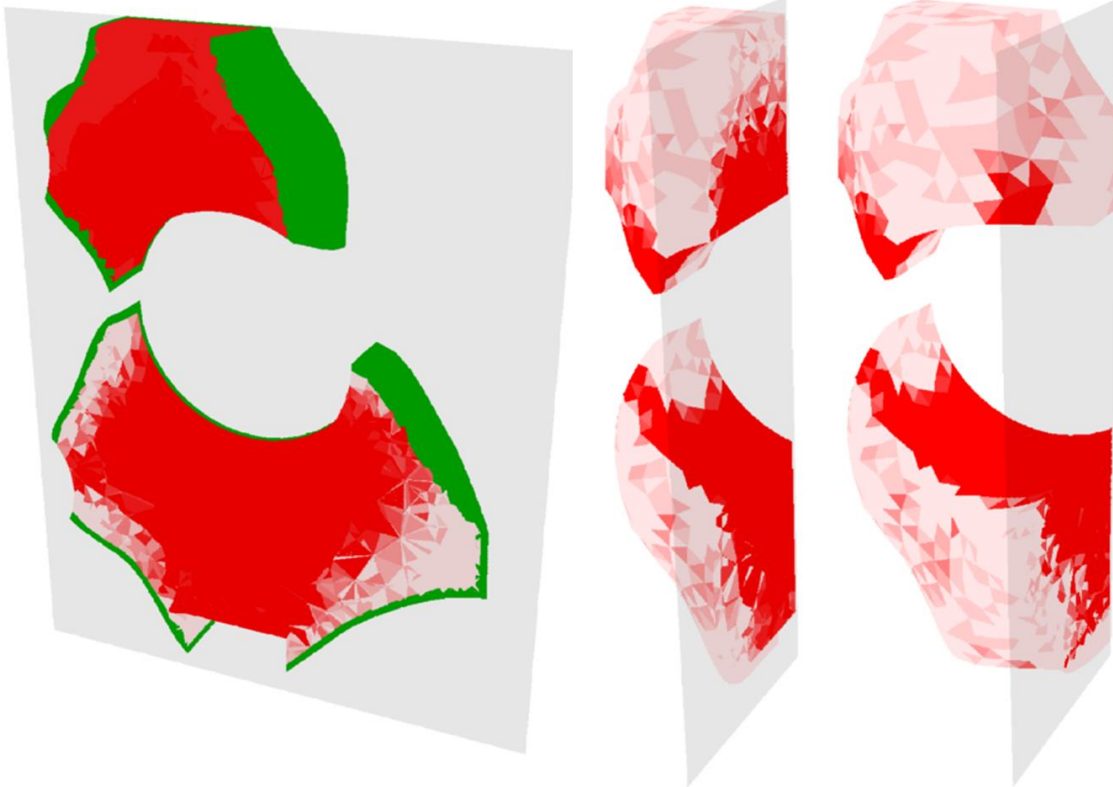


Figure 81. Result of Optimization Problem 1

It is not possible to find wide regions assigned to low density values. Therefore, the feedback it is not necessary in this case.

### 7.2.3 Optimization Problem 2 - Upright

With the cell size and manufacturing constraints calculated, we can get the range of bar thickness in the same way it has been done for the previous example:

$$A_{i,min} = \text{constant} = 1.77 \text{ mm}^2 \text{ (with } t_{min} = 1.5 \text{ mm)}$$

$$A_{max} = \frac{d_{max} L^2}{(3 + 4\sqrt{3})} = 4.52 \text{ mm}^2$$

Before running the optimization, the model has to be prepared. Here the cell topology and size are the same for the hole part. Anyway, the trim part is still pretty long and even more complicated than the other because of the complexity of the external skin. Once the model is ready and do not give any problem with double nodes or sticking out bars, we can run the Optimization Problem 2, that gives the area distribution shown in Fig.82

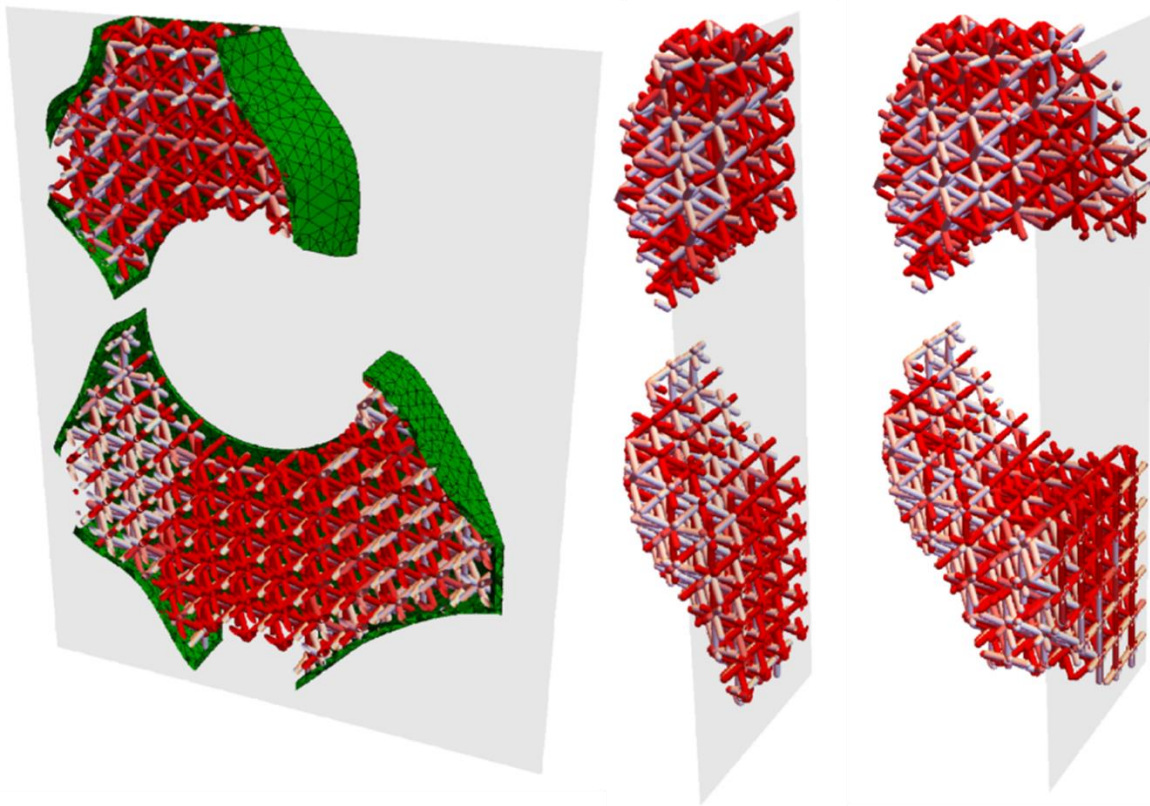


Figure 82. Result of Optimization Problem 2

From the figure above, it is possible already to see that the two optimization results seem to agree, but not as much as in the case of the bottle test piece. This consideration will be evident in the next chapter.

A prototype of solution Fig. 82 (without skin), as built, is displayed in Fig. 83.



Figure 83. A prototype of solution in Fig. 82 (without skin), as built.

## 7.2.4 Results

The results in terms of compliance and stiffness increment are reported in Table 7. The loads have been scaled in order to have compliance  $\hat{C}=1$  for the model with uniform density distribution (or constant bar section area).

Therefore, the stiffness increment is considered with respect to the model for compliance  $\hat{C}=1$ .

Partition	Original Partition		Refined Partition	
	<i>Opt. Problem 1</i>	<i>Opt. Problem 2</i>	<i>Opt. Problem 1</i>	<i>Opt. Problem 2</i>
Optimization Problem				
Compliance	0.92	0.80	NaN	NaN
Stiffness increment	+8%	+20%	NaN	NaN

Table 7. Results of FEM simulation of the Upright

Note that this time the solutions of the Optimization Problems 1 and 2 differs by a 12% on the mean compliance. The reason why the difference is bigger than before is not very clear. Anyway, the optimization problem 1 was mainly used for the feedback to find new internal subdivision, that we did not use in this case.

The result of optimization problem 2 is the one to look for, and useful to evaluate the effectiveness of the optimization process proposed. Also in this case a modest improvement in stiffness of about 20% from a design with uniform lattice density is achieved.

## 8 Conclusions

The procedure described addresses some of the issues that are relevant in the design of a good lattice infill for additive manufacturing:

- it can be used for design of real 3D objects;
- it allows users to select the small-scale topology of the infill;
- it allows the use of different topologies in different subdomains, and different effective densities within each subdomain; the selection of the lattice topology can insure that the part is printed from one direction;
- it takes in consideration manufacturing constraints (printability), that makes the output always printable, and once printed it does not need post processing because no support material has been used (support material is needed just to print the external skin if it overcomes the maximum overhang angle or the maximum bridging length);
- it can create complete closed object with an external skin to protect the internal structure or accomplish some aesthetic requirements.

The strategy still has to overcome some important drawbacks:

- to allow for the use of different lattice scales and facilitate their connection, it requires the introduction of separating walls, not object of optimization;
- it provides only some guidance on how to place these walls, relying on designer experience for this step;
- crucially, it requires that the user has access to a good trimming algorithm, capable of trimming the lattice to the boundaries of the subdomains in a more automatic or faster way;
- it does not take in consideration the anisotropy, on the printing direction, introduced by the deposition process

With the methodology as it is, an improvement of 20% in performance (stiffness), with respect to a constant density lattice infill with the same total mass, has been demonstrated for the two examples considered. The refinement of the partition explained in Chapter 5 and shown in the example of the bottle shape piece has shown no improvements in

mechanical performance. It could be reasonable considering that we are eliminating and adding material in regions of low stress where modifications are less likely to change the macroscale behaviour.

Anyway, the innovation carried by this methodology is important. It is the first one concerning about printability and that open the possibilities to FDM technology to build optimized structures. For this reason, we believe that more effort should be spent on working on this idea. For this purpose, some possible future work is presented here.

## 8.1 Future Work

The topic that were not treated in this thesis, but could be implemented in the future, are presented here ordered roughly by priority.

1. *Compare the result obtained with this methodology to Altair Optistruct optimization.*

Keeping in mind that the target is to bring lattice optimization to FDM technology, from the comparison, one could evaluate if it is worthy to keep working on this methodology or it might be better to find a way of introducing manufacturing constraints during the generation of a mesh. In this way one could use Optistruct and the truss model generated by the mesh would respect the printability requirements of FDM (and others) technology.

2. *Introducing other lattice cells and their orientation as a parameter.* Only one choice of lattice microstructure topology throughout the body was investigated, while it is likely that using several topologies, and including their optimal orientation (for anisotropy cells) as part of the optimization problems, will result in improvements in performance.
3. *Introduce printing variables in the optimization.* If the methodology presented is applied as it is, the printed object will probably behave different than expected in real experiment tests. Parts printed with most additive manufacturing technologies, present strong anisotropy on the printing direction. Adding orientation of the cell and anisotropy in the model one could also account these anisotropies introduced by the deposition process.

4. *Eliminate internal walls.* Another important task is to find another way to connect lattices of different scales or topologies because now it is a significant drawback of this methodology. This limitation can be removed, but only at the expense of considerable investment in effort on the geometric modelling side of the problem. For some problems this is a justifiable investment that is being pursued elsewhere. One could also try to find a way of generating an automatic interface between two subdomains that do not make use of such a big amount of material like the current walls used
5. *Include buckling and strength.* The strategy considered only stiffness as the main design criterion, while strength and buckling are likely to play a role in the design. However, there is nothing that prevents introduction of these additional performance criteria in future work, while keeping the essence of the methodology intact.

## Symbols List

$E$	Young's Modulus
$p$	Penalization factor
$\rho_c$	Cell density
$\rho_o$	Material density
$d$	Relative density
$t$	Bar diameter
$L$	Cell size
$\alpha$	Overhang angle
$w$	Wall thickness
$\Omega$	Entire body domain
$\Omega_B$	Skin domain
$\Omega_D$	Design domain
$\Omega_i$	Subdomain
$N_\Omega$	Number of subdomains
$\mathbf{D}$	Effective elastic tensor
$f(d)$	Effective properties factor
$\mathbf{D}^0$	Solid elastic matrix
$A$	Bar section area
$\boldsymbol{\sigma}$	Stress vector
$\boldsymbol{\varepsilon}$	Strain vector
$D_i$	Prescribed dimension of a subdomain
$n$	Number of cell each side of a coupon
$\hat{D}_i$	Sphere diameter

- $v$  Percentage of material assigned
- $\mathbf{U}$  Global displacement vector
- $\mathbf{F}$  Force vector
- $\mathbf{K}$  Global stiffness matrix
- $\hat{C}$  Compliance

## Figure Index

Figure 1. SuperDraco engine produced with EOS metal 3D printer and made of Inconel superalloy. <sup>2</sup> .....	9
Figure 2. 3D printing process compared to traditional manufacturing process.....	10
Figure 3. Comparison between AM and conventional manufacturing. Laser beam Melting is one of the AM main technologies. The same pattern is valid for the other AM technologies.....	10
Figure 4. Example of complex 3D printed geometry .....	11
Figure 5. Resume of the main 3D printing technologies. Image from Ref. [12].....	13
Figure 6. Typical scheme of an SLA machine. Image from Ref. [12]. .....	14
Figure 7. A part being printed with SLA technology. Image from Ref. [12]. .....	14
Figure 8. Typical scheme of a SLS printer .....	15
Figure 9. A general SLS printer in action.....	16
Figure 10. Scheme of a 3D double nozzle FDM printer. Image from Ref. [12]. .....	17
Figure 11. FDM printer in action to print one of the practical example of this thesis. ..	17
Figure 12. Working scheme of a Material Jetting machine. Image from Ref. [12]. .....	18
Figure 13. An example of part produced with Material Jetting. The white part is stiff, while the black part is made up of another material flexible. Image from Ref. [12]. ...	18
Figure 14. Another example with a clear use of two different materials, one glossy and one matte. Image from Ref. [12]. .....	19
Figure 15. Working scheme of a binder jetting printer .....	19
Figure 16. Example of a multicolour part produced with Binder jetting technology.....	20
Figure 17. Working scheme of an EBAM machine. ....	21
Figure 18. LENS system in action. ....	21
Figure 19. Scheme of a typical Sheet Lamination machine. ....	22
Figure 20. Example of multi-material (copper and aluminium) part printed with Sheet Lamination.....	22
Figure 21. Example of full colour print object printed with Sheet Lamination. ....	23
Figure 22. Result of a standard topology optimization with SIMP model for $p \geq 3$ . Image from [10]. .....	25
Figure 23. Result of the optimization problem allowing mid-densities elements. ....	26

Figure 24. Typical 2D cells. From the left: Honeycomb cell, Triangular cell, Kagome cell. .....	27
Figure 25. Some of the 3D cells. From the left BCC cell, Octet-truss cell, cubic-octet foam. ....	27
Figure 26. Optimization procedure presented in Ref [2]. First Fem simulation to get rid of very useless part of the domain (a); new design domain (b); toolpath of even layers (c); toolpath of odd layers (d); final aspect (e); printed object (f) .....	28
Figure 27. Kagome cell dimension, and result of the optimization presented in Ref [1]. .....	30
Figure 28. Real 2.5D part of Ref [1] printed. ....	30
Figure 29. Bracket optimized through Altair Optistruct (Ref. [10]). ....	31
Figure 30. Titanium 3D printed structural object optimized with Optistruct. ....	32
Figure 31. Design process for additively manufactured parts. ....	33
Figure 32. Resume of the additive manufacturing technologies grouped by the function of the printed part. ....	34
Figure 33. Attempt by the 3D printer to make a bridge. ....	38
Figure 34. Effect of bridging handled in a bad way (top) and a good way (bottom). ....	39
Figure 35. Definition of overhang angle. $\alpha_1$ is printable. $\alpha_2$ might be printable worse quality, $\alpha_3$ is not printable. ....	40
Figure 36. Sphere printed without support. A thin wall could cause the collapse of the shape caused by its own weight.....	41
Figure 37. Wall attached to other two walls (a). Minimum wall thickness can be used (generally 0.4mm) Wall not attached to any other wall. Minimum thickness should be increased. ....	41
Figure 38. Cylinders of different diameters, without any support material. The thicker the longer can be printed. ....	42
Figure 39. Result of the bridging test on the machine used in this thesis. ....	43
Figure 40. Result of the overhang angle test on the machine used in this thesis. ....	44
Figure 41. Result of the thin wall test on the machine used in this thesis. ....	45
Figure 42. Scheme of the cylinder test in Ref. [13]. ....	46
Figure 43. Result of cylinder test in Ref [13]. ....	46
Figure 44. Five cell patterns of different thicknesses. ....	47

Figure 45. Zoom on one of the pattern (2 mm diameter bars) and comparison to the CAD model. ....	47
Figure 46. Component used for illustration. $\Omega_B$ is the “skin”, of prescribed shape. $\Omega_D$ is the design domain to be optimized. ....	48
Figure 47. Possible division of the internal domain through two internal walls. $\Omega_i \in \Omega_D$ are filled with lattice infill. ....	49
Figure 48. Body Centred Cell (BCC) used as infill. Two setups with same cell size but different bar thickness ....	50
Figure 49. Each subdomain contains cells of same topology and size. Thicknesses of the bars may change. ....	51
Figure 50. Dogbone mesh for Optimization Problem 1. Each tetrahedra is an element of the optimization. Mechanical properties are given to each element by averaging the microscopic dimensions of the cell. ....	52
Figure 51. Body after Optimization Problem 2. Each subdomain $\Omega_i$ is assigned to a lattice pattern of length $L_i$ . Note that this time the cells have independent diameter. ....	53
Figure 52. Flowchart of the methodology proposed. ....	54
Figure 53. Elementary lattices with cubic symmetry. Simple Cubic (SC) (a); Body-Centred Cubic (BCC) (b); and Face-Centred Cubic (FCC) or Octet truss (c). ....	56
Figure 54. Isotropic cubic cells resulting from the combination of elementary cells in Fig. 53. ....	56
Figure 55. Numerical results of the simulation of cells in Fig. 54. Anisotropy analysis (a), f(d) that being isotropic cell is just the relative Young’s Modulus (b) ....	57
Figure 56. Octet truss cell, 3x3x3 Octet cell pattern ....	58
Figure 57. Cubic-Octet Foam cell ....	59
Figure 58. The BCC lattice cell topology with its parameters and a 3x3x3 coupon of the same cell. ....	62
Figure 59. Result of the homogenization procedure for the BCC cell of different lengths L, thickness t, and coupon size n. Blue vertical lines represent the deviations of the results, while the red dashed line follows (13). ....	64
Figure 60. Contour plot of the relative densities as a function of the cell length L and bar thickness t. The plot is bounded by the manufacturing constraints, and shows the range of possible densities. (Dimensions t and L in mm) ....	66

Figure 61. Result of standard topology optimization on Dogbone geometry. (a) Just internal material, (b) internal material and external skin.....	67
Figure 62. Subdivision of the design domain based on constraint (16). Three spheres of different diameters show the need of different cell dimensions and walls to separate them. ....	69
Figure 63. Possible scenarios where small features impose restrictions on cell size. ....	70
Figure 64. Iterative procedure of design domain subdivision. ....	71
Figure 65. Tetrahedral mesh of the model. Each tetrahedra has different relative density and consequently different effective properties.....	73
Figure 66. Typical condition at the boundary of each subdomain, where truss elements cross tetra elements.....	77
Figure 67. Lattice infill trim starting point (a), after trimming (b).....	78
Figure 68. Lattice infill after transformation from solid to truss elements.....	78
Figure 69. Aspect of the model after conversion from solid to truss full of sticking out bars (a) Aspect after cleaning the model (b).....	79
Figure 70. Test piece. External shape with forces and constraints (a). Mid-section with the three regions defined (b). A wall is placed to allow the connection between lattices of different scale lengths, defined by the blue spheres, from (17) with $n=3$ . ....	81
Figure 71. Result of Optimization Problem 1 for the “bottle” test piece. ....	82
Figure 72. Choice of the position of the new internal walls (a). Modified subdivision and new labels (b).....	83
Figure 73. Result of the Optimization Problem 1 for the new subdivision of the design domain. ....	84
Figure 74. Result of Optimization Problem 2 for both partitions set. ....	85
Figure 75. A prototype of solution in Fig. 74 (half), as built. ....	87
Figure 76. Upright designed with standard manufacturing technique and position in the assembly of the suspension.....	88
Figure 77. Design domain (a) and result of standard topology optimization (b) from Ref. [11].....	89
Figure 78. Problem set-up. Initial design domain given by [11] (a), result of the standard topology optimization (b), new design domain (c).....	90

Figure 79. Upright geometry. External skin and mounts $\Omega_B$ showing forces and constraints (a), Subdomains $\Omega_1, \Omega_2$ to be filled by lattice (b).....	91
Figure 80. Sphere method to evaluate cell dimension. All spehere in the picture have diameter=36mm.....	91
Figure 81. Result of Optimization Problem 1.....	92
Figure 82. Result of Optimization Problem 2.....	93
Figure 83. A prototype of solution in Fig. 82 (without skin), as built.....	94

## Table Index

Table 1. Characteristic of additive manufacturing technologies for high strength prints. .....	36
Table 2. Resume of the geometrical characteristics and effective properties of the three cells of the literature. ....	60
Table 3. Density ranges for various cell size $L_i$ .....	75
Table 4. Area ranges for various cell sizes $L_i$ .....	76
Table 5. Results of FEM simulation of the “bottle” test piece .....	86
Table 6. Load cases .....	89
Table 7. Results of FEM simulation of the Upright .....	95

## Bibliography

- [1] Campagna, F and Diaz, AR: Optimization of lattice infill distribution in additive manufacturing. *43rd Design Automation Conference* (Vol. 2A-2017). American Society of Mechanical Engineers (ASME). (2017) DOI: 10.1115/DETC2017-67582 .
- [2] Tancogne-Dejean, T and Mohr, D: Elastically-isotropic truss lattice materials of reduced plastic anisotropy, International. *Journal of Solids and Structures* (2017), <https://doi.org/10.1016/j.ijsolstr.2017.12.025>
- [3] Steuben, JC; Iliopoulos, AP and Michopoulos, JG: Implicit slicing for functionally tailored additive manufacturing. *International Design Engineering Technical Conferences and Computers and Information in Engineering Conference*, Volume 1A: (2016) 107-119. American Society of Mechanical Engineers (ASME). (2016) DOI:10.1115/DETC2016-59638.
- [4] Hedayati, R; Mojtaba S; Mohammad M-A and Hosseini-Toudeshky, H: Comparison of elastic properties of open-cell metallic biomaterials with different unit cell types. *Journal of biomedical materials research. Part B, Applied biomaterials* 106 1 (2018): 386-398.
- [5] Berger, JB; Wadley, HNG and McMeeking, RM: Mechanical metamaterials at the theoretical limit of isotropic elastic stiffness, *Nature* (2017), vol 543 , no. 7646 , pp. 533-537 . DOI: 10.1038/nature21075
- [6] Vigliotti, A and Pasini, D: Stiffness and strength of tridimensional periodic lattices, *Comput. Methods Appl. Mech. Engrg.* Volumes 229–232 (2012) Pages 27–43. <https://doi.org/10.1016/j.cma.2012.03.018>
- [7] Oller, S: Homogenization Theory. In: Numerical Simulation of Mechanical Behavior of Composite Materials. *Lecture Notes on Numerical Methods in Engineering and Sciences*. Springer, Cham (2014).
- [8] Bendsoe, MP and Sigmund: O. *Topology Optimization: Theory, Methods, and Applications*. Springer Berlin Heidelberg (2003).
- [9] Svanberg, K: The method of moving asymptotes – a new method for structural optimization. *Int. J. Numer. Methods* (1987). Eng. 24(2): 359-73.
- [10] Altair Engineering Inc. Optistruct: Lattice optimization; <http://insider.altairhyperworks.com/design-andoptimization-of-lattice-structures-for-3D-printing-using-altairoptistruct/> Quoted 2/27/2018.

- [11] Maranan, VJC: *Design and Processing of an Additive Manufacturing Component*. Thesis, Baccalaureate Degree in Engineering Science, Department of Engineering Science and Mechanics, Pennsylvania State University (2013).
- [12] 3D Hubs, <https://www.3dhubs.com/knowledge-base> , Last time consulted 16/03/2018
- [13] Xometry, <https://support.xometry.com/hc/en-us/articles/217723698-What-is-the-smallest-feature-that-you-can-print->, Last time consulted 16/03/2018
- [14] Claus Aumund-Kopp, Adeline Riou: *Introduction to additive manufacturing technology*. European Powder Metallurgy Association (EPMA):